

1 **Understanding Arctic Ocean circulation:**
2 **a review of ocean dynamics in a changing climate**

3 **Mary-Louise Timmermans¹ and John Marshall²**

4 ¹Department of Geology and Geophysics, Yale University, New Haven, Connecticut, USA

5 ²Department of Earth, Atmospheric and Planetary Sciences, Massachusetts Institute of Technology,
6 Cambridge, Massachusetts, USA

7 **Key Points:**

- 8 • Major features of Arctic Ocean circulation are reviewed and interpreted theoret-
9 ically
- 10 • Fundamental ocean dynamics are set in the context of a changing Arctic climate
- 11 • We describe how Arctic dynamics might change in the future

Corresponding author: Mary-Louise Timmermans, mary-louise.timmermans@yale.edu

Abstract

The Arctic Ocean is a focal point of climate change, with ocean warming, freshening, sea-ice decline and circulation that link to the changing atmospheric and terrestrial environment. Major features of the Arctic and the interconnected nature of its wind- and buoyancy-driven circulation are reviewed here by presenting a synthesis of observational data interpreted from the perspective of geophysical fluid dynamics (GFD). The general circulation is seen to be the superposition of Atlantic Water flowing into and around the Arctic basin, and the two main wind-driven circulation features of the interior stratified Arctic Ocean: the Transpolar Drift Stream and the Beaufort Gyre. The specific drivers of these systems, including wind forcing, ice-ocean interactions and surface buoyancy fluxes, and their associated GFD are explored. The essential understanding guides an assessment of how Arctic Ocean structure and dynamics might fundamentally change as the Arctic warms, sea-ice cover declines and the ice that remains becomes more mobile.

1 Introduction

The Arctic Ocean, centered over the north pole and surrounded by land, is covered entirely by a thin (order 1 m) layer of sea ice in winter, which can shrink by up to 2/3 every summer. Arctic summer sea ice appears to be in rapid decline in recent decades (D. Perovich et al., 2019). Moreover the north polar regions are warming faster than the global-mean (Overland et al., 2019) — a phenomenon known as Arctic amplification — and Arctic change is accelerating. For these reasons the Arctic is particularly vulnerable to climate change. In the coming decades we may expect to enter a new regime, in which the interior Arctic Ocean is entirely ice free in summer and sea ice is thinner and more mobile in winter (e.g., T. W. Haine & Martin, 2017). Some climate model scenarios suggest the Arctic Ocean may be seasonally ice free by ~ 2050 (Collins et al., 2013). A seasonally ice-free Arctic will have vast implications for Arctic oceanography, the marine ecosystems it supports and the larger-scale climate. It will also have wide-ranging consequences for Arctic communities, geopolitics and policy as Arctic coastal environments and sea routes change and Arctic resources become more accessible. Urgent challenges will be to implement effective observing strategies, and synthesize observations in theoretical and modeling analyses to better understand the ocean’s role and interrelationships in the Arctic system.

43 In this review we summarize some major aspects of Arctic Ocean physical oceanog-
44 raphy by presenting key observations in a common format, discuss the cause of its gen-
45 eral circulation and how it might change as the Arctic enters a new sea-ice regime. The
46 physical oceanography is complex and, due to the presence of sea ice, difficult to observe.
47 The first ocean measurements from the central Arctic Ocean were made during Fridtjof
48 Nansen’s 1893-1896 drift of the Fram (Nansen, 1897). Observations revealed it to be a
49 vast deep basin, and confirmed the existence of the Transpolar Drift Stream, the flow
50 of ice and water from the coast of Siberia across the Arctic to the North Atlantic via the
51 east coast of Greenland. It was during Nansen’s expedition that the observation was made
52 that sea ice drifts somewhat to the right of the prevailing wind direction — an obser-
53 vation that was the foundation of Ekman’s theory describing the friction-Coriolis force
54 balance in geophysical fluid boundary layers (Ekman et al., 1905). Rudels et al. (2012)
55 provides a concise review of the exploration history leading to the general picture in the
56 mid-1900s of the Arctic being a deep ocean characterized by complex bathymetry and
57 relatively warm water of Atlantic Ocean origins underlying relatively cool and fresh sur-
58 face waters capped with ice (Figure 1).

59 The Arctic Ocean receives inflows from the Atlantic and Pacific oceans and North
60 American and Siberian rivers. Its stratification is predominantly set by salinity (there
61 is a halocline rather than a thermocline) with melting and freezing of sea ice being a cen-
62 tral player in the freshwater cycle and in the mediation of the wind stress acting at the
63 surface. Familiar, textbook paradigms of ocean circulation, such as *Sverdrup balance*, that
64 underpin theories of the mid-latitude oceans, are not applicable in the Arctic where the
65 north-south gradient of the Coriolis parameter is too small to influence the dynamics.
66 The rapid changes that are presently underway have raised new questions about the Arc-
67 tic Ocean’s future dynamics, the relative importance of influences exterior and interior
68 to the Arctic, and the complex ocean-ice-atmosphere interactions and feedbacks which
69 involve and evolve as sea ice declines. Our review is led by observations, and we apply
70 the underlying theory of geophysical fluid dynamics to shed light on contemporary cir-
71 culation characteristics presenting what we consider to be the key ideas. We then spec-
72 ulate how the fundamental dynamics may be transformed under continued Arctic change.

73 Our review is outlined as follows. In Section 2 we describe the geographical and
74 bathymetric setting of the Arctic, how it connects to the rest of the world ocean, Arc-
75 tic Ocean surface properties, and the wind patterns driving the circulation. Two key cen-

76 ters of meteorological action are the Beaufort High and the Icelandic Low, introducing
77 anticyclonic and cyclonic vorticity tendencies, respectively. In Section 3 we describe the
78 Arctic Ocean temperature and salinity structure and buoyancy forcing (dominated by
79 surface freshwater fluxes). Mixing and stirring in the Arctic Ocean are described in Sec-
80 tion 4. The observed circulation of warm, salty Atlantic Water entering and circulating
81 around the Arctic basin is described in Section 5. Its transformation within the semi-
82 enclosed Arctic basin is associated with mixing of cold, fresh water from above (Section
83 5.1). The wind provides a source of energy for mixing, but also its cyclonic curl exter-
84 nal to the basin (associated with the Icelandic Low) plays an important role in draw-
85 ing Atlantic Water, strongly steered by topography, in to the Arctic basin (Section 5.2).
86 Interior to the Arctic basin, the two main wind-driven circulation features are the Trans-
87 polar Drift Stream and the anticyclonic Beaufort Gyre, under the influence of the Beau-
88 fort High, as discussed in Sections 6 and 7, respectively. In Section 8 we describe how
89 the Arctic system is changing as the Earth warms and how those changes may manifest
90 themselves in the circulation dynamics. In Section 9, we attempt to synthesize the over-
91 all ocean structure and dynamics in a conceptual framework within which we can con-
92 template and reconcile ongoing and future Arctic change.

93 **2 Geographical setting and Arctic Ocean surface properties**

94 The Arctic Ocean, along with the Greenland, Iceland and Norwegian seas (the Nordic
95 Seas) have together been referred to as the *Arctic Mediterranean* because, as shown in
96 Figure 1a, it is a large deep basin of water surrounded by land and shallower channels
97 (see e.g., Sverdrup, Johnson, Fleming, et al., 1942)¹. The main entry to the Arctic Mediter-
98 reanean is marked by the Greenland-Scotland Ridge. Relatively warm and salty Atlantic
99 Ocean water flows across the Greenland-Scotland Ridge into the Nordic Seas (Hansen
100 et al., 2008). Atlantic water enters the Arctic via Fram Strait and the Barents Sea Open-
101 ing (see e.g., Beszczynska-Möller, Fahrbach, Schauer, & Hansen, 2012; Ingvaldsen, Lo-
102 eng, & Asplin, 2002; Schauer, Fahrbach, Osterhus, & Rohardt, 2004). The only oceanic

¹ The *Arctic Mediterranean* as described has also be referred to as the Arctic Ocean (i.e., the Nordic Seas and Barents Sea are included in the region that is considered the Arctic Ocean); indeed, this is the International Hydrographic Organization’s official definition of the Arctic Ocean (see Jakobsson & Macnab, 2006, their Figure 1).

103 gateway between the Pacific and Arctic oceans is Bering Strait where Pacific Water in-
104 flows provide an important source of fresh water and heat to the Arctic Ocean (T. W. N. Haine
105 et al., 2015; Woodgate, Weingartner, & Lindsay, 2010). Waters leave the Arctic Ocean
106 via straits in the Canadian Arctic Archipelago (e.g., LeBlond, 1980; Münchow, Melling,
107 & Falkner, 2006), and in the East Greenland current that flows south on the west side
108 of Fram Strait (e.g., Woodgate, Fahrbach, & Rohardt, 1999).

109 The bathymetric and topographic complexity within the Arctic is extreme and ex-
110 erts strong controls on circulation pathways, ventilation and exchange processes between
111 Arctic basins. Bathymetry also influences the spatial variability of diapycnal mixing and
112 baroclinic instability, as described in Section 4. The roughly 4000 m deep Arctic basin
113 is divided by the Lomonosov Ridge, with a mean depth of around 1500 m (Cochran, Ed-
114 wards, & Coakley, 2006), separating the Eurasian and Canadian basins. These two basins
115 are subdivided into the Amundsen and Nansen basins (separated by the Gakkel Ridge,
116 typically deeper than ~ 4000 m) and the Makarov and Canada basins (separated by the
117 ~ 2200 -m-deep Alpha and Mendelejev Ridges), Figure 1.

118 The Arctic is under the influence of two major wind-patterns: the Beaufort High
119 centered over the Canadian Basin, introducing anticyclonic tendencies, and the Icelandic
120 Low centered just outside of the Arctic basin inducing cyclonic tendencies and orches-
121 trating the Arctic gateway to the Atlantic (Figure 2c). Wind-stress curl patterns are such
122 that there is broad Ekman downwelling over much of the Arctic Ocean, and relatively
123 strong upwelling over the Nordic Seas (indicated by the blue and red colors in Figure
124 2c, respectively), with sea ice modifying stress on the surface ocean, as will be discussed
125 in Section 7.2. Sea-ice motion (Figure 2a, white arrows), and surface ocean geostrophic
126 flow (Figure 2d), generally follow the wind with the anticyclonic flow of the Beaufort Gyre
127 (the dominant upper-ocean circulation feature of the Canadian Basin) and Transpolar
128 Drift Stream being clearly evident.

129 Arctic sea-ice cover extends throughout the Arctic Ocean in winter (approximately
130 where white arrows are present in Figure 2a), and is characterized by an average thick-
131 ness of around 2 m. Sea-ice has a large seasonal cycle, with summer sea-ice extent in re-
132 cent years generally around one-third of the winter extent. The winter maximum extent
133 occurs in March, while the sea-ice minimum is in September. The August 2018 sea-ice
134 distribution is shown in Figure 2b (colored white) together with the August mean ex-

135 tent for 1981-2010 (black contour). Since 1979 (the start of the satellite record) a lin-
136 ear trend indicates summer (September) sea ice has been declining at a rate of about 1
137 million square kilometers per decade, with sea ice covering about 4.5 million square kilo-
138 meters in September in recent years (e.g., D. Perovich et al., 2019; D. K. Perovich & Richter-
139 Menge, 2009; Richter-Menge, Jeffries, & Osborne, 2018). Declining sea-ice volume (i.e.,
140 a shift to a thinner, more mobile sea-ice pack) accompanies these sea-ice area losses. In
141 the 1980s, average winter (fall) sea-ice thickness was around 3.6 m (2.7 m), while in 2018,
142 average winter (fall) ice thickness was ~ 2 m (1.5 m) (Kwok, 2018). The loss of Arctic
143 sea ice is not only a conspicuous indicator of climate change, it also sustains a funda-
144 mental global climate feedback through its influence on Earth’s planetary albedo (Pi-
145 stone, Eisenman, & Ramanathan, 2014). Arctic Ocean warming (e.g., Onarheim, Elde-
146 vik, Smedsrud, & Stroeve, 2018; I. V. Polyakov et al., 2010; Timmermans, 2015; Tim-
147 mermans, Toole, & Krishfield, 2018; Woodgate, 2018), freshening (e.g., A. Proshutin-
148 sky et al., 2009; Rabe et al., 2014), and changing stratification, circulation dynamics, and
149 momentum transfer to the ocean (e.g., Davis, Lique, & Johnson, 2014; Meneghello, Mar-
150 shall, Timmermans, & Scott, 2018; Peralta-Ferriz & Woodgate, 2015; I. V. Polyakov et
151 al., 2017) all link to the sea ice.

152 The amount and mobility of sea ice is of great relevance to the balance of forces
153 that drive the large-scale ocean circulation, because it acts as a critical mediator of wind-
154 stress in the Arctic, as explored in Section 7. Further, sea-ice cover, sea-surface salin-
155 ity and temperature are also strongly coupled. Surface salinities are much fresher in the
156 Arctic Ocean compared to the north Pacific and Atlantic oceans (Figure 2a), the broad
157 result of northward transport of atmospheric fresh water from equatorial regions, with
158 contributions from seasonal sea-ice melt and relatively fresh ocean flows from the Pa-
159 cific Ocean. Arctic Ocean sea-surface temperatures are at the freezing point (around -
160 2°C for seawater) in winter and in regions where sea ice persists year round. Outside of
161 the winter months, an opening in the sea-ice pack can leave the ocean exposed to direct
162 solar forcing, increasing sea-surface temperatures. These warmed surface waters can melt
163 the surrounding sea ice, exposing more open water and a positive feedback (the *ice-albedo*
164 *feedback*) ensues. Summer sea-surface temperatures at the ice-free margins of the Arc-
165 tic basin can be up to a few degrees above 0°C , with higher sea-surface temperatures (again
166 several degrees above 0°C) in the vicinity of Pacific and Atlantic Water inflows (Figure
167 2b and see Timmermans and Ladd (2019)). Owing to the halocline stratification, which

168 we describe next, the warm waters originating in the Pacific and Atlantic oceans do not
169 need to be confined to the surface Arctic Ocean, and can reside at depth.

170 **3 Arctic Ocean stratification and buoyancy forcing**

171 A trans-Arctic section crossing from the Pacific to the Atlantic oceans illustrates
172 the essential Arctic Ocean water-mass distribution and stratification: relatively cold, fresh
173 water overlies relatively warm, salty water (Figure 1b). Marked gradients in tempera-
174 ture, salinity and density are confined to the top few hundred meters of the water col-
175 umn, which features various components of the Arctic halocline (Figure 3). We consider
176 the potential density surface $\sigma = 27.4 \text{ kg m}^{-3}$ to approximately represent the base of
177 the halocline (see the deepest dashed line in Figure 3b), and plot its depth across the
178 Arctic Ocean (Figure 3a). In the Canada Basin, this isopycnal surface is as deep as $\sim 200 \text{ m}$,
179 marking the imprint of the anticyclonic Beaufort Gyre which is in thermal wind balance
180 with lateral density gradients. Also evident is the signature of the Transpolar Drift Stream
181 at the confluence of the Canadian and Eurasian Basins.

182 Representative vertical profiles of temperature, salinity and density in the Cana-
183 dian and Eurasian Basins illustrate the details of the upper water column (Figure 3b).
184 Underlying the surface mixed layer ($\lesssim 50 \text{ m}$ deep), is a relatively warm near-surface layer
185 in the Canadian Basin, absent in the Eurasian Basin. It derives from the $\sim 1 \text{ Sv}$ ($1 \text{ Sv} =$
186 $10^6 \text{ m}^3 \text{ s}^{-1}$) northward flow through the $\sim 50 \text{ m}$ deep and $\sim 80 \text{ km}$ wide Bering Strait
187 (e.g., Woodgate et al., 2010). Bering Strait inflow is driven both by local wind variabil-
188 ity, and a sea-surface height difference between the Bering Sea Shelf and the Chukchi and
189 East Siberian seas (with sea level being highest in the Bering Sea) (see Danielson et al.,
190 2014; Peralta-Ferriz & Woodgate, 2017; Woodgate & Aagaard, 2005).

191 This layer, with origins in the Pacific Ocean, has temperatures in the range -1 to
192 1°C , and sits at around 50 to 100-m depth in the Canadian Basin (Figure 3b,c), is called
193 Pacific Summer Water since it ventilates the region in summer (e.g., Steele et al., 2004;
194 Timmermans et al., 2014). Below the Pacific Summer Water layer in the Canadian Basin
195 sits relatively cooler and saltier Pacific Winter Water (e.g., Pickart, Weingartner, Pratt,
196 Zimmermann, & Torres, 2005), which ventilates the region in winter (Figure 3b,c). The
197 base of the Pacific Winter Water layer is approximately bounded by the $\sigma = 27.4 \text{ kg}$
198 m^{-3} surface. In both the Canadian and Eurasian basins, a layer of warm Atlantic-origin

199 water, characterized by temperatures around 0 - 3°C (colored red in Figure 3c), resides
200 between roughly 150 and 500-m depth, at or below the $\sigma = 27.4 \text{ kg m}^{-3}$ surface. We
201 discuss these Atlantic-origin waters in detail in Section 5.

202 A defining feature of the Arctic Ocean with a profound influence on the behavior
203 of the Arctic system and climate is that it is predominantly salinity-stratified. This ba-
204 sic stratification of fresher waters overlying saltier waters, separated by a strong halo-
205 cline, is known as a β -ocean, where β refers to the saline contraction coefficient. By con-
206 trast, the subtropical α -oceans (where α refers to the thermal expansion coefficient) have
207 their stratification set mainly by temperature, with warmer waters overlying cooler wa-
208 ters. This broad stratification distinction, evident at around 45°N in both the Pacific
209 and Atlantic sectors (Figure 1b), is a vital aspect of ocean and climate relevance; for ex-
210 ample, sea ice can only grow at the surface of β -oceans where the salinity stratification
211 inhibits deep convection — an α -ocean would convect (see E. C. Carmack, 2007). In the
212 mid-latitude α -oceans, there is a net warming and evaporation. The atmospheric mois-
213 ture is transported polewards where it precipitates over the high-latitude β -oceans. The
214 non-linear equation of state of seawater also factors in this distinction with α increas-
215 ing with temperature, such that in the upper water column it is about an order of mag-
216 nitude larger at 20°C compared to its value at much colder (near freezing) Arctic Ocean
217 temperatures (see Timmermans & Jayne, 2016). In Section 8 we return to discuss this
218 α - β transition in the context of a changing Arctic Ocean under increasingly Atlantic
219 influence.

220 River discharge, predominantly from the six main Arctic rivers (the Ob, Yenisey,
221 Lena, Kolyma, Yukon, and Mackenzie rivers), is a major source of fresh water to the Arc-
222 tic Ocean (Holmes et al., 2012; McClelland, Holmes, Dunton, & Macdonald, 2012). While
223 the Arctic Ocean constitutes only 1% of the World’s ocean by volume, it catches around
224 10% of its river discharge (Aagaard & Carmack, 1989). The Arctic Ocean also receives
225 fresh water through net precipitation (e.g., M. C. Serreze et al., 2006) and relatively fresh
226 water from the Pacific Ocean via Bering Strait (Woodgate & Aagaard, 2005). In the an-
227 nual mean, the partitioning of this freshwater input is around 1/2 river discharge, 1/4
228 Pacific water inflow and 1/4 net precipitation (E. C. Carmack, 2000; E. C. Carmack et
229 al., 2016; T. W. N. Haine et al., 2015; M. C. Serreze et al., 2006); much smaller contri-
230 butions (less than a few percent) derive from meltwater fluxes from Greenland and north-
231 ward sea-ice fluxes through Bering Strait (T. W. N. Haine et al., 2015). Surface fresh

232 water from all of these sources is drawn toward the center of the Canadian basin by the
233 anticyclonic winds of the Beaufort High, ensuring the maintenance of the Arctic’s strong
234 halocline stratification (Figure 3).

235 As Arctic sea ice grows and moves, and brine is rejected, there is a distillation of
236 fresh water. While some fraction of this fresh water returns to liquid form during sea-
237 ice melt each summer, export of sea ice from the Arctic Ocean is a sink of fresh water
238 (in solid form) (see Aagaard & Carmack, 1989). Fresh water leaves the Arctic via ocean
239 and sea-ice flows through channels in the Canadian Arctic Archipelago and through Fram
240 Strait. Around 1/3 of the total freshwater export is in liquid form via each of Fram Strait
241 and Davis Strait, with 1/4 of the total exported in solid sea-ice fluxes through Fram Strait
242 (T. W. N. Haine et al., 2015).

243 Brine rejection from sea-ice growth produces dense, salty water in the shelf regions.
244 Cavalieri and Martin (1994) examine dense-water production across the Arctic in sites
245 of sustained sea-ice growth (e.g., coastal polynyas) to estimate a total dense-water flux
246 in the range 0.7 to 1.2 Sv. The overall contribution of this flux in modifying interior water-
247 column properties is unclear. For example, while instances of down-slope flows off con-
248 tinental shelves have been documented in the observations (predominantly in the Bar-
249 ents, Kara and Laptev seas V. Ivanov, Shapiro, Huthnance, Aleynik, & Golovin, 2004),
250 the strong halocline stratification limits the penetration of dense shelf water to the up-
251 per several hundred meters of the water column, and planetary rotation confines flows
252 to the continental slopes (e.g., V. V. Ivanov & Golovin, 2007).

253 The Arctic Ocean warms in summer via surface-water heating in ice-free regions
254 that is dominated by solar radiation (e.g., D. K. Perovich, Richter-Menge, Jones, & Light,
255 2008). The net surface heat flux is the sum of incoming shortwave radiation, longwave
256 emission, and sensible plus latent heat fluxes. Throughout the year over most of the Arc-
257 tic Ocean, vertical sensible and latent heat fluxes are small contributions (having mag-
258 nitudes $\lesssim 10 \text{ W m}^{-2}$) (e.g., M. C. Serreze et al., 2007). The net longwave flux is larger
259 (around 50 W m^{-2} upward) and remains approximately constant throughout the year.
260 The net shortwave component has a strong seasonal cycle, dominating in summer when
261 average values over the Arctic Ocean are around 150 W m^{-2} downward. Incoming so-
262 lar radiation is effectively zero between October and March (e.g., M. C. Serreze et al.,
263 2007).

264 The Arctic Ocean also receives heat via warm inflows from the Atlantic and Pa-
265 cific oceans (e.g., Beszczynska-Möller et al., 2012; Woodgate, Weingartner, & Lindsay,
266 2012). For the Arctic waters at low temperatures, α is sufficiently small that ocean tem-
267 perature does not strongly influence ocean dynamics. This may change as the ocean con-
268 tinues to warm, and we discuss potential implications of this in Section 8. While ocean
269 temperature may have only a weak influence on ocean dynamics, it is crucially impor-
270 tant to the fate of Arctic sea-ice cover should heat be mixed to the surface. We there-
271 fore now outline the primary mixing processes at work in the Arctic.

272 4 Mixing and stirring in the Arctic Ocean

273 The Arctic Ocean exhibits a variety of ocean mixing processes that differ from the
274 mid-latitudes because of the presence of sea ice, the high latitude, and the distinct halo-
275 cline stratification structure with warm water underlying cooler water. These processes
276 include convection by surface buoyancy fluxes resulting from brine rejection during ice
277 formation, turbulence driven by stress at the ice-ocean interface, mixing by internal waves
278 (where the internal wave field is affected by the high latitude Coriolis effect and sea-ice
279 cover), and double-diffusive mixing (see the review of these processes by Padman, 1995).
280 The Arctic Ocean is also baroclinically unstable and the mean flow emerges only after
281 averaging over a relatively energetic mesoscale and submesoscale.

282 4.1 Small-scale diapycnal processes

283 Arctic Ocean mixing levels are critical to the fate of sea ice because the ocean heat
284 stored at depth is enough to melt the entirety of the Arctic sea ice (G. A. Maykut & Un-
285 tersteiner, 1971). However, this would require some mechanism (e.g., dissipation of in-
286 ternal wave energy or double diffusion or vertical eddy heat flux) to mix that heat to the
287 surface layer in contact with sea ice. At present, the Arctic Ocean exhibits generally low
288 mixing rates compared to the mid-latitude ice-free oceans (e.g., D’Asaro & Morison, 1992;
289 Rainville & Winsor, 2008).

290 There is relatively weak tidal forcing in the Arctic and most of the region is above
291 the critical latitude north of which the semi-diurnal lunar tide can propagate freely (Kowa-
292 lik & Proshutinsky, 1993). Topographic waves generated over bathymetric slopes and
293 rough topography, forced by the tides, are the main source of energy for higher tidal dis-

294 sipation observed over topography (Holloway & Proshutinsky, 2007; Kowalik & Proshutin-
 295 sky, 1995; Luneva, Aksenov, Harle, & Holt, 2015; Padman, Plueddemann, Muench, &
 296 Pinkel, 1992; Rippeth et al., 2017). Sea-ice cover is present for most of the year and acts
 297 as a buffer to wind-driven momentum input to the upper ocean; further, internal wave
 298 energy can be dissipated under sea ice (Morison, Long, & Levine, 1985; Pinkel, 2005).
 299 In the fully-ice covered winter months, inertial wave energy and shear are generally weaker
 300 than in the seasonal absence of sea ice (Dosser, Rainville, & Toole, 2014; Halle & Pinkel,
 301 2003; Rainville & Woodgate, 2009). In the summer months, even though winds are weaker
 302 than in winter, median inertial wave amplitudes are around 10 to 20% larger than in win-
 303 ter. The additional energy is a consequence of increased atmosphere to ocean momen-
 304 tum transfer in open water regions and the absence of sea-ice damping of internal waves
 305 (e.g. Dosser & Rainville, 2016). In Section 8, we discuss the implications of Arctic sea-
 306 ice loss on ocean mixing levels.

307 Microstructure measurements indicate turbulent kinetic energy dissipation ϵ in the
 308 halocline of the deep basins to be around 5×10^{-10} to 2×10^{-9} W kg $^{-1}$ (Fer, 2009; Lenn
 309 et al., 2009; Lincoln et al., 2016; Rippeth et al., 2015). These values may be compared
 310 to typical midlatitude ocean thermocline values of around 10^{-9} W kg $^{-1}$ (J. M. Toole,
 311 Schmitt, & Polzin, 1994). In the Arctic’s continental shelf regions, ϵ is estimated to be
 312 two orders of magnitude larger than over the abyssal plain; in the region just north of
 313 Svalbard, for example, $\epsilon \sim 3 - 20 \times 10^{-8}$ W kg $^{-1}$ (Rippeth et al., 2015). This can be
 314 compared to values estimated by Ledwell et al. (2000) of around 10^{-8} W kg $^{-1}$ over the
 315 rough topography of the Mid-Atlantic Ridge. Elevated rates of dissipation of kinetic en-
 316 ergy are also found over the Canada Basin shelf regions where $\epsilon \approx 2 \times 10^{-8}$ W kg $^{-1}$
 317 (Lincoln et al., 2016; Rippeth et al., 2015).

318 Diapycnal diffusivity K_ρ takes values around 10^{-4} m 2 s $^{-1}$ at the base of the mixed
 319 layer to $\sim 1-7 \times 10^{-6}$ m 2 s $^{-1}$ in the strongly-stratified halocline away from topographic
 320 features (D’Asaro & Morison, 1992; Fer, 2009; Padman & Dillon, 1989; Rainville & Win-
 321 sor, 2008). In model studies, the Atlantic Water circulation direction and strength is found
 322 to be highly sensitive to the level of vertical mixing. Zhang and Steele (2007) find val-
 323 ues of $K_\rho \approx 10^{-6}$ m 2 s $^{-1}$ yield Atlantic Water circulation patterns and water proper-
 324 ties that best agree with climatology (values typically appropriate for midlatitudes, around
 325 10^{-5} m 2 s $^{-1}$, returned an anticyclonic Atlantic Water circulation, inconsistent with ob-
 326 servations).

327 Low mixing levels in the interior basin allow for the persistence of a double-diffusive
328 staircase at the top boundary of the Atlantic Water layer (see Figure 3b, inset panel),
329 and double-diffusive fluxes are the main mechanism for vertical heat transport from the
330 Atlantic Water. Vertical heat fluxes across the double-diffusive staircases in the central
331 basins are only in the range $0.02\text{--}0.3\text{ W m}^{-2}$, however (Guthrie, Fer, & Morison, 2015;
332 Padman & Dillon, 1987, 1989; Shibley, Timmermans, Carpenter, & Toole, 2017; Sire-
333 vaag & Fer, 2012; Timmermans, Toole, Krishfield, & Winsor, 2008). For context, these
334 heat fluxes are about one tenth of the mean surface ocean heat flux to the sea ice. An-
335 nual average ocean-to-ice heat fluxes are around $3\text{--}5\text{ W m}^{-2}$, with monthly-average
336 values up to 30 W m^{-2} in July and August, and maximum values up to 60 W m^{-2} (R. A. Kr-
337 ishfield & Perovich, 2005; G. Maykut & McPhee, 1995; Wettlaufer, 1991). In these re-
338 gions, summer solar heating of the surface ocean layer (in ice-free regions or through thin
339 ice) provides the main heat source for ocean-to-ice heat fluxes (Fer, 2009; G. Maykut &
340 McPhee, 1995; G. A. Maykut & Untersteiner, 1971; Timmermans, 2015; J. M. Toole et
341 al., 2010).

342 A well-defined double-diffusive staircase is absent around most Arctic Ocean con-
343 tinental shelf-slope regions (i.e., coinciding with pathways of the Atlantic Water) (Shi-
344 bley et al., 2017), likely because of higher mixing levels in those regions (e.g., Rippeth
345 et al., 2015). Staircases do appear at the eastern boundary of the Eurasian Basin and
346 in the vicinity of the east Siberian continental slope, where double-diffusive heat fluxes
347 are estimated to be higher (order 1 W m^{-2}) compared to interior basin values (Lenn et
348 al., 2009; I. V. Polyakov et al., 2012). Note that ocean-to-ice heat fluxes can be order
349 100 W m^{-2} where the Atlantic Water enters the Arctic Ocean and where stratification
350 and turbulence levels are not amenable to the formation of a double-diffusive staircase
351 (Peterson, Fer, McPhee, & Randelhoff, 2017).

352 Related to the double-diffusive staircase at the top boundary of the Atlantic Wa-
353 ter layer, are prominent thermohaline intrusions underlying the staircase and emanat-
354 ing from the core of the Atlantic Water (e.g., Bebieva & Timmermans, 2017; E. Carmack
355 et al., 1998; Rudels, Kuzmina, Schauer, Stipa, & Zhurbas, 2009). These intrusions have
356 a lateral component of motion, driven partly by double-diffusive vertical buoyancy flux
357 divergences, and carry warm Atlantic Water from the boundaries to the interior basins
358 (Bebieva & Timmermans, 2016; F. McLaughlin et al., 2004; Walsh & Carmack, 2003;
359 Woodgate, Aagaard, Swift, Smethie Jr, & Falkner, 2007). Walsh and Carmack (2003)

360 estimated lateral diffusivities associated with these thermohaline intrusions to be around
361 $50 \text{ m}^2 \text{ s}^{-1}$. In this way, diapycnal mixing can redistribute Atlantic Water heat laterally,
362 with Atlantic Water intrusions taking around a decade to propagate across the Canada
363 Basin (see for example Bebieva & Timmermans, 2019).

364 While diapycnal mixing of deeper ocean heat can delay the onset of freezing at the
365 start of the ice-growth season, and yield reductions in total sea-ice thickness (e.g., G. A. Maykut
366 & Untersteiner, 1971; D. K. Perovich et al., 2011; Steele, Ermold, & Zhang, 2008; Tim-
367 mermans, 2015), its role in the large-scale ocean circulation is less clear. Diapycnal mix-
368 ing has been presumed to play a role in driving the Atlantic Water inflow to the Arc-
369 tic Ocean, as we will discuss in Section 5.1. Lateral eddy fluxes, on the other hand, have
370 been shown to be a key player in the fundamental dynamics of the Beaufort Gyre, as we
371 discuss in Section 7.

372 **4.2 Eddies, baroclinic instability and isopycnal eddy diffusivity**

373 Baroclinic eddies are a ubiquitous feature of the Arctic Ocean, which is observed
374 to have a vigorous mesoscale and submesoscale eddy field (e.g., Carpenter & Timmer-
375 mans, 2012; Kozlov, Artamonova, Manucharyan, & Kubryakov, 2019; Manley & Hunk-
376 ins, 1985; G. E. Manucharyan, Thompson, & Spall, 2017; Mensa, Timmermans, Kozlov,
377 Williams, & Özgökmen, 2018; Pnyushkov, Polyakov, Padman, & Nguyen, 2018; Spall,
378 Pickart, Fratantoni, & Plueddemann, 2008; Timmermans, Toole, Proshutinsky, Krish-
379 field, & Plueddemann, 2008; M. Zhao et al., 2014; M. Zhao, Timmermans, Cole, Krish-
380 field, & Toole, 2016). Water column kinetic energy in the Arctic’s halocline is dominated
381 by eddies (M. Zhao, Timmermans, Krishfield, & Manucharyan, 2018), and we expect eddy
382 buoyancy fluxes and along-isopycnal stirring by eddies to play an important role in the
383 general circulation, as will be shown in Section 7.

384 The horizontal length scale that tends to characterize eddies and baroclinic insta-
385 bilities of the ocean mean state is the first baroclinic Rossby radius of deformation, $R_d =$
386 ND/f where D is the vertical scale over which horizontal currents vary, f is the Cori-
387 olis parameter, and $N^2(z) = -(g/\rho_0)(\partial\rho/\partial z)$ is the stratification. Chelton, Deszoeke,
388 Schlax, El Naggar, and Siwertz (1998) estimated R_d from hydrographic climatology by
389 solving the quasi-geostrophic equations for a given stratification profile, $N^2(z)$. In Fig-
390 ure 4a we follow the methodology of Chelton et al. (1998) to compute R_d from Arctic

391 Ocean climatology (see also Nurser and Bacon (2014); M. Zhao et al. (2014)). Shallow
 392 shelf regions are generally characterized by a much smaller deformation radius (of or-
 393 der a few kilometers) than the deep basins (where it is around 7 - 15 km), while vari-
 394 ations in R_d between deep basins arise due to stratification differences (see M. Zhao et
 395 al., 2014). The Beaufort Gyre is more strongly stratified than the Eurasian Basin wa-
 396 ter column; typical values of R_d in the Beaufort Gyre region are around 15 km, twice
 397 as large as values in the deep Eurasian Basin. Observed eddies have horizontal scales which
 398 are roughly consistent with values of R_d . Eddies in the Canadian Basin have larger di-
 399 ameters than those in the Eurasian Basin (M. Zhao et al., 2014). We note that the hor-
 400 izontal scales of the energy-containing eddies may differ from the deformation radius be-
 401 cause there is an inverse energy cascade. The upscale energy transfer on a β -plane may
 402 be arrested at the Rhines scale, which can characterize a transition to a Rossby wave regime
 403 (see Rhines (1975) and the discussion by, for example, Tulloch, Marshall, Hill, and Smith
 404 (2011)). In the Arctic Ocean, the Coriolis parameter f is approximately constant (i.e.,
 405 an f -plane), and the Rhines scale is set by topographic beta. Nevertheless, the scales
 406 apparent in Figure 4a highlight the challenges for numerical modeling of ocean processes
 407 in the region where model grid scales must be smaller than a few kilometers to resolve
 408 mesoscale eddies.

Related to the Rossby deformation radius, we may analyze hydrography to exam-
 ine the linear stability characteristics of the mean state of the Arctic Ocean. If the mean
 current has speed U , then we expect an inverse timescale (growth rate) $\omega \sim U/R_d$. This
 may be expressed in terms of the Richardson Number, $Ri = N^2 D^2 / U^2$, where D is the
 vertical scale over which U varies, as $\omega \sim f / \sqrt{Ri}$ (the Eady growth rate). More detailed
 calculations calibrated against linear stability yield (see Smith, 2007; Tulloch et al., 2011):

$$\omega = f \sqrt{\frac{1}{6H} \int_H^0 \frac{dz}{Ri(z)}}, \quad (1)$$

409 where the Richardson number $Ri(z)$ may be estimated as a function of the stratification
 410 and the thermal wind shear, $Ri = N^2 / [(\partial u / \partial z)^2 + (\partial v / \partial z)^2]$. Tulloch et al. (2011)
 411 examine hydrographic climatology for the global oceans south of 60°N and show that
 412 spatial patterns of growth rates and their magnitudes estimated from (1) are in reason-
 413 able correspondence to growth rates computed from the full stability analysis.

414 If the generation of eddies is associated with baroclinic instability, we expect the
 415 Eady timescale ω^{-1} to be short where there is anomalously high eddy kinetic energy and/or

416 weak stratification. Around the Arctic basin margins, timescales are of the order of two
417 weeks or shorter, while in the central Canada Basin/Beaufort Gyre and Nordic Seas re-
418 gions, Eady timescales computed from (1) are between a few weeks and a couple of months
419 (Figure 4b). This spatial pattern is consistent with satellite-derived eddy kinetic energy
420 estimates, which show the shelf and boundary-current regions to have higher eddy ki-
421 netic energy compared to the interior Canada Basin and Nordic Seas (Armitage et al.,
422 2017). Notably, the central Eurasian Basin exhibits shorter timescales (faster growth rates)
423 than the Canada Basin, and this may be attributed to the significantly weaker strati-
424 fication there (Figure 3b); satellite-derived estimates of eddy kinetic energy are not avail-
425 able for the Eurasian Basin. In interpreting the Eady growth-rate map (Figure 4b), it
426 should be noted that the presence of sea ice is likely to efficiently damp unstable near-
427 surface baroclinic instabilities, but that the interior halocline modes are less suscepti-
428 ble because they do not have a strong surface expression. Early studies of baroclinic in-
429 stability in the Arctic, interpreting observations of mesoscale eddies, argued that fric-
430 tional drag against sea ice was a significant stabilizing influence (e.g., Hunkins, 1974; Man-
431 ley & Hunkins, 1985).

432 M. Zhao et al. (2018) show how the specific halocline structure of the Beaufort Gyre
433 influences the evolution of water-column kinetic energy, and its dissipation. They an-
434 alyze mooring velocity measurements to deduce that most kinetic energy in the Beau-
435 fort Gyre water column is contained within the barotropic and the first two baroclinic
436 modes, and that this partitioning is a result of the specific halocline stratification which
437 determines interactions between modes. M. Zhao et al. (2018) find energy has a tendency
438 to concentrate in the second baroclinic mode (consistent with ubiquitous intrahalocline
439 eddies), with a much smaller tendency to transfer to the barotropic mode. Ultimately
440 kinetic energy may be dissipated by drag at the sea floor or under sea-ice cover. How-
441 ever, the inefficiency of energy transfer to the barotropic mode suggests an ineffective
442 pathway for kinetic energy dissipation at the sea floor, and an important role for under-
443 ice dissipation when kinetic energy is transferred to the (surface intensified) first baro-
444 clinic mode.

445 For the Beaufort Gyre, satellite-based estimates of eddy kinetic energy, and the ap-
446 plication of mixing-length theory, have been used to infer eddy diffusivities (Armitage
447 et al., 2017). A similar approach has been used to estimate eddy diffusivities in the Beau-
448 fort Gyre from eddy kinetic energy based on in-situ mooring velocity measurements (Meneghello,

449 Marshall, Cole, & Timmermans, 2017). These studies yield eddy diffusivity values in the
450 range $100\text{-}600\text{ m}^2\text{ s}^{-1}$, decaying from higher to lower values with depth (Meneghello et
451 al., 2017). As described in Section 7, eddy diffusivities of such magnitude suggest that
452 eddy-induced circulation can be as large as the Eulerian circulation, with important im-
453 plications for the general circulation and tracer transport in the Arctic.

454 Water-mass distribution, stratification structure and strength, mixing and lateral
455 eddy processes, are intimately connected with ocean circulation pathways, which we de-
456 scribe next, beginning with an analysis of the circulation of Atlantic Water into and around
457 the Arctic basin.

458 **5 The Circulation of Atlantic Water in the Arctic**

459 On route to the Arctic Ocean, Atlantic waters cross the Scotland-Greenland Ridge
460 and propagate into the Nordic Seas in branches stemming from the North Atlantic Cur-
461 rent extension of the Gulf Stream. In the Norwegian Sea, the northward flow follows two
462 topographically steered western and eastern branches of the Norwegian Atlantic Cur-
463 rent (e.g., Orvik & Niiler, 2002). These waters enter the Arctic Ocean at the $\sim 2600\text{ m}$
464 deep, $\sim 450\text{ km}$ wide, Fram Strait, which is the deepest connection between the Nordic
465 Seas and the Arctic Ocean (Figure 5). At Fram Strait there is an exchange flow between
466 inflowing Atlantic Water and outflowing relatively cooler and fresher upper Arctic Ocean
467 waters (Figure 5c). The West Spitsbergen Current (WSC) carries relatively warm and
468 salty Atlantic Water north (around 7 Sv) into the Arctic Ocean on the eastern side of
469 Fram Strait, with a recirculation within Fram Strait (see e.g., Beszczynska-Möller et al.,
470 2012; Schauer et al., 2004). The East Greenland Current (EGC) flows south (around 9 Sv)
471 out of the Arctic Ocean along the western side of Fram Strait (de Steur, Hansen, Mau-
472 ritzen, Beszczynska-Möller, & Fahrbach, 2014). Net transport through Fram Strait has
473 been estimated to be several Sv to the south, with month-to-month variability that can
474 be as large (Schauer & Beszczynska-Möller, 2009). Atlantic Water also enters the Arc-
475 tic Ocean from the Nordic Seas via the Barents Sea Opening ($\sim 2\text{ Sv}$) (Ingvaldsen et
476 al., 2002; Schauer, Loeng, Rudels, Ozhigin, & Dieck, 2002). Observations indicate that
477 Atlantic Water heat transport to the Arctic Ocean is higher through the Barents Sea Open-
478 ing ($\sim 70\text{ TW}$, Smedsrud et al. (2013)) than through Fram Strait ($\sim 40\text{ TW}$, Schauer and
479 Beszczynska-Möller (2009), where these estimates use 0°C as a reference temperature).

480 Where Atlantic Water enters the Arctic Ocean through Fram Strait and the Bar-
481 ents Sea Opening, the overlying sea ice melts and the upper-most waters undergo a cool-
482 ing and freshening transformation such that the Atlantic Water temperature maximum
483 resides at depth within the Arctic Ocean (e.g., Rudels, Anderson, & Jones, 1996; Un-
484 tersteiner, 1988). The spatial distribution of maximum Atlantic Water temperature has
485 been used to infer its cyclonic pathway around the boundary of the Eurasian Basin (e.g.,
486 L. Coachman & Barnes, 1963) and is shown in Figure 5a,b,d. There is believed to be a
487 recirculation within the Eurasian Basin, as schematized by Rudels, Jones, Anderson, and
488 Kattner (1994), see their Figure 9. Atlantic Water penetrates the Makarov and Canada
489 basins (where the Atlantic Water core referenced by the depth of the temperature max-
490 imum is located around 400 m depth, Figure 5d) and circulates cyclonically around the
491 basin margins, visibly following isobaths. Mooring measurements indicate Atlantic Wa-
492 ter boundary current speeds to be around 2 to 4 cm s⁻¹ (Woodgate et al., 2001). This
493 is consistent with transient tracer data which suggest Atlantic Water propagation from
494 the Eurasian Basin to the southern Canada Basin (a distance of around 6000 km) takes
495 around 7.5 years (Mauldin et al., 2010).

496 Below the Atlantic Water layer, the Arctic Ocean’s deep and bottom waters are
497 generally inferred (from sparse measurements) to follow a cyclonic pathway in both the
498 Eurasian and Canadian basins, in the same sense as the intermediate Atlantic Water (e.g.
499 Aagaard, 1981; Rudels, 2015). Deepest waters also exhibit variable bottom-trapped cur-
500 rents and waves (Aagaard, 1981; Timmermans, Rainville, Thomas, & Proshutinsky, 2010;
501 B. Zhao & Timmermans, 2018). Note that, distinct from the Atlantic Water boundary
502 current, there also exist narrow, energetic, seasonally-varying boundary currents, with
503 typical speeds around 15 cm s⁻¹, trapped at the shelf breaks in the Eurasian and Cana-
504 dian basins (e.g., Aksenov et al., 2011; Dmitrenko et al., 2016; Nikolopoulos et al., 2009;
505 Pickart, 2004); the properties of these shelf-break currents depend strongly on local and
506 remote winds and buoyancy forcing.

507 Ascertaining what drives the Atlantic Water inflow and its circulation within the
508 Arctic Ocean has been the subject of study since Nansen (1902) first identified warm sub-
509 surface water within the Arctic Ocean as having originated in the North Atlantic. We
510 now briefly review two bodies of work that explore the mechanisms from rather differ-
511 ent perspectives: the first, using an estuary framework, invokes wind-driven mixing in-

terior to the Arctic to draw water in; the second invokes winds exterior to the Arctic to
drive water in to the Arctic following bathymetric contours.

5.1 An estuary framework

The earliest models of Arctic Ocean circulation were *estuarine-like* (see e.g., Aagaard, Swift, & Carmack, 1985), motivated by the idea that the Arctic is a semi-enclosed basin in which the inflow from the Nordic Seas is balanced by an outflow of relatively fresh water, and this exchange flux depends upon the level of mixing within the Arctic basin (Figure 6). The circulation is driven by buoyancy; winds only play a role in mixing upper and intermediate waters in the estuary basin.

Stigebrandt (1981) modeled the upper Arctic Ocean water column as a function of buoyancy input, wind-driven mixing and topographic control at the connecting straits (here, primarily Fram Strait and Lancaster Sound) that are sufficiently wide that the effects of Earth’s rotation are important. His model couples conservation of volume and salt, and a weir formula for the hydraulically-controlled (and rotationally-influenced) volume flow through the straits, plus a horizontally uniform vertical entrainment velocity that is a function of both wind-driven mixing and convection. This estuarine description of the circulation shows how the buoyancy input and mixing in the interior Arctic Ocean can uphold a steady exchange flow between the Arctic Ocean and Nordic Seas.

Consider an idealized system in which there is a volume flux Q_1 of Polar Water (upper layer of salinity S_1) leaving the Arctic Ocean (e.g., via Fram Strait) and a volume flux Q_2 of Atlantic Water (lower layer, of salinity S_2) entering the Arctic Ocean from the Nordic Seas (Figure 6). For a flux through the Bering Strait of Q_B (of salinity S_B) and net freshwater flux Q_f (approximately the sum of river influxes and net precipitation, minus a sea-ice export flux from the Arctic Ocean) into the upper layer in the Arctic Ocean, conservation of volume may be written

$$Q_1 = Q_2 + Q_B + Q_f. \quad (2)$$

For a hydraulically controlled flow of the upper layer (of thickness H_1) through Fram Strait, the flow rate is given by (Whitehead, 1998)

$$Q_1 = \frac{g' H_1^2}{2f}, \quad (3)$$

where $g' = g(\rho_2 - \rho_1)/\rho_0$ is the reduced gravity between the Polar Water ρ_1 and Atlantic Water ρ_2 layers (ρ_0 is a reference density). A good approximation is given by $g' = g\beta(S_2 - S_1)$, which neglects temperature influences on density. Equation (3) applies because Fram Strait (around 500 km wide) is much wider than the internal Rossby deformation radius, with typical parameter values yielding $(2g'H_1)^{1/2}/f \approx 10$ km, in accord with Figure 4a. Conservation of salt in the upper layer is given by

$$Q_1 S_1 = Q_2 S_2 + Q_B S_B. \quad (4)$$

The remaining model component is an entrainment flux of lower layer water across the halocline (Figure 6) which may be written in terms of the area A of the halocline and an entrainment velocity w_e as:

$$Q_2 = w_e A. \quad (5)$$

Specification of w_e requires some quantification of the mixing processes. Mixing between the Atlantic Water and the Polar Water may be driven by processes ranging from double-diffusive convection to shear-driven mixing by winds and sea-ice motion, to surface buoyancy fluxes driving convection, such as sea-ice growth generating dense brine. Stigebrandt (1981) formulates the following expression for entrainment velocity

$$w_e = \frac{2.5u_*^3}{g\beta(S_2 - S_1)H_1} + \gamma \frac{Q_f S_1}{A(S_2 - S_1)}. \quad (6)$$

530 The first term on the right relates the injection of kinetic energy to the interface to a change
 531 of potential energy of the system (mixing), where u_* is a friction velocity characteriz-
 532 ing the mixing levels. The second term quantifies the contribution (scaled by a param-
 533 eter γ) to w_e by surface freshwater buoyancy fluxes.

534 Choosing typical values of external parameters ($A = 10^{13}$ m², $Q_B = 1.5 \times 10^6$ m³ s⁻¹,
 535 $S_B = 32.4$, $\gamma = 0.05$ and $S_2 = 35$; see Stigebrandt (1981)), the system (2) to (6) may
 536 be solved to determine the Atlantic Water influx Q_2 , and the properties of the upper layer
 537 H_1 and S_1 exiting the Arctic Ocean through Fram Strait as functions of net freshwater
 538 input Q_f and mixing levels (quantified by specifying u_*), Figure 6b. For larger net fresh-
 539 water fluxes Q_f into the Arctic Ocean (i.e., river influxes and net precipitation domi-
 540 nate over a sea-ice export flux), the outflowing upper layer is thinner and fresher, and
 541 there is a smaller Atlantic Water volume influx Q_2 to the Arctic Ocean. Further, for fixed
 542 Q_f , an increase in mixing gives rise to a thicker, saltier upper layer exiting the Arctic
 543 Ocean, and a larger volume influx of Atlantic Water. For a range of appropriate param-
 544 eters, the solutions generally yield plausible results for the exchange flow at Fram Strait.

545 Rudels (1989) employs the formalism of Stigebrandt (1981) and incorporates spatially-
546 variable mixing (water-mass transformations in the shelf regions) to deduce a magnitude
547 for the Atlantic Water inflow to the Arctic Ocean and strength of the stratification that
548 depends on the buoyancy input.

549 These general ideas have been extended further by considering the Arctic Mediter-
550 ranean to be a double-estuary (Eldevik & Nilsen, 2013; Lambert, Eldevik, & Haugan,
551 2016). This conceptualizes cooling and dense water formation in the Nordic Seas as a
552 negative estuary, and positive buoyancy forcing (freshwater input) in the Arctic Ocean
553 (i.e., a positive estuary). Heat loss in the Nordic Seas drives an overturning circulation
554 there (Mauritzen, 1996) while the freshwater input to the north drives an estuarine cir-
555 culation with the Atlantic Water layer. Lambert et al. (2016) find that because of the
556 Arctic estuary circulation, an Atlantic Water inflow to the Arctic can persist even in the
557 absence of deep convection in the Nordic Seas. This is an important point in the con-
558 text of discussions related to Atlantic Water heat entering the Arctic being influenced
559 by the strength of the Atlantic Meridional Overturning Circulation (AMOC). Based on
560 climate model simulations, it has been put forward, for example, that a strengthened AMOC
561 has been partly responsible for Arctic Ocean warming and sea-ice loss (e.g., Delworth
562 et al., 2016).

563 The estuary view of Arctic circulation has been invoked in an attempt to explain
564 the presence of the halocline. Indeed, it is in accord with the traditional model of the
565 Arctic halocline (Aagaard et al., 1985): the required mixing within the Arctic basin (rep-
566 resented by the upward circular arrows in Figure 6a) has been associated with the en-
567 trainment of ambient water by plumes that flow down continental slopes powered by con-
568 centrations of dense brine formed by ice formation over the continental shelves, although
569 the extent to which this is relevant on an Arctic-wide scale has been debated, (e.g., Östlund,
570 Possnert, & Swift, 1987). The structure of the interior Arctic halocline, however, requires
571 additional processes, such as advection by wind-driven circulation and lateral eddy fluxes,
572 to bring the ventilating dense water away from continental slopes and into the interior.
573 Spall (2013) presents a conceptual model in which the halocline structure and Atlantic
574 Water flow are set by the combined effects of horizontal eddy fluxes taking water from
575 the basin boundaries to the interior and vertical diapycnal mixing in the interior basin.
576 In his idealized simulations, an effectively barotropic Atlantic Water inflow (and cyclonic
577 Atlantic Water boundary current) is balanced by outflowing cooler water including a surface-

578 intensified fresh outflow. The essential common feature between this and other models
579 of the Arctic estuary is that buoyancy forcing and mixing in the interior drives the Arctic-
580 Nordic Seas exchange.

581 Bathymetric influences (aside from those of the straits) and recirculations within
582 the Arctic basin are not represented in estuary models. Nor do they account for recir-
583 culations in the vicinity of the connecting straits. Further, it is unclear whether the re-
584 quired mixing between the surface fresh layers and the inflowing Atlantic Water is re-
585 alistic. In an alternative framework, the wind directly drives the topography-following
586 Atlantic Water circulation. In the next section, we describe studies which have shown
587 how the prevailing wind field over the Arctic is such that the wind-stress curl can set the
588 observed ocean transport.

589 **5.2 Wind-driven flow along f/H contours**

590 Wind-stress curl patterns over the Arctic are such that there is broad Ekman down-
591 welling over much of the interior basin, with relatively strong upwelling over the Nordic
592 Seas (Figures 2c and Figure 7a). Over most of the tropical and subtropical oceans, wind-
593 stress curl is balanced by the depth-integrated meridional transport, i.e., Sverdrup bal-
594 ance (e.g., Gray & Riser, 2014; Wunsch, 2011). However, where topography has a strong
595 influence, and in the higher latitudes where the β -effect (here, β refers to the meridional
596 gradient of the Coriolis parameter) is negligible, Sverdrup balance does not hold. Nøst
597 and Isachsen (2003) analyzed Arctic wind forcing and hydrographic climatology to show
598 that patterns of Ekman downwelling and upwelling differ markedly from the depth-integrated
599 meridional transport predicted based on Sverdrup balance. Instead of being constrained
600 by the β -effect, the potential vorticity-conserving barotropic flow is controlled by sea-
601 floor topography.

602 In the Nordic Seas and Arctic Ocean potential vorticity contours $q = f/H$ (where
603 H is water depth) effectively coincide with isobaths because f is approximately constant.
604 These f/H contours (Figure 7a) can be seen to close within basins (rather than being
605 blocked by isobaths as typical of midlatitude ocean basins), and potential vorticity gra-
606 dients (directed across isolines of f/H) are dominated by topographic slopes. One might
607 expect that depth-integrated flow would have a proclivity to conserve q and thus follow
608 bathymetry. This is schematized in Figure 8; idealized closed f/H contours (black) lie

609 either entirely within the Arctic basins, or enclose both the Nordic Seas and the Arc-
610 tic Ocean. These are the ‘railway tracks’ along which the barotropic flow circulates, as
611 indicated by the arrows in Figure 8. The sense of the flow along f/H contours depends
612 on the sign of the vorticity input, set by the wind-stress curl integrated over the area within
613 the q contour in question. (By Stokes’ Theorem, this is equivalent to the integral of the
614 wind stress around the closed contour.)

615 Isachsen, LaCasce, Mauritzen, and Häkkinen (2003) exploited this idea to describe
616 the time-varying depth-averaged Arctic Ocean and Nordic Seas circulation. They inte-
617 grated the governing vorticity equation over an area bounded by a closed f/H contour
618 and showed that the flow in the bounded region co-varies with the difference between
619 transport in the wind-driven surface Ekman layer and the bottom Ekman layer. This
620 is the barotropic mode excited by time-varying winds. It is a solution that is close to a
621 free mode, where the free mode is one that is exactly along f/H contours; in the absence
622 of wind forcing, the f/H following flow will continue, ultimately spinning down as a re-
623 sult of bottom friction (see Hughes, Meredith, & Heywood, 1999; LaCasce, Nøst, & Isach-
624 sen, 2008).

Nøst and Isachsen (2003) developed a related model for the local flow using an in-
integrated vorticity balance in an area surrounded by an f/H contour, but for the time-
mean bottom velocities of the Arctic Ocean and Nordic Seas. The steady-state balance
between vorticity input and output is given by

$$\iint_A \nabla \times \boldsymbol{\tau}_s dA = \oint_C \boldsymbol{\tau}_b \cdot d\mathbf{l}, \quad (7)$$

where $\boldsymbol{\tau}_s$ is the surface stress and $\boldsymbol{\tau}_b$ the bottom stress. This states that the surface vor-
ticity input by the wind within q surfaces is balanced by bottom stress integrated around
closed q contours. Relating the bottom stress to bottom velocity \mathbf{v}_b through a linear drag
law, $\boldsymbol{\tau}_b = -\rho_0 \mu \mathbf{v}_b$ (where μ is a linear friction parameter), (7) can be rearranged as

$$\mathbf{v}_b \approx -\frac{1}{\rho_0 \mu L} \iint_A \nabla \times \boldsymbol{\tau}_s dA \frac{|\nabla q|}{\frac{1}{L} \oint_C |\nabla q| dl}. \quad (8)$$

625 This says that the flow at any location along an f/H contour can be estimated as the
626 product of the surface wind-stress curl $\nabla \times \boldsymbol{\tau}_s$ integrated over the area within the con-
627 tour, divided by the length L of the $q = f/H$ contour, and the magnitude of the lo-
628 cal slope relative to the average slope of the f/H contour. That is, the magnitude of the
629 cross-stream vorticity gradient, $|\nabla q|$, modulates the strength of the bottom current by

630 a factor $|\nabla q| / (\frac{1}{L} \oint_C |\nabla q| dl)$. Nøst and Isachsen (2003) show that (8) gives reasonable
631 agreement with current-meter measurements of the bottom flow in the Arctic Ocean. Sur-
632 face flows may then be computed from the bottom-velocity prediction (equation 8) us-
633 ing climatological hydrographic data to obtain thermal wind shear from the bottom to
634 the surface. Note, however, that the presence of sea ice is not accounted for in estimates
635 of surface-ocean stresses although in Section 7 we return to the role of sea ice as a con-
636 trol on ocean dynamics.

637 Considering each of the closed f/H contours plotted in Figure 7a, we compute the
638 total area-integrated wind-stress curl within each contour (divided by the length of the
639 contour), and plot it as a function of area enclosed by the contour (Figure 7, where the
640 plotted points are colored by the depth of the f/H contour in question; see also Figure
641 13 of Nøst and Isachsen (2003)). The area-integrated wind forcing for f/H contours that
642 enclose both the Nordic Seas and the entire Arctic Basin is cyclonic: comprised of con-
643 tributions of strong cyclonic forcing in the Nordic Seas, and relatively weak anticyclonic
644 wind forcing in the Canadian Basin. In this sense, the cyclonic Atlantic Water bound-
645 ary current in the Canadian Basin is driven by the cyclonic atmospheric forcing in the
646 Nordic Seas. This is the concept that flow following f/H contours is driven by *remote*
647 wind stresses (outside the Arctic Ocean), while the balancing bottom drag is distributed
648 throughout the Arctic basin. The concept is consistent with a recent climate model study
649 that suggests intensified Atlantic Water inflow to the Nordic Seas and Arctic Ocean is
650 related to a strengthening of the Icelandic Low (Årthun, Eldevik, & Smedsrud, 2019).

651 The interior anticyclonic flow in the Canada Basin (i.e., the Beaufort Gyre), around
652 closed f/H contours entirely within the Canada Basin, is then also explained by the area-
653 integrated anticyclonic wind forcing for closed contours in that region (Figure 7a,b). We
654 note that these ideas are distinct from others that are based on an integral constraint
655 of potential vorticity (e.g., Karcher, Kauker, Gerdes, Hunke, & Zhang, 2007; Yang, 2005),
656 where if the net potential vorticity introduced to the Arctic basin via the strait inflows
657 is positive (negative), the result is an interior cyclonic (anticyclonic) circulation; further,
658 large buoyancy fluxes in the Barents Sea are an important source of potential vorticity.

5.2.1 Eddy influences

So far, we have only discussed a model in which energy dissipation is confined to the bottom boundary layer. Lateral eddy momentum fluxes, eddy-topography interactions and diapycnal fluxes have been neglected. It has been shown, for example, that lateral eddy momentum fluxes may be at least as important as bottom friction in balancing surface forcing (Dewar, 1998), much as synoptic eddy momentum fluxes maintain the surface wind patterns in the atmosphere.

Dewar (1998) presents an analytical layered model of abyssal flow in the Atlantic (invoking area integration around closed f/H contours) in which eddy fluxes arising from baroclinic instability are parameterized as down-gradient potential vorticity diffusion (see Marshall, Jamous, & Nilsson, 2001), a generalization of thickness diffusion. Applied to a 2-layer model forced by anticyclonic winds, wind-driven Ekman pumping in the upper layer deepens the layer which is balanced by a divergent eddy mass flux in that layer. In the deep layer, eddies mix thickness gradients with outward mass fluxes over a bowl-shaped basin, and inward mass fluxes over a seamount (assuming the tilt of the isopycnal interface between the two layers remains small compared to the topographic slope). These must be balanced by fluxes in the opposite sense in the bottom boundary; inward mass flux in the bottom boundary gives rise to a mean flow that tends to be cyclonic in the bowl case, and vice versa. In this way, a gyre can be set up in the deep layer, which is cyclonic around closed f/H contours in a deep basin and anticyclonic over a seamount, i.e., the direction of circulation in the deep layer depends on the bathymetry rather than the sign of the wind-curl forcing.

The applicability of this description to the Arctic's Atlantic Water circulation is unclear. The formalism would predict a cyclonic circulation in the deep Beaufort Gyre, whereas observations indicate that the deep flow is in the same direction (i.e., anticyclonic) as the upper-ocean circulation (e.g., Dosser & Timmermans, 2018). Furthermore, in the two-layer model within a bowl-shaped basin described above, a reversal with depth of the horizontal potential vorticity gradients is absent, yet is a necessary condition for baroclinic instability.

Lastly, with respect to eddy influences, it has been shown that accounting for eddy interactions with seafloor topography can give rise to a mean cyclonic circulation along f/H contours in a deep basin, a result referred to as the *Neptune Effect* (Holloway, 1992,

691 2004). (see also Bretherton & Haidvogel, 1976, who describe how eddies can force a cir-
692 culation along f/H contours). The circulation results from the stress generated by eddy
693 pressure anomalies correlated with seafloor slope. This effect is likely to influence prop-
694 agation speeds and diffusion of the cyclonic Atlantic Water flow. For example, includ-
695 ing a parameterization of the Neptune Effect in an ocean model yields an Arctic Ocean
696 flow field that is more consistent with that inferred from tracer observations; the over-
697 all cyclonic flow is enhanced around individual basins, most intense over topographic bound-
698 aries (Nazarenko, Holloway, & Tausnev, 1998; I. Polyakov, 2001).

699 **5.3 Estuary vs. f/H -following perspectives**

700 We have analyzed the processes driving the circulation of Atlantic Water into and
701 around the Arctic Ocean basin. Both the estuary model invoking diabatic processes, and
702 the f/H -following wind-driven model that invokes dynamical forcing by the winds, pro-
703 vide important perspectives. Diabatic processes must play an essential role because At-
704 lantic Water flowing in to the Arctic has its properties changed as it circuits the basin.
705 Similarly, fresh water input to the Arctic Ocean is modified before it leaves the Arctic
706 Ocean. Surface buoyancy forcing, a range of mixing mechanisms and eddy stirring all
707 play a role. Furthermore, winds through cyclonic curl forcing over the Nordic seas set
708 the sense of circulation around f/H contours and orchestrate the gateway into the Ar-
709 ctic. Both wind- and buoyancy-driven processes work together to facilitate Atlantic Wa-
710 ter inflow and circulation around the Arctic, processes that do not depend on the strength
711 and structure of the AMOC. It remains unclear how this concept relates to modeling stud-
712 ies. Delworth et al. (2016) examine climate model output to deduce a positive relation-
713 ship between AMOC strength and ocean heat transport into the Barents Sea, where they
714 attribute AMOC fluctuations to changes in the North Atlantic Oscillation. Other cli-
715 mate model studies find this same result for internal climate variability, but suggest the
716 opposite result under climate change (greenhouse gas forcing): ocean heat transport to
717 the Nordic Seas and Arctic increases at the same time as the AMOC weakens (Årthun
718 et al., 2019; Oldenburg, Armour, Thompson, & Bitz, 2018). No doubt feedbacks on the
719 regional atmospheric circulation (e.g., the Icelandic Low) are also important.

720 Co-existing with the arterial Atlantic Water flow are relatively cold, fresh, wind-
721 driven surface-intensified patterns in the interior Arctic basins: the Transpolar Drift Stream
722 and the Beaufort Gyre. In the model of Nøst and Isachsen (2003), the prevailing anti-

723 cyclonic winds set up the anticyclonic Beaufort Gyre circulation in the Canadian Basin
724 (see magenta contours in Figure 7a), and bottom friction provides the balance to the wind-
725 stress curl. The role of bottom friction and topographic influences on the Beaufort Gyre
726 (which can at times be centered over the Canada Basin’s abyssal plain) and Transpo-
727 lar Drift Stream dynamics are less obvious; the circulation is surface intensified in these
728 strongly-stratified, wind-driven systems. We now outline some of the essential features
729 of the Transpolar Drift Stream, before moving on in Section 7 to review the present state
730 of understanding of Beaufort Gyre dynamics.

731 **6 The Transpolar Drift Stream**

732 The Transpolar Drift Stream of ice and water flows from the Siberian Shelf towards
733 Greenland and the Nordic Seas, as is evident in the wind and sea-ice fields shown in Fig-
734 ures 2a and c. Many studies have addressed the sea-ice drift component of the Trans-
735 polar Drift Stream, readily monitored by remote sensing and drift of floe-tracking buoys
736 (e.g. Kwok, 2009; Rigor, Wallace, & Colony, 2002; M. C. Serreze, McLaren, & Barry, 1989).
737 The strength and orientation of the Transpolar Drift Stream is associated with the rel-
738 ative domains and intensity of the Beaufort High and Icelandic Low pressure systems.
739 During conditions of a weakened Beaufort High, and deepened Icelandic Low, ice drifts
740 cyclonically in the Eurasian Basin, transiting from the Laptev Sea towards the Cana-
741 dian Basin before drifting towards Fram Strait (Kwok, Spreen, & Pang, 2013). A stronger
742 Beaufort High, characterized by an expanded anticyclonic circulation, and a weaker Ice-
743 landic Low, are associated with a more direct path from the Laptev Sea to Fram Strait
744 of ice drift in the Transpolar Drift Stream (e.g., Kwok et al., 2013).

745 The geostrophic ocean flow is aligned with the sea-ice Transpolar Drift Stream in
746 the vicinity of the front between relatively warm and fresh surface waters, associated with
747 the northern extent of the Beaufort Gyre, and colder, saltier surface waters that com-
748 prise the Transpolar Drift Stream (see Figure 3a, the confluence of contours at the north-
749 ern boundary of the Beaufort Gyre, and aligned with the Transpolar Drift Stream) (Mori-
750 son, Steele, & Andersen, 1998; Morison, Steele, Kikuchi, Falkner, & Smethie, 2006; Steele
751 et al., 2004). This surface front also bounds the northern extent of Pacific Water influ-
752 ence in the upper halocline (F. McLaughlin, Carmack, Macdonald, & Bishop, 1996; Mori-
753 son et al., 1998), and is a region of water mass exchange owing to frontal baroclinic in-
754 stability (Timmermans, Toole, Proshutinsky, et al., 2008). Currents in the upper 20 m

755 of the water column are around 6 - 10 cm s⁻¹ (e.g., Armitage et al., 2017), suggesting
756 the transport of water from the Siberian shelf to Fram Strait takes approximately one
757 year.

758 The position of the Atlantic-Pacific boundary has been observed to be in the vicin-
759 ity of the Lomonosov Ridge to as far south as the Mendeleyev Ridge separating the Canada
760 and Makarov basins (Boyd, Steele, Muench, & Gunn, 2002; Morison et al., 1998; Steele
761 & Boyd, 1998). Positional changes have been attributed to changes in large-scale wind
762 forcing patterns which re-direct freshwater inputs from Siberian rivers and shift the axis
763 of the Transpolar Drift Stream (Boyd et al., 2002; Morison et al., 1998; Steele & Boyd,
764 1998; Timmermans et al., 2011); the shift is schematized in Figure 4 of Morison et al.
765 (2012). Further complicating this general picture and the spatial distribution of surface
766 freshwater and circulation patterns may be the fact that a weakened Beaufort Gyre al-
767 lows for fresh water release (Timmermans et al., 2011). This is explored further in Sec-
768 tion 8.

769 Timescales of ocean baroclinic adjustment to atmospheric forcing changes over the
770 central Arctic are uncertain. Morison et al. (2006) consider atmospheric forcing in con-
771 text with annual hydrographic measurements in the central Arctic Ocean to infer the
772 timescale of the response of the upper ocean to large-scale atmospheric circulation changes
773 is around 3 to 7 years. These adjustment timescales are influenced by processes balanc-
774 ing momentum input by the winds, mediated by sea-ice cover. We describe these pro-
775 cesses as they control Beaufort Gyre dynamics in the next section.

776 **7 The Beaufort Gyre**

777 The anticyclonic Beaufort Gyre, with a diameter around 800 km, dominates the Cana-
778 dian Basin circulation. It is characterized by typical speeds in the upper water column
779 of several cm/s (McPhee, 2013; M. Zhao et al., 2018); water parcels at the gyre periph-
780 ery take roughly 2 years to complete a revolution. The Beaufort Gyre has been much
781 more intensively studied than the Transpolar Drift Stream, in part because it is the largest
782 reservoir of fresh water in the Arctic Ocean (e.g., L. K. Coachman, 1969; A. Proshutin-
783 sky, Dukhovskoy, Timmermans, Krishfield, & Bamber, 2015; A. Y. Proshutinsky & John-
784 son, 1997; Worthington, 1953). The presence of upper-ocean fresh water allows for the
785 persistence of sea ice because the associated stratification acts as a barrier to upward heat

786 transport (e.g., Aagaard, Coachman, & Carmack, 1981). Further, the release of Beau-
787 fort Gyre fresh water may affect climate dynamics in the North Atlantic by changing the
788 stratification there (e.g., Belkin, Levitus, Antonov, & Malmberg, 1998). Mixed-layer salin-
789 ities are freshest in the Beaufort Gyre center, the result of surface Ekman convergence
790 of fresh water deriving from river discharge, net precipitation and sea-ice melt, and there
791 is a surface gradient towards higher salinities away from the center (Figure 2a). The Beau-
792 fort Gyre center (characterized by a maximum in sea-surface height and maximum depth
793 of halocline density surfaces, Figures 3, 9 and 10) generally coincides with the atmospheric
794 Beaufort High center and its intensity is associated with the strength of the wind-stress
795 curl, Figure 2c (e.g., Armitage et al., 2017; L. K. Coachman, 1969; A. Proshutinsky et
796 al., 2009; A. Y. Proshutinsky & Johnson, 1997).

797 Related to the accumulation and release of Beaufort Gyre fresh water, A. Y. Proshutin-
798 sky and Johnson (1997) put forward that there are two regimes of atmospheric circu-
799 lation over the Arctic Ocean – one in which the Beaufort High atmospheric pressure dom-
800 inates (an anticyclonic regime), and the other in which the Icelandic Low pressure sys-
801 tem is expanded and dominates (a cyclonic regime). These regimes shift from one to an-
802 other on a timescale of around 5 - 7 years, although the precise mechanism for this shift
803 is unclear (A. Proshutinsky et al., 2015). Observations and numerical experiments sug-
804 gest that during an anticyclonic regime, the Beaufort Gyre accumulates fresh water, and
805 during a cyclonic regime, it can be released to exit the Arctic Ocean into the North At-
806 lantic (A. Proshutinsky, Bourke, & McLaughlin, 2002). Only since the early 2000s have
807 we had sufficient year-round observations of the coupled atmosphere-ice-ocean system
808 to build up a deeper understanding of the relationships between atmospheric forcing and
809 Beaufort Gyre fresh water. For example, the accumulation of fresh water requires the
810 availability of fresh water (e.g., sea-ice melt water or river influxes) to coincide with at-
811 mospheric forcing that drives Ekman convergence in the surface ocean layer. A. e. a. Proshutin-
812 sky (2019) show that the dominant contributions to recent fresh water accumulation in
813 the Beaufort Gyre have been Pacific Water inflows through Bering Strait and fresh wa-
814 ter from the Mackenzie River; changes to either could yield changes in Beaufort Gyre
815 fresh water content even while the atmospheric forcing remains the same. We re-visit
816 changes in Beaufort Gyre fresh water in Section 8.

7.1 Potential vorticity and ventilation

The field of potential vorticity is useful for understanding the large-scale circulation of the Beaufort Gyre. Just as low Rossby number barotropic flow associated with the Atlantic Water is steered by f/H contours, the flow on density surfaces in the Beaufort Gyre's stratified halocline follows f/h contours where h is the vertical distance between two density surfaces whose density difference is $\delta\sigma$. We then define the potential vorticity $q = (\delta\sigma/\rho_0)(f/h)$. The possible geometry of q contours is shown schematically in Figure 8 (blue contours). A closed q contour suggests that water can circulate around the contour without having its potential vorticity reset. If, instead, q contours thread back to density outcrops at the surface, ventilation is possible in which fluid flow along these contours enters/exits the halocline from/to the surface mixed-layer. In this way, inspection of the field of potential vorticity allows one to distinguish between waters that are relatively isolated from the surface and those that are ventilated.

We select the layer defined by $\sigma = 25 - 27.4 \text{ kg m}^{-3}$ to represent the main halocline (Figure 3b,c). In the central basins its top surface is consistently below the mixed layer so that it is not subject to seasonally-varying surface buoyancy and wind forcing (Figure 9a). The layer is characterized by a potential vorticity minimum in the central Beaufort Gyre, and a potential vorticity maximum (higher stratification, a consequence of surface Ekman transport towards the Beaufort Gyre) approximately paralleling the Lomonosov Ridge at the front between Canadian and Eurasian Basin water, i.e., the Atlantic-Pacific boundary described in Section 6 (Figure 9b). The outcrop of the layer can be seen at the margins of the Beaufort Gyre, where there is a surface front between saltier Chukchi Sea water and relatively fresh Beaufort Gyre water (see Figure 2a), and in the Eurasian Basin. We see that q contours in the halocline layer thread to the outcrop in the Chukchi Sea indicating ventilation (Figure 9b). This supports the idea that the halocline layer is ventilated by waters whose temperature and salinity properties are set at the surface. Timmermans et al. (2014) and Timmermans, Marshall, Proshutinsky, and Scott (2017) argue that the Beaufort Gyre is ventilated by water that is transferred from the surface in the Chukchi Sea region down and laterally into the halocline by wind-driven Ekman pumping and the large-scale geostrophic circulation. The process is analogous to mid-latitude thermocline ventilation (e.g., Iselin, 1939; Luyten, Pedlosky, & Stommel, 1983; H. M. Stommel, 1979). In this way Pacific Water is swept into the Beaufort Gyre such

849 that it penetrates and ventilates the entire interior Canada Basin halocline where Pa-
850 cific Water layers reside beneath the surface mixed layer (see Timmermans et al., 2014).

851 We note here that, prior to Pacific Water ventilation of the interior Canada Basin
852 halocline, Pacific Water inflows en route to the northern Chukchi Sea/Canada Basin shelf
853 slope are observed to follow a circuitous and highly temporally-variable pathway, strongly
854 influenced by regional wind forcing and modified by intense local buoyancy forcing (see
855 e.g., Pickart et al., 2019; Weingartner et al., 2005). A major portion of Pacific Water that
856 enters through Bering Strait is advected through Barrow Canyon (at the northeast bound-
857 ary of the Chukchi Sea where it meets the Canada Basin), with more than half of this
858 then transported west in the Chukchi Slope Current (Spall et al., 2018).

859 As a consequence of its ventilation, the halocline of the Beaufort Gyre is charac-
860 terized by two stratification maxima (Figures 3b and 10c). The first and shallowest cor-
861 responds to the mixed-layer base and is maintained by sustained surface Ekman conver-
862 gence of fresh water. The second peak in the stratification around 200 m depth is at the
863 base of the Pacific Winter Water Layer (Figure 10b,c), and is thought to originate at the
864 surface in the Chukchi Sea and ventilate the region in winter (Timmermans et al., 2017,
865 2014). Deeper down, waters from the cyclonic Atlantic Water boundary current are car-
866 ried into the interior of the Canada Basin by thermohaline intrusions and eddies (F. A. McLaugh-
867 lin et al., 2009). Below the Atlantic Water Layer, the deep and bottom waters share the
868 same large-scale circulation patterns, although are much weaker in strength than the over-
869 lying anticyclonic circulation (see Dosser & Timmermans, 2018; M. Zhao et al., 2018).

870 There is a vast store of available potential energy in the Beaufort Gyre halocline
871 that is susceptible to baroclinic instability. The basic state isopycnals indicate a change
872 in sign with depth of the horizontal potential vorticity gradient satisfying the necessary
873 criterion for baroclinic instability (Figure 10d). If the planetary potential vorticity gra-
874 dient is negligible, the sign of the interior meridional background potential vorticity gra-
875 dient may be determined by the sign of the meridional isopycnal layer thickness gradi-
876 ent. In the schematic representation of the Beaufort Gyre, the horizontal potential vor-
877 ticity gradient changes sign between the layers shown, indicating how the gyre may be
878 baroclinically unstable (Figure 10d). The observed energetic eddy field (Figure 10e) and
879 predicted scales and growth rates (Section 4.2 and Figure 4) suggest that the gyre is in-

880 deed baroclinically unstable, with important implications for its dynamics, as we now
 881 discuss.

882 **7.2 Fundamental dynamics of the Beaufort Gyre**

883 Fundamental dynamics of the Beaufort Gyre differ from mid-latitude wind-driven
 884 gyres which are characterized by a Sverdrup interior and frictional balance at western
 885 boundary currents (Munk, 1950; H. Stommel, 1948). It appears that the dynamics of
 886 the Beaufort Gyre have much in common with the dynamics of the Antarctic Circum-
 887 polar Current (ACC). Meridional barriers are also absent in the Southern Ocean and mesoscale
 888 eddy transfer is key to satisfying large-scale budgets of the ACC (see Marshall & Radko,
 889 2003). Residual-mean theory is central to understanding the dynamics of such systems.

890 **7.2.1 Residual-mean theory**

We consider the Beaufort Gyre as a system in which the prevailing winds pump
 fresh water in to the interior of the gyre, thickening halocline layers. This process is bal-
 anced by mesoscale eddy fluxes (i.e., bolus fluxes) that reduce thickness variations. The
 total transport in an isopycnal layer (due to the mean flow $\bar{\mathbf{v}}$ plus transport by eddies)
 is known as the residual-mean (as reviewed by, e.g., Andrews, Leovy, & Holton, 1987)
 defined by

$$\underbrace{\frac{\overline{\mathbf{v}h}}{h}}_{\text{Residual-mean}} = \underbrace{\bar{\mathbf{v}}}_{\text{Eulerian-mean}} + \underbrace{\frac{\overline{\mathbf{v}'h'}}{h}}_{\text{Eddy-induced transport}}, \quad (9)$$

891 where h is the thickness of a density layer, overbars denote an average and primes de-
 892 partures from that average. The residual-mean transport through a layer has a compo-
 893 nent in addition to the Eulerian mean because there can be correlations between the lat-
 894 eral flow and the thickness of the layer, leading to a significant bolus transport, $\overline{\mathbf{v}'h'}$. In
 895 the ACC, for example, bolus fluxes are significant and residual and Eulerian transports
 896 differ greatly from one-another, a fact that has fundamental implications for our under-
 897 standing of its dynamics (see the review by Marshall & Speer, 2012). This is also true
 898 for the Beaufort Gyre (G. E. Manucharyan, Spall, & Thompson, 2016; Meneghello et al.,
 899 2017; Yang, Proshutinsky, & Lin, 2016).

Meneghello et al. (2017) show that observations are consistent with the large-scale
 wind-driven Ekman transport integrated over the Beaufort Gyre being largely balanced

by eddy fluxes (i.e., the left hand side of equation (9) is a residual of the terms on the right hand side which tend to cancel one-another). They consider the zero residual-mean limit (analogous to studies to understand Southern Ocean dynamics, e.g., Marshall & Radko, 2003) and test whether the Eulerian-mean circulation can balance the bolus transport by eddies. Introducing an eddy diffusivity K_D to characterize eddy transport (as in Gent & McWilliams, 1990), a zero residual-mean balance yields

$$K_D = \frac{1}{\rho_0 f_0} \frac{\iint \nabla \times \boldsymbol{\tau}_s dA}{\iint \nabla^2 h dA}, \quad (10)$$

where $h(r)$ refers to the depth of an isopycnal in the stratified Beaufort Gyre, and $\boldsymbol{\tau}_s$ is the stress on the surface ocean, influenced by the presence of sea-ice cover (we discuss the role of sea ice shortly). The integrals are over an area enclosed by a particular geopotential height contour in the (r, z) plane. The numerator of (10) represents the area integrated Ekman pumping and the denominator can be considered as the balancing thickness flux. As described in Section 4.2, mooring measurements of velocity in the Beaufort Gyre allow for observational estimates of K_D invoking a mixing length theory. The magnitude and vertical structure of these estimates are in rough agreement with values inferred from (10) as shown by Meneghello et al. (2017). This suggests that in the Beaufort Gyre, eddy fluxes may be sufficient to balance Ekman pumping leading to a small residual-mean flow. We note that (10) yields the scaling for the depth of the halocline:

$$h \sim \frac{R\tau_s}{\rho_0 f_0 K_D}, \quad (11)$$

900 where R is an estimate for the radius of the gyre. Taking typical values for these param-
 901 eters ($R = 400$ km, $\tau_s = 0.5 \times 10^{-2}$ N m $^{-2}$, $f = 10^{-4}$ s $^{-1}$, and $K_D = 400$ m 2 s $^{-1}$),
 902 gives $h \approx 50$ m, broadly in accord with the depth scale of the upper halocline and Fig-
 903 ures 3c and 10c (see e.g., Meneghello et al., 2017). This is the same as the scaling for
 904 the vertical scale of the ACC discussed by Marshall and Radko (2003) and the same dy-
 905 namics are at work.

906 The axisymmetric model described above, although highly instructive, cannot cap-
 907 ture important asymmetries induced by topographic effects. Notably, the west side of
 908 the southern Canada Basin is bounded by the steep Northwind Ridge; the ridge has a
 909 slope of more than 10 degrees in places from the abyssal plain of the Canada Basin (around
 910 3800 m deep) to the Chukchi Borderland and Northwind Abyssal Plain regions, shallower
 911 than 1000 m in parts (Jakobsson et al., 2008, 2012). This prominent topographic fea-

912 ture may affect the symmetry of the gyre, and its susceptibility to baroclinic instabil-
913 ity (e.g., G. Manucharyan & Isachsen, 2019).

914 **7.2.2 Wind forcing mediated by sea ice**

915 In the absence of sea ice there is a direct relationship between the wind-stress act-
916 ing on the ocean and the associated Ekman pumping. In the presence of sea ice, how-
917 ever, wind applies stress to the ice which, less the lateral stresses within the ice, applies
918 stress to the ocean. Moreover, the strength and sign of Ekman pumping in the surface
919 ocean can be influenced by geostrophic ocean currents moving against the sea ice (Dewey
920 et al., 2018; Meneghello, Marshall, Campin, Doddridge, & Timmermans, 2018; Meneghello,
921 Marshall, Timmermans, & Scott, 2018). Consider, for example, a situation in which the
922 Arctic Ocean is almost completely ice covered in winter and internal lateral stresses in
923 the ice pack are sufficiently large that the sea-ice motion in response to the prevailing
924 anticyclonic wind forcing is small. At the same time, there is a persistent ocean geostrophic
925 flow of the anticyclonic Beaufort Gyre acting against the near-motionless sea ice. This
926 gives rise to Ekman divergence in the surface ocean layer and upwelling from the inte-
927 rior. Meneghello, Marshall, Timmermans, and Scott (2018) show that this upwelling each
928 winter greatly reduces the annual cumulative Ekman downwelling from the value it would
929 have had in the ice-free case; observations of ocean geostrophic flow, winds and sea-ice
930 drift indicate that cumulative Ekman downwelling can be up to 80% lower than an in-
931 ferred value that neglects the presence of ice. Meneghello, Marshall, Campin, et al. (2018)
932 describe how this effect acts as a self-regulator, which they call the *ice-ocean stress gov-*
933 *ernor*, and which sets the speed of the Beaufort Gyre. As the gyre increases in speed in
934 response to sustained anticyclonic wind forcing, and/or sea-ice drift slows in winter when
935 internal ice stresses increase, ocean currents ultimately reach ice speeds and the surface
936 stress on the ocean shuts off. In this way, the ice-ocean stress governor can equilibrate
937 the gyre, which implies a limit on freshwater accumulation. This is another example of
938 the internal system dynamics arranging to “turn off” the residual flow and the forcing
939 thereof. The implications for the future Arctic, where ice will likely be absent in sum-
940 mer and more mobile in winter, are discussed in the next section.

8 Arctic Ocean variability, climate change and future perspectives

The rapid changes that are underway in the Arctic compel an assessment of how Arctic Ocean dynamics might fundamentally change in the future. One conspicuous scenario to consider is a seasonally ice-free Arctic Ocean, with no sea ice for part of the summer/fall and a thinner, more mobile sea-ice pack in winter/spring. How will Arctic oceanography be different in this regime? Here, we contemplate two aspects of such a change; the first relates to ocean heat storage and the second relates to fresh water content and energetics of the large-scale circulation.

8.1 Changing ocean heat storage

In recent decades, a general warming of the upper Arctic Ocean has been widely documented in observations (e.g., E. Carmack et al., 2015; I. V. Polyakov et al., 2017; Timmermans, Toole, & Krishfield, 2018). Linear trends indicate summer mixed-layer temperatures increasing at about 0.5°C per decade over 1982-2018 in large areas of the Arctic Ocean that are ice-free in summer (Timmermans & Ladd, 2019). Increasing mixed-layer temperatures predominantly result from increased summertime solar absorption into the surface ocean that is associated with sea-ice losses and decreased Arctic Ocean albedo; the ice-albedo feedback mechanism has been a dominant factor of recent sea-ice losses (D. K. Perovich & Richter-Menge, 2009). Further, the heat absorbed by the surface ocean has implications that persist beyond the melt season. Timmermans (2015) showed that in the Canadian Basin, the excess heat absorbed by the surface ocean can lead to sea ice that is 25% thinner at the end of the growth season. Similar estimates apply for the region to the northeast of Svalbard, where observations indicate a delayed onset of freezing that follows excess solar absorption by the oceans (V. Ivanov et al., 2016).

Heat advected from the Pacific Ocean is also increasing, and has been implicated in triggering the ice-albedo feedback mechanism in the Chukchi Sea (Woodgate et al., 2010), which has experienced the fastest rate of sea-ice decline in the summer months in the entire Arctic Ocean (Comiso, 2012; M. C. Serreze, Crawford, Stroeve, Barrett, & Woodgate, 2016). Heat transport from the Pacific Ocean through Bering Strait increased by 60% during 2001-2014, from around 10 TW in 2001 to 16 TW in 2014; this was attributed to increases in both volume flux and temperature (Woodgate, 2018; Woodgate, Stafford, & Prael, 2015).

972 Some of the additional ocean heat in the Chukchi Sea, that derives both from ex-
973 cess solar absorption as a consequence of reduced sea-ice cover, and increased advection
974 from the Pacific Ocean, is accumulated and stored within the Beaufort Gyre halocline,
975 away from the influence of surface-ocean buoyancy fluxes and wind-driven mixing. As
976 described in Section 7.1, anomalously warm waters at the surface in the Chukchi Sea are
977 saltier (and therefore more dense) than the fresher, cooler waters at the surface in the
978 interior Beaufort Gyre, and there is a surface front between the two water types (approx-
979 imately at the $\sigma = 25 \text{ kg m}^{-3}$ outcrop in the southwest Beaufort Sea, see Figure 9);
980 the denser (warmer) water type ventilates the Beaufort Gyre halocline. In the interior
981 Beaufort Gyre, Pacific Water Layer maximum temperatures increased by about 0.5°C
982 between 2009 and 2013 (Timmermans et al., 2014), and integrated heat content in the
983 warm Pacific Water Layer approximately doubled over the period 1987-2017 (Timmer-
984 mans, Toole, & Krishfield, 2018). The amount of additional heat is enough to melt al-
985 most 1 m of sea ice should it reach the surface. Understanding the fate of this stored heat
986 is the subject of ongoing research.

987 It may be expected that under seasonally ice-free conditions (i.e., open water for
988 longer periods each summer in the Chukchi Sea), intensified solar absorption by the ocean
989 should continue, and therefore stored ocean heat should increase. On the other hand,
990 a different scenario may unfold. Ventilation of the Beaufort Gyre halocline relies on the
991 presence of the surface front (where the density contrast exists because of the salinity
992 differences) between Chukchi Sea waters and Beaufort Gyre waters. At present Arctic
993 Ocean temperatures, the coefficient of thermal expansion α is small and temperature has
994 a negligible effect on density. Therefore, although the summertime surface Chukchi Sea
995 waters are several degrees warmer than the Beaufort Gyre surface waters, the saltier Chukchi
996 Sea surface waters are more dense than those of the Beaufort Gyre, and the summer-
997 time solar-warmed water can continue to ventilate the Beaufort Gyre halocline. How-
998 ever, as warming continues, α will increase, and temperature will have an increasingly
999 important influence on the density, just as it does in the mid-latitude oceans character-
1000 ized by a thermocline. A possible future scenario is that the warming of Chukchi Sea wa-
1001 ters will be sufficiently strong as to have a compensating effect on the salinity differences
1002 on density, and the front will become weaker or disappear (Timmermans & Jayne, 2016).
1003 This would shut off the Beaufort Gyre halocline ventilation, and the mechanism for the
1004 accumulation of ocean heat, during the warmest periods.

1005 8.2 Atlantification of the Arctic

1006 The concept and implications of polar water-masses becoming closer to those typ-
1007 ical of mid-latitude oceans has also been explored on the Atlantic Ocean side of the Arc-
1008 tic. Mean Atlantic Water temperatures at Fram Strait and the Barents Sea Opening in-
1009 creased by around 1-1.5°C from 1980-2012 with long-term trends in volume inflow es-
1010 timates difficult to infer given observation limitations (Mulwijk, Smedsrud, Ilicak, & Drange,
1011 2018). Recent changes in the vicinity of the Atlantic Water inflow to the Arctic Ocean,
1012 including reduced sea ice, weaker stratification and enhanced Atlantic Water Layer heat
1013 fluxes further northeast into the Eurasian Basin, have been referred to as the *Atlantifi-*
1014 *cation* of the Arctic Ocean (Årthun, Eldevik, Smedsrud, Skagseth, & Ingvaldsen, 2012;
1015 Lind, Ingvaldsen, & Furevik, 2018; I. V. Polyakov et al., 2017). In the Eurasian Basin,
1016 vertical heat fluxes from the Atlantic Water Layer were estimated to be around 2-4 times
1017 larger in the 2014-2015 period compared with 2007-2008 (I. V. Polyakov et al., 2017).

1018 The Atlantification concept alludes to the possibility of a northward progression
1019 of the warm α -oceans – North Atlantic water masses encroaching on the Arctic Ocean.
1020 Around 45°N in both the North Pacific and Atlantic (with significant east-west variabil-
1021 ity in this position), there is a transition from an upper ocean that exhibits α stratifi-
1022 cation to a β stratification at the subarctic frontal zone, where warmer, saltier surface
1023 waters to the south meet cooler, fresher surface waters to the north (Roden, 1970, 1991),
1024 Figure 1b. The exact position of the subarctic front is related to the wind field, with the
1025 front being found in the vicinity of the maximum Ekman transport convergence (Roden,
1026 1991). While the North Atlantic subarctic front covers a much broader range of latitudes,
1027 in both the Pacific and Atlantic oceans this α - β boundary, where the local surface den-
1028 sity is maximal (a consequence of lateral mixing and the non-linear seawater equation
1029 of state), is characterized by temperatures around 10°C (see e.g., Belkin & Levitus, 1996;
1030 E. C. Carmack, 2007), Figure 1b. Cabbelling, a process of sinking where two water masses
1031 of the same density but differing temperature and salinity mix and become more dense,
1032 is active in this frontal boundary region (see Garrett & Horne, 1978; Schanze & Schmitt,
1033 2013).

1034 As mentioned in Section 3, the α - β stratification boundary is of importance to
1035 climate in that it establishes the southern extent of winter sea ice cover. Sediment core
1036 proxy data suggest significant changes in the position of the subarctic front over the Holocene

1037 (Moros, Jansen, Oppo, Giraudeau, & Kuijpers, 2012; Perner et al., 2018), and much fur-
1038 ther back in the climate record, where the shifting influence of Atlantic and Polar Wa-
1039 ter types is related to changes in sea-ice extent (e.g., Stein, Fahl, Gierz, Niessen, & Lohmann,
1040 2017). During the last major interglacial period (\sim 130,000 and 80,000 years ago, char-
1041 acterized by conditions warmer than today), Arctic sea ice biomarker proxy records and
1042 modeling suggest the Barents Sea was ice free for much of the year under the strong in-
1043 fluence of inflowing Atlantic Water (Stein et al., 2017). The Barents Sea has been an in-
1044 creasingly dominant region of winter sea-ice loss in recent decades, largely resulting from
1045 increased Atlantic Water heat transport into the region (Smedsrud et al., 2013).

1046 Climate model ensemble means (under continued increasing emissions) show a sus-
1047 tained incursion of Atlantic Water (marked by contours of the 1°C isotherm at 200 m
1048 depth in Figure 12 of Årthun et al. (2019)), from its present location in the vicinity of
1049 Fram Strait and the Barents Sea, (see e.g., Barton, Lenn, & Lique, 2018) to almost par-
1050 alleling the Lomonosov Ridge in the 2070s such that warm Atlantic Water fills the en-
1051 tire Eurasian Basin (Årthun et al., 2019). The main effect of this is a decrease in win-
1052 ter sea-ice thickness, by around 1.2 m between the 2010s and 2070s; average ocean-to-
1053 ice heat fluxes increase from around 0.5 W m^{-2} to 5 W m^{-2} in the Eurasian Basin be-
1054 tween these two periods. Increased Atlantic Water influence is likely to be a major player
1055 in the march towards a seasonally-ice-free Arctic Ocean. A potentially relevant feedback
1056 is increased mixing within the Arctic (discussed next) driving increased Atlantic Water
1057 influxes.

1058 **8.3 Sea-ice loss and ocean mixing levels**

1059 Loss of sea ice is not only linked to a build-up of ocean heat in the Arctic (and the
1060 indirect dynamical effects of this) but also has direct dynamical influences on the ocean.
1061 First, as implied in Section 4, wind-driven momentum input and therefore mixing lev-
1062 els are expected to increase under continued sea-ice losses and the absence of the buffer-
1063 ing effects of sea-ice cover. While no studies have shown an increasing trend in Arctic
1064 Ocean mixing levels (it may be that sufficient data are not yet available), future condi-
1065 tions may be inferred from observations of more energetic inertial motions in the upper
1066 water column when sea-ice concentrations are lower (e.g., Plueddemann, Krishfield, Tak-
1067 izawa, Hatakeyama, & Honjo, 1998). Mooring observations indicate that upper water-
1068 column inertial wave energy levels in the absence of sea ice can be as large as mid-latitude

1069 levels (Rainville & Woodgate, 2009). Increased mixing will likely drive larger vertical heat
1070 fluxes (D’Asaro & Morison, 1992), causing further sea-ice melt. On the other hand, it
1071 may be that increased wind-driven momentum input does not lead to higher mixing lev-
1072 els because sea-ice losses are concurrent with increased halocline stratification, which sup-
1073 presses mixing.

1074 Stratification increases, linked to freshening of the surface ocean (where fresh wa-
1075 ter originates from river influxes, land-ice melt, net precipitation, sea ice growth/melt,
1076 and northwards advection of mid-latitude waters), can inhibit convective and shear-driven
1077 mixed-layer deepening and suppress turbulent diapycnal diffusivities in the halocline. These
1078 processes regulate vertical heat transfer between the ocean interior and the surface. Arc-
1079 tic Ocean mixed-layer depths are typically around 25 to 50 m in winter and around 5-
1080 30 m in summer (e.g., Peralta-Ferriz & Woodgate, 2015; J. M. Toole et al., 2010). Be-
1081 tween 1979 and 2012, central Arctic Ocean observations indicate a mixed layer shoal-
1082 ing of 0.5 to 1 m yr⁻¹ (Peralta-Ferriz & Woodgate, 2015). Complicating the inferred con-
1083 sequences of this, Rainville, Lee, and Woodgate (2011) point out that the presence of
1084 thinner mixed layers can lead to more effective wind-driven momentum transfer to the
1085 ocean layers below; faster mixed-layer currents are generated because the same energy
1086 input is distributed over a thinner layer.

1087 In recent decades, the the Arctic shelf seas (e.g., the East Siberian, Laptev, Chukchi,
1088 Kara and Barents seas) have seen freshwater decreases (Armitage et al., 2016). For ex-
1089 ample, freshwater content in the top 100 m of the northern Barents Sea decreased by about
1090 1/3 between 1970-1999 and 2010-2016 (Lind et al., 2018). Mixed-layer deepening trends
1091 have been observed in these marginal regions in the past few decades, attributed to winds
1092 driving surface fresh water offshore (Peralta-Ferriz & Woodgate, 2015), and weakening
1093 stratification associated with Atlantification (I. V. Polyakov et al., 2017). The state of
1094 halocline strength and structure, and therefore mixing levels, in the coming decades will
1095 depend on the combined evolution of fresh water availability and its dynamical redis-
1096 tribution by winds, modified to varying degrees by sea ice depending on season and re-
1097 gion.

1098 **8.4 Changes in fresh water storage**

1099 Between 1992 to 2012 Arctic Ocean total freshwater content (integrated fresh wa-
1100 ter relative to a salinity of 34.8) increased at a rate of around $600\pm 300 \text{ km}^3 \text{ yr}^{-1}$; about
1101 two-thirds has been attributed to salinity decreases, with the remainder a result of a thick-
1102 ening of the freshwater layer (E. C. Carmack et al., 2016; T. W. N. Haine et al., 2015;
1103 Rabe et al., 2014). The most comprehensive in-situ hydrographic measurements are from
1104 the Beaufort Gyre region where observations indicate an overall increase in total fresh-
1105 water content by almost 40% since the 1970s (from around $17\times 10^3 \text{ km}^3$ to 23.5×10^3
1106 km^3 in 2018) (A. Proshutinsky, Krishfield, & Timmermans, 2019; A. e. a. Proshutinsky,
1107 2019). Such increases are associated with the strengthening of the Beaufort Gyre respond-
1108 ing to anticyclonic wind forcing over the Canadian Basin, freshwater accumulation from
1109 sea ice melt, increasing freshwater flux through Bering Strait and greater influence of Macken-
1110 zie River water (R. A. Krishfield et al., 2014; A. Proshutinsky et al., 2015; A. e. a. Proshutin-
1111 sky, 2019).

1112 Anticipating the fate of Arctic fresh water as it is influenced by, and influences, sea-
1113 ice losses (via setting the stratification and regulating wind-energy input) is a priority
1114 for future climate projections. Currently the Beaufort Gyre is subject to sustained wind
1115 forcing, with eddy fluxes and particularly the ice-ocean stress governor playing a role in
1116 equilibrating the gyre and its freshwater content (Meneghello, Doddridge, Marshall, Scott,
1117 & Campin, 2020). A future, seasonally ice-free Beaufort Gyre, with a corresponding thin-
1118 ner, more mobile winter sea-ice pack, would be characterized by a much less effective ice-
1119 ocean stress governor. Recent increases in Beaufort Gyre freshwater content may in part
1120 already be a manifestation of a less effective ice-ocean stress governor under recent sea-
1121 ice losses. Anticyclonic wind forcing balanced only by eddy fluxes will likely yield an equi-
1122 librium freshwater content that is larger, with a deeper halocline. That said, the new equi-
1123 librium may be uncertain given the changing fresh water availability (e.g., increased net
1124 precipitation, see Vihma et al., 2016) and topographic influences on gyre stability (that
1125 change with positional shifts in the gyre center).

1126 Predicting future prevailing wind forcing is also a major source of uncertainty in
1127 understanding the fate of fresh water. A weakening of the Beaufort High and dominance
1128 of the Icelandic Low will favor freshwater release, which may also be accompanied by a
1129 greater volume of Atlantic Water. For example, coupled modeling comparing the time

1130 periods 1979-88 and 1989-96 indicates a reduced Beaufort Gyre in the later period, a man-
1131 ifestation of a weakened Beaufort High and an expansion of the Icelandic low pressure
1132 system (Zhang, Rothrock, & Steele, 1998). Accompanying these changes is an increased
1133 penetration of Atlantic Water into the Arctic Ocean in the later period, and increased
1134 Polar Water outflow (i.e., an intensified East Greenland Current associated with fresh
1135 water release from the Beaufort Gyre). These changes are also evidenced in observations.
1136 Morison et al. (1998) analyze 1993 hydrographic observations that show increased in-
1137 fluence of Atlantic Water/Eurasian Basin water types in the Arctic Ocean, with a shift
1138 in the position of the front between Eurasian Basin and Canadian Basin water types,
1139 which are characterized by fresher surface waters, Pacific Water influence and cooler At-
1140 lantic Waters (see also Morison et al. (2012)). Consistent with a weakening of the Beau-
1141 fort High and expanded influence of the Icelandic Low, the front shifts from its previ-
1142 ous position around the location of the Lomonosov Ridge to a position roughly paral-
1143 leling the Alpha and Mendelejev Ridges; at the same time hydrographic measurements
1144 indicate a general warming of the Atlantic Water core temperatures. Morison et al. (1998)
1145 point out that the increased Atlantic sector influence (and reduced fresh water) in the
1146 Arctic Ocean persists for at least several years.

1147 It may be that general Arctic warming and sea-ice loss will lead to a reduced Beau-
1148 fort High. A reversal of the prevailing anticyclonic circulation was documented in win-
1149 ter 2017, for example (Moore, Schweiger, Zhang, & Steele, 2018). This was attributed
1150 to warm surface air temperatures during the previous autumn, and reduced sea ice ex-
1151 tents which generated an intensified low over the Barents Sea and increased cyclone prop-
1152 agation into the Beaufort Sea region (Moore et al., 2018). Such circulation patterns could
1153 become increasingly prevalent in a warming Arctic, which would have significant impli-
1154 cations and feedbacks with respect to fresh water fluxes out of the Beaufort Gyre region.
1155 This highlights the importance of understanding how the meteorology of the Arctic will
1156 change as it warms at a rate greater than twice the global average (see the review of Arc-
1157 tic amplification by M. Serreze, Barrett, Stroeve, Kindig, & Holland, 2009).

1158 **9 A framework for interpreting Arctic Ocean circulation in a chang-** 1159 **ing system, and future challenges**

1160 We have provided a general description of two distinct circulation patterns in the
1161 Arctic Ocean. Relatively warm and salty Atlantic waters enter through Fram Strait and

1162 the Barents Sea Opening, and circulate cyclonically around the Arctic basin boundaries
1163 and within Arctic sub-basins, ostensibly under strong topographic control. Co-existing
1164 with these arterial flows are wind-driven surface-intensified patterns driven interior to
1165 the Arctic – the Beaufort Gyre and the Transpolar Drift Stream. The ocean is capped
1166 by seasonally-varying sea-ice cover, with a distribution that is largely independent of to-
1167 pographic features. Pacific Ocean and river influxes further modify surface-water prop-
1168 erties.

1169 Both the estuary and f/H -following models for Atlantic Water circulation incor-
1170 porate key essential processes, and on their own cannot provide a complete picture. In
1171 the estuary model, there is no role for topography within the Arctic Ocean and no al-
1172 lowance for winds to play a dynamic role. The simplest f/H -following model is barotropic,
1173 while strong stratification exists along the cyclonic pathway of the Atlantic Water. This
1174 is particularly true in the interior Canada Basin where stratification is strongest, eddies
1175 are active and flow is surface-intensified. Further, while bottom friction may be impor-
1176 tant, a complete model should also take into account diabatic halocline mixing, lateral
1177 eddy fluxes, eddy pressure anomalies at the sea-floor slope, and under-ice stresses.

1178 There are undoubtedly complicated relationships between the arterial Atlantic Wa-
1179 ter and stratified Arctic Ocean interior flow. Coupled ice-ocean modeling, for example,
1180 suggests the Beaufort Gyre and Atlantic Water circulation can influence each other (e.g.,
1181 Lique, Johnson, & Davis, 2015). For example, an intensified Beaufort Gyre (under anoma-
1182 lously strong anticyclonic wind forcing) has been found to weaken and even reverse the
1183 Atlantic Water boundary current although the precise interactions remain unclear (Karcher
1184 et al., 2007). At least, the structure and water-mass properties of mesoscale eddies sam-
1185 pled within the Beaufort Gyre indicate efficient eddy fluxes from the Atlantic Water bound-
1186 ary current (and overlying Eurasian Basin halocline water types) to the Beaufort Gyre
1187 (Carpenter & Timmermans, 2012; M. Zhao & Timmermans, 2015).

1188 The community has built up a consistent description of the wind-driven Beaufort
1189 Gyre circulation and dissipation processes – both ocean-ice stresses and baroclinic eddy
1190 activity play key roles in balancing wind forcing – yet many open questions remain. One
1191 major understanding gap is that adjustment timescales for the Beaufort Gyre and upper-
1192 ocean response to wind forcing in the Eurasian Basin are not well known. These will be
1193 essential to constrain if we are to make viable assessments about how the Beaufort Gyre

1194 will change with further sea-ice decline, the fate of freshwater, stratification and mix-
1195 ing processes, and how the fundamental dynamics will change with continued warming
1196 to a scenario where the dynamical influence of temperature will be more important.

1197 While conceptual models provide the context in which to contemplate the Arctic's
1198 changing dynamics as the Earth warms, we require continued exploration of novel ways
1199 to make use of atmosphere-ocean-sea-ice coupled general circulation models to probe the
1200 Arctic system response to external drivers (as described by, for example, Johnson, Cor-
1201 nish, Kostov, Beer, & Lique, 2018; Marshall, Scott, & Proshutinsky, 2017; Muilwijk et
1202 al., 2019). These modeling efforts require constraints provided by sustained observations.

1203 Many gaps in our understanding exist because of the obstacles to acquiring suffi-
1204 cient measurements. While satellite remote sensing of ocean properties, including the
1205 meso- and smaller-scale flow field (and eddy kinetic energy) will continue to become more
1206 effective as sea ice declines, sea-ice cover will continue to remain an impediment for much
1207 of the year. Although sea ice can be a barrier to sustained remote and in-situ Arctic Ocean
1208 observing, sensors mounted in sea ice have provided invaluable measurements of the Arc-
1209 tic atmosphere-ice-ocean system (see the review by Timmermans, Krishfield, Lee, & Toole,
1210 2018). However, there remain challenges of observing and quantifying ice-ocean stresses
1211 and eddy fluxes in the upper ocean, which we know to be critical in the dynamical bal-
1212 ances. High spatial and temporal resolution measurements in the ice-ocean boundary
1213 layer are generally only possible through the use of sea ice as a platform from which to
1214 sample (and these are therefore Lagrangian measurements). Further, year-round mea-
1215 surements in the boundary layer are currently not practical because seasonal sea-ice growth
1216 and dynamical ridging processes can compromise deployment. For this same reason, moored
1217 sensors must be placed deeper than a couple of tens of meters below the ice-ocean in-
1218 terface to avoid the possibility of being damaged by deep ice keels drifting past.

1219 Year round measurement of the Arctic basin boundary regions (including its marginal
1220 seas) also remains a critical observational gap. As we have seen, these regions are char-
1221 acterized by the smallest flow scales and highest eddy kinetic energy. In addition, basin
1222 boundaries are the pathways for river influxes, Atlantic and Pacific inflows and bound-
1223 ary currents, and are the ocean regions with the strongest summertime solar warming.
1224 However, characterizing year-round dynamics and variability there is challenging for both
1225 political reasons (i.e., observing in Exclusive Economic Zones) and environmental rea-

1226 sons (i.e., ocean and sea-ice flows in boundary regions are exceptionally dynamic and de-
1227 structive and exhibit strong seasonal variability). A range of observing approaches will
1228 be required to provide new observations in under-ice boundary layers and in the impor-
1229 tant basin margins – observations which will be vital to guide and constrain theoret-
1230 cal and modeling analyses to better understand the ocean’s changing dynamical balances.

1231 **Acknowledgments**

1232 Support was provided by the National Science Foundation Division of Polar Programs
1233 under award 1603542. The Ice-Tethered Profiler data were collected and made available
1234 by the Ice-Tethered Profiler program (R. Krishfield, Toole, Proshutinsky, & Timmermans,
1235 2008; J. Toole, Krishfield, Timmermans, & Proshutinsky, 2011) based at the Woods Hole
1236 Oceanographic Institution (<http://www.whoi.edu/itp>). Hydrographic climatology data
1237 are from the World Ocean Atlas 2018 (WOA18; <https://www.nodc.noaa.gov/OC5/woa18/>).
1238 Beaufort Gyre hydrographic data were collected and made available by the Beaufort Gyre
1239 Exploration Program based at the Woods Hole Oceanographic Institution (<http://www.whoi.edu/beaufortgyre>)
1240 in collaboration with researchers from Fisheries and Oceans Canada at the Institute of
1241 Ocean Sciences; Data are available online at <http://www.whoi.edu/website/beaufortgyre/data>.
1242 We thank Chris Garrett and two anonymous reviewers for their valuable comments and
1243 suggestions.

1244 **References**

- 1245 Aagaard, K. (1981). On the deep circulation in the Arctic Ocean. *Deep Sea Research*
1246 *Part A. Oceanographic Research Papers*, 28(3), 251–268.
- 1247 Aagaard, K., & Carmack, E. C. (1989). The role of sea ice and other fresh water
1248 in the Arctic circulation. *Journal of Geophysical Research: Oceans*, 94(C10),
1249 14485–14498.
- 1250 Aagaard, K., Coachman, L., & Carmack, E. (1981). On the halocline of the Arctic
1251 Ocean. *Deep Sea Research Part A. Oceanographic Research Papers*, 28(6),
1252 529–545.
- 1253 Aagaard, K., Swift, J., & Carmack, E. (1985). Thermohaline circulation in the
1254 Arctic Mediterranean seas. *Journal of Geophysical Research: Oceans*, 90(C3),
1255 4833–4846.
- 1256 Aksenov, Y., Ivanov, V. V., Nurser, A. G., Bacon, S., Polyakov, I. V., Coward,
1257 A. C., ... Beszczynska-Moeller, A. (2011). The Arctic circumpolar boundary
1258 current. *Journal of Geophysical Research: Oceans*, 116(C9).
- 1259 Andrews, D. G., Leovy, C. B., & Holton, J. R. (1987). *Middle atmosphere dynamics*
1260 (Vol. 40). Academic press.
- 1261 Armitage, T. W. K., Bacon, S., Ridout, A. L., Petty, A. A., Wolbach, S., &
1262 Tsamados, M. (2017). Arctic Ocean geostrophic circulation 2003-

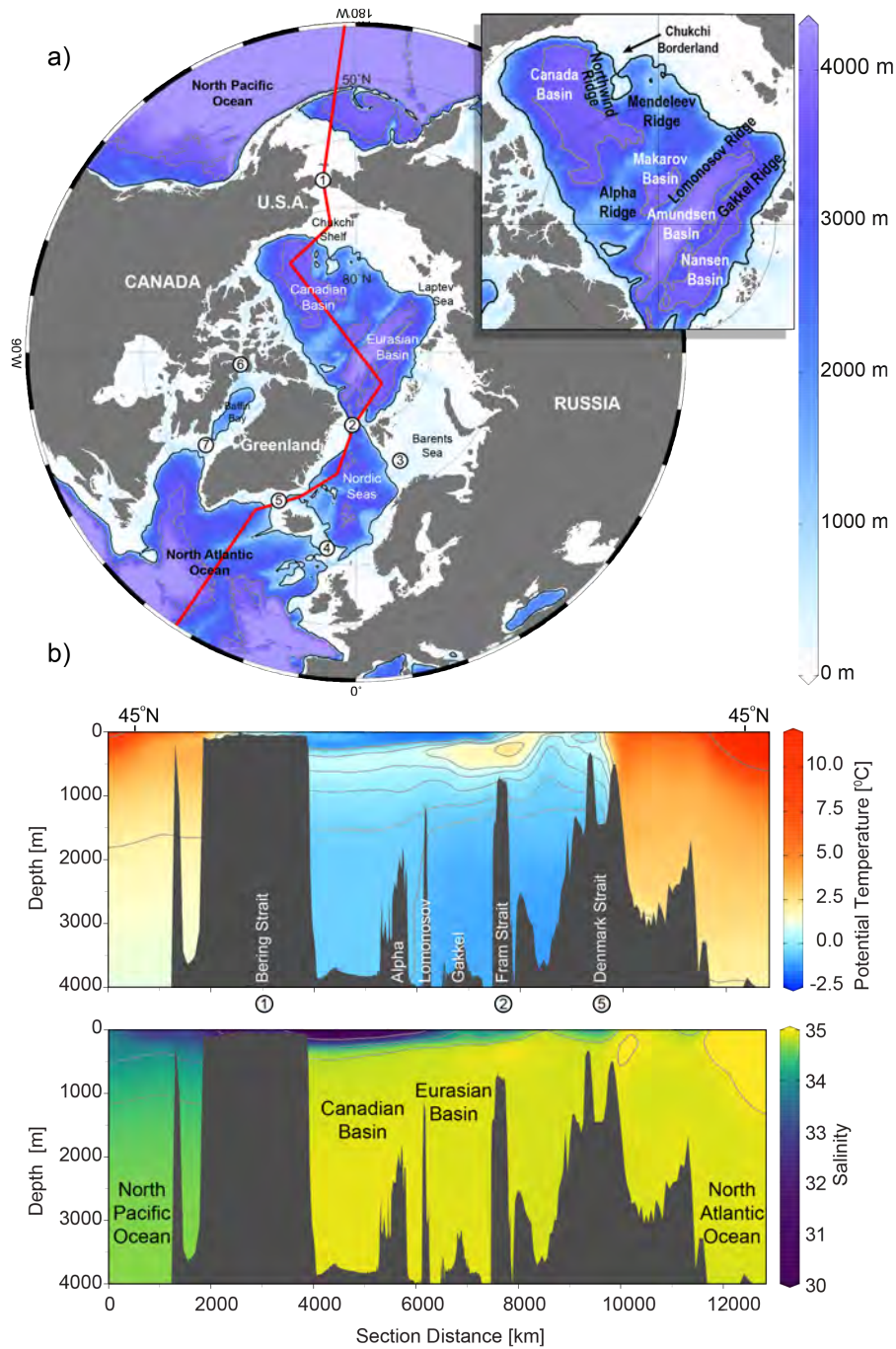


Figure 1. a) Map showing the main geographic features of the Arctic Mediterranean; the inset shows the Arctic Ocean in detail. 1000 m and 3500 m bathymetric contours are shown and numbers refer to 1. Bering Strait, 2. Fram Strait, 3. Barents Sea Opening, 4. Greenland-Scotland Ridge, 5. Denmark Strait, 6. Lancaster Sound, 7. Davis Strait. The red line marks the section shown in b) (top) Potential temperature ($^{\circ}\text{C}$) and (bottom) salinity sections from the Pacific Ocean (left), through the Arctic Ocean to the Atlantic Ocean (right). Data are from the World Ocean Database (WOD18), all data in the period 2005-2017 (Boyer, 2018), compiled as the World Ocean Atlas (WOA18) (Garcia et al., 2019).

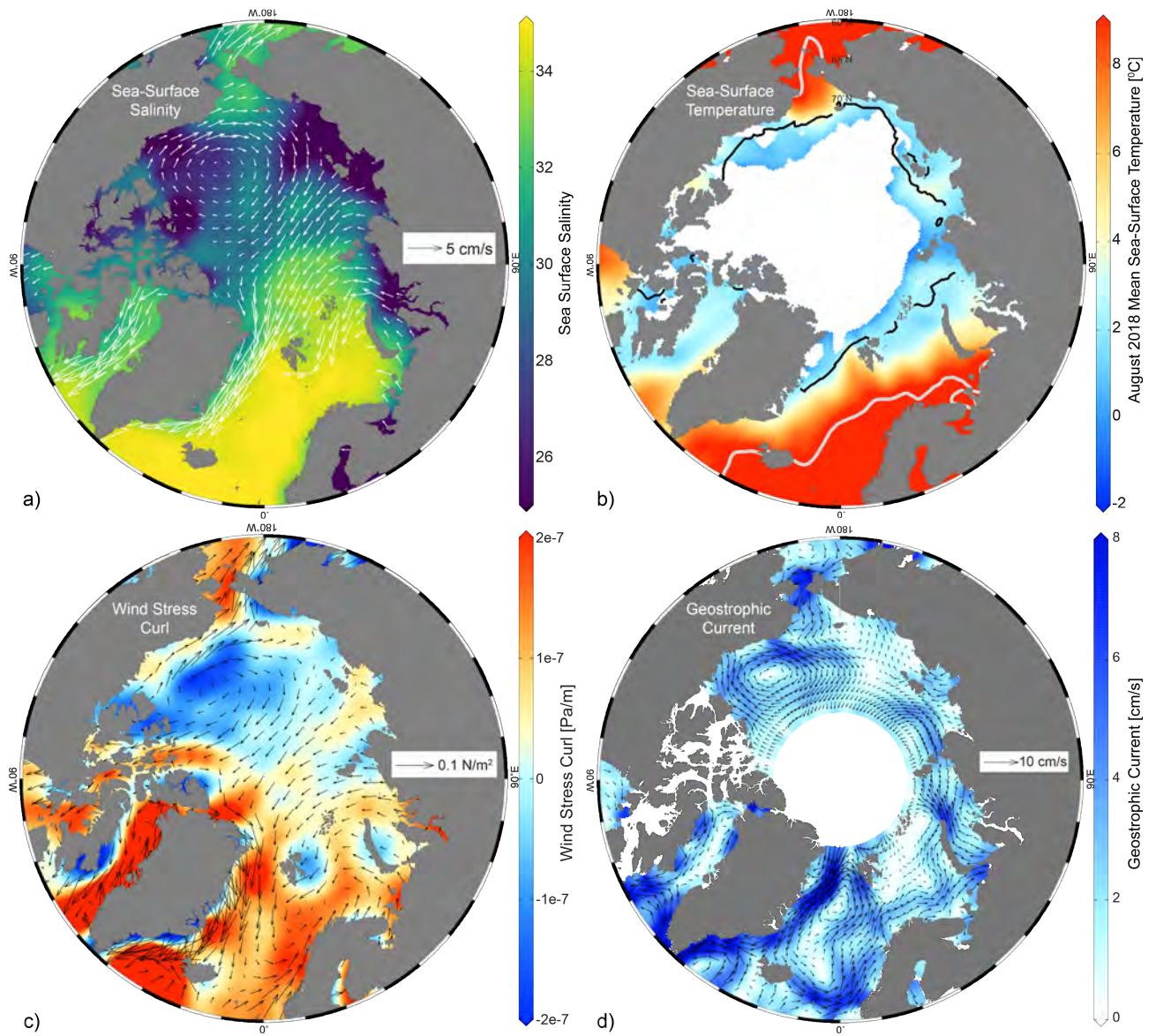


Figure 2. Maps of a) sea-surface salinity (WOD18, 2005-2017) [color] and March average sea-ice motion [white vectors] for the period 2005-17 from the Polar Pathfinder Daily 25 km EASE-Grid Sea Ice Motion Vectors data set available at the NASA National Snow and Ice Data Center Distributed Active Archive Center (Tschudi et al., 2016); b) August mean sea-surface temperature ($^{\circ}\text{C}$) from the NOAA Optimum Interpolation (OI) SST Version 2 product (OISSTv2), which is a blend of in situ and satellite measurements (Reynolds et al., 2007); c) annual average surface wind stress [black vectors] and wind-stress curl (2005-17) [color] from NCEP/NCAR Reanalysis Monthly Means (Kalnay et al., 1996); d) Mean ocean geostrophic flow (cm/s) estimated for 2003-2014 from satellite-derived dynamic topography, where data are provided by the Centre for Polar Observation and Modelling, University College London (Armitage et al., 2017). In panel b), thick gray contours indicate the 10°C isotherm, white shading is the August 2018 mean sea ice extent, and the black line indicates the median ice edge for August 1982-2010. Sea ice extent data are from NSIDC Sea Ice Index, Version 3 (Fetterer et al., 2017).

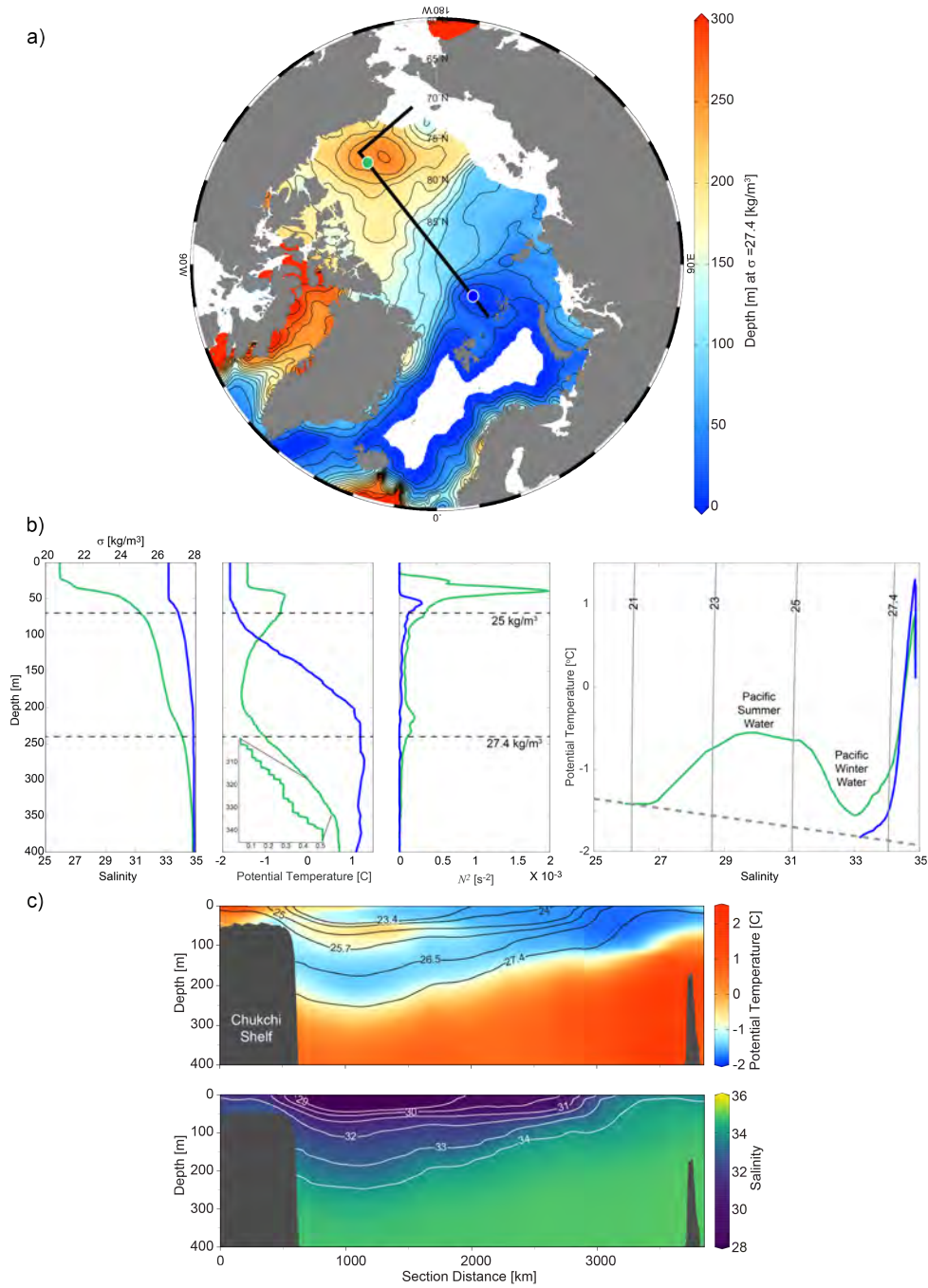


Figure 3. a) Depth of the $\sigma=27.4 \text{ kg m}^{-3}$ isopycnal. b) Example salinity, potential temperature ($^{\circ}\text{C}$) and buoyancy frequency (N^2 , s^{-2}) profiles, and corresponding potential temperature-salinity plot (from Ice-Tethered Profilers) from March 2010 in the Canada Basin (green profiles corresponding to the green marker in panel a) and Eurasian Basin (blue profiles, blue marker). The top x -axis in the left panel indicates the corresponding density and horizontal dashed lines mark the depths of $\sigma=25 \text{ kg m}^{-3}$ and $\sigma=27.4 \text{ kg m}^{-3}$ in the Canada Basin. The inset on the potential temperature profile shows the double-diffusive staircase structure. Grey contours in the right panel are isopycnals (kg m^{-3}) and the grey dashed line is the freezing line (referenced to zero pressure). c) Sections of (top) potential temperature ($^{\circ}\text{C}$) and (bottom) salinity from the Chukchi Sea (left) to the Eurasian Basin (right) along the black line shown in panel a). Data in a) and c) are from WOD18, 2005-2017.

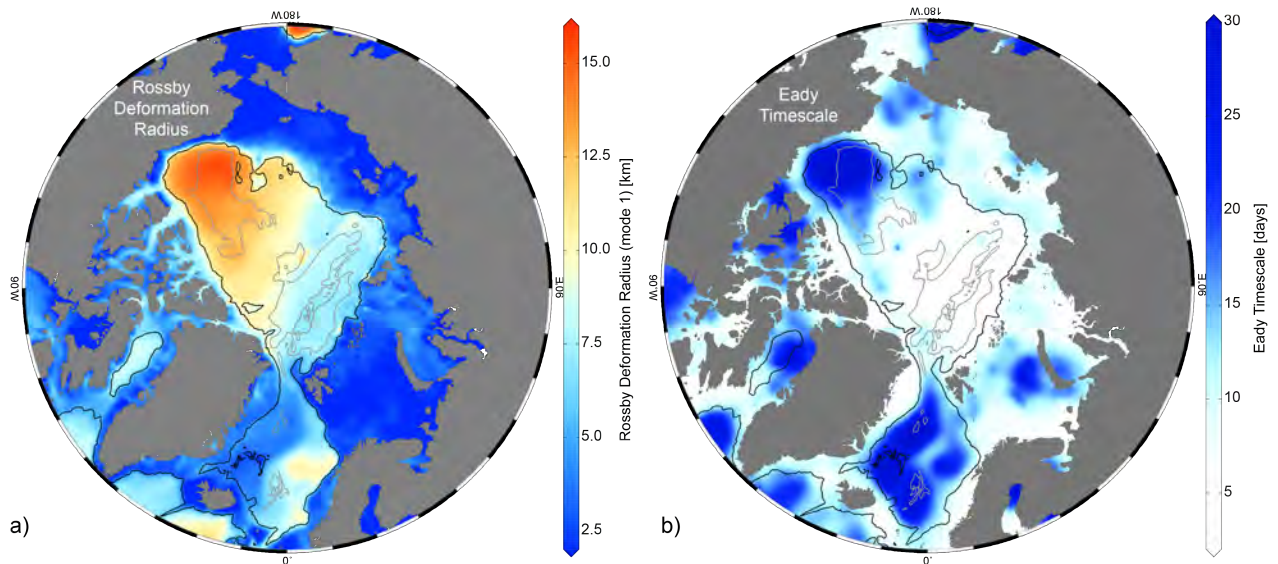


Figure 4. a) First baroclinic Rossby radius of deformation (km, computed from hydrographic climatology: WOD18, 2005-2017) following the method outlined by Chelton et al. (1998). b) An approximate Eady timescale ω^{-1} (days) calculated from (1) (see Tulloch et al., 2011) using the thermal wind shear estimated from the WOD18 climatology. 1000 m (black) and 3500 m (grey) bathymetric contours are shown.

- 1263 2014. *The Cryosphere Discussions, 2017*, 1–32. Retrieved from [http://](http://www.the-cryosphere-discuss.net/tc-2017-22/)
1264 www.the-cryosphere-discuss.net/tc-2017-22/ doi: 10.5194/tc-2017-22
- 1265 Armitage, T. W. K., Bacon, S., Ridout, A. L., Thomas, S. F., Aksenov, Y., & Wing-
1266 ham, D. J. (2016). Arctic sea surface height variability and change from
1267 satellite radar altimetry and GRACE, 2003-2014. *Journal of Geophysical*
1268 *Research: Oceans, 121*(6), 4303–4322. doi: 10.1002/2015JC011579
- 1269 Årthun, M., Eldevik, T., Smedsrud, L., Skagseth, Ø., & Ingvaldsen, R. (2012).
1270 Quantifying the influence of Atlantic heat on Barents Sea ice variability and
1271 retreat. *Journal of Climate, 25*(13), 4736–4743.
- 1272 Årthun, M., Eldevik, T., & Smedsrud, L. H. (2019). The role of Atlantic heat
1273 transport in future Arctic winter sea ice loss. *Journal of Climate, 32*(11),
1274 3327–3341.
- 1275 Barton, B. I., Lenn, Y.-D., & Lique, C. (2018). Observed Atlantification of the Bar-
1276 ents Sea causes the Polar Front to limit the expansion of winter sea ice. *Jour-
1277 nal of Physical Oceanography, 48*(8), 1849–1866.

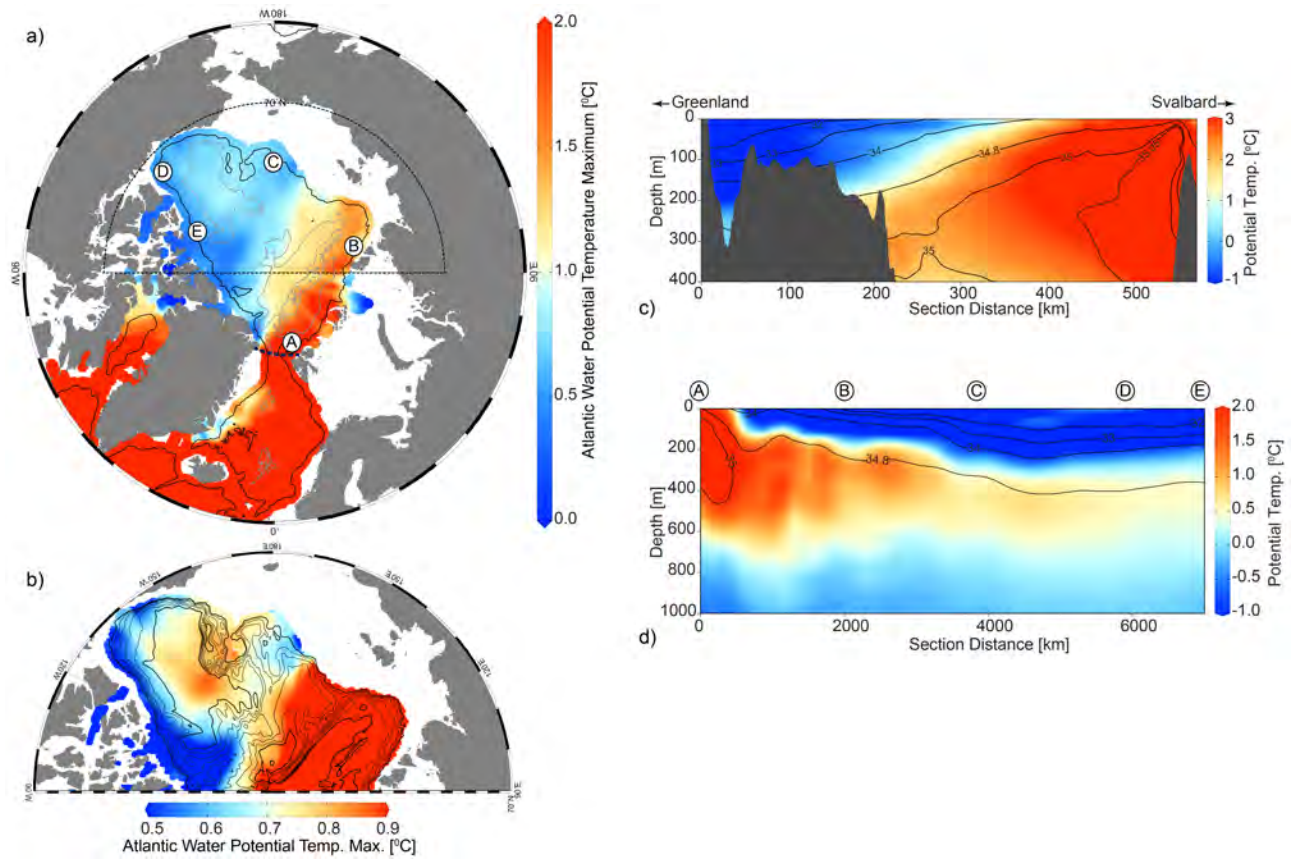


Figure 5. Maps of Atlantic Water potential temperature maximum ($^{\circ}\text{C}$) for a) the Arctic Ocean and b) the sector bounded by the thin dotted black lines in a). Bathymetric contours in b) are in intervals of 500 m; the deepest contour shown is 3500 m. Sections of potential temperature ($^{\circ}\text{C}$, colors) and salinity (contours) c) across Fram Strait from west to east along 80°N (thick dotted line shown in panel a; cooler, fresher water in the west flows south, while the warmer, saltier water to the east flows north, entering the Arctic Ocean from the Nordic Seas) and d) along the 1000 m isobath moving cyclonically around the Arctic Basin with letters A-E corresponding to their locations marked in panel a. Data are from WOD18, 2005-2017.

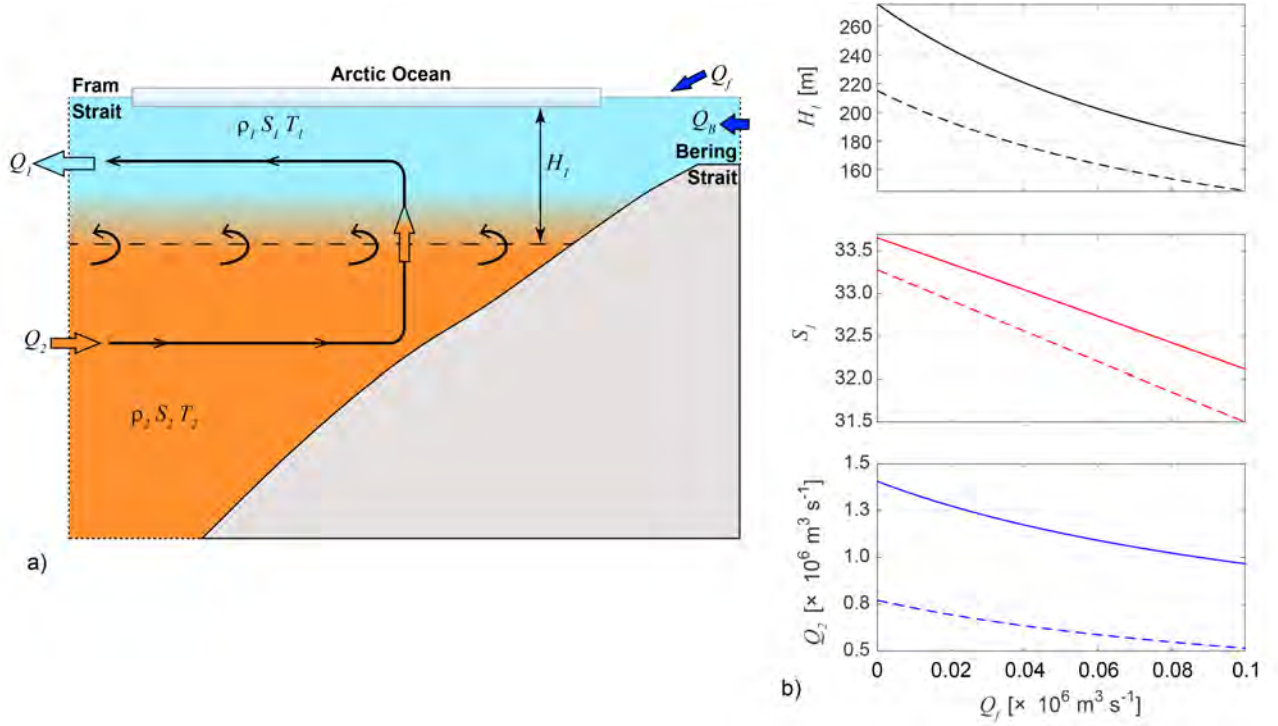


Figure 6. a) Schematic of an idealized 2-layer estuary (see Stigebrandt, 1981, his Figure 2). The upper layer constitutes Polar Water that flows from the Arctic Ocean to the Nordic Seas on the left side of the diagram, while the lower layer is renewed by Atlantic Water inflowing from the Nordic Seas to the Arctic Ocean. Mixing and entrainment of Atlantic Water into the upper layer drives the Atlantic Water inflow. b) Solutions to the system of equations (2)-(6): Upper layer thickness H_1 (top), upper layer salinity S_1 (middle) and Atlantic Water volume influx Q_2 (bottom) as functions of net freshwater input Q_f . Parameter values chosen for the calculations are given in the text, and solutions are shown for two different values of the mixing rate: $u_* = 0.55$ cm s^{-1} (solid lines) and $u_* = 0.45$ cm s^{-1} (dashed lines). For a fixed value of Q_f , larger mixing gives rise to a thicker, saltier upper layer exiting the Arctic Ocean, and a larger Atlantic Water volume influx Q_2 (see Rudels, 1989; Stigebrandt, 1981).

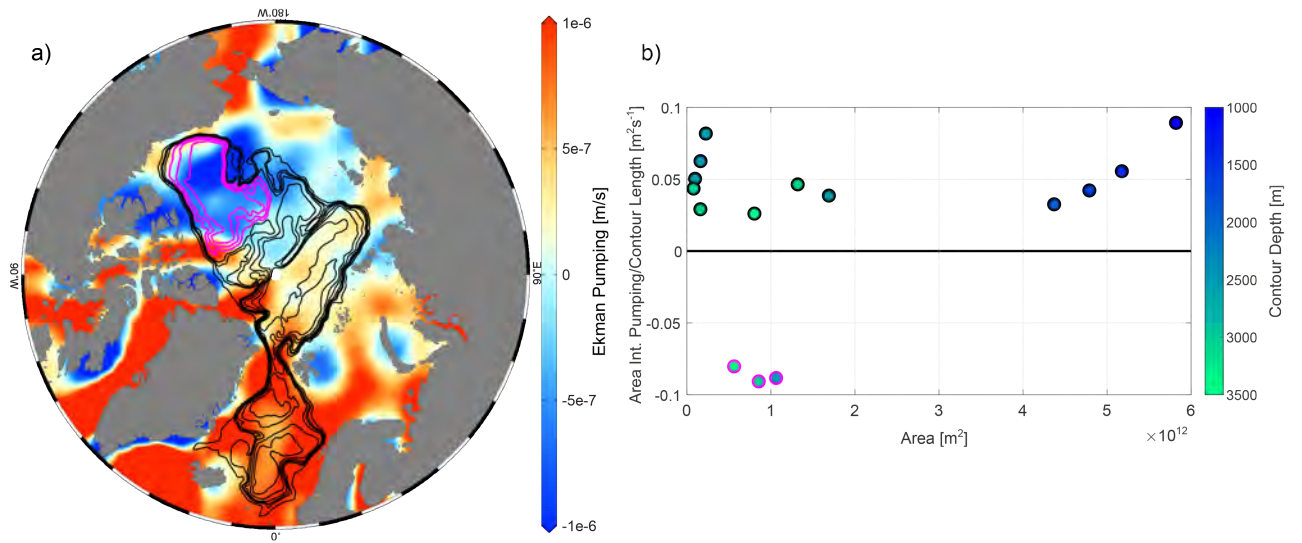


Figure 7. a) Annual average Ekman pumping (m/s, 2005-17) [color] and a selection of closed f/H contours; f/H contours effectively coincide with bathymetric contours at these latitudes. Black (magenta) contours enclose an area for which the area-integral of wind-stress curl is positive (negative). b) Area-integrated Ekman pumping per contour length (m^2s^{-1}) vs. area enclosed by the contour (m^2) for the contours shown in panel a (markers correspondingly outlined by black and magenta). Marker colors indicate the depth of the contours. See Nøst and Isachsen (2003), their figures 13 and 14.

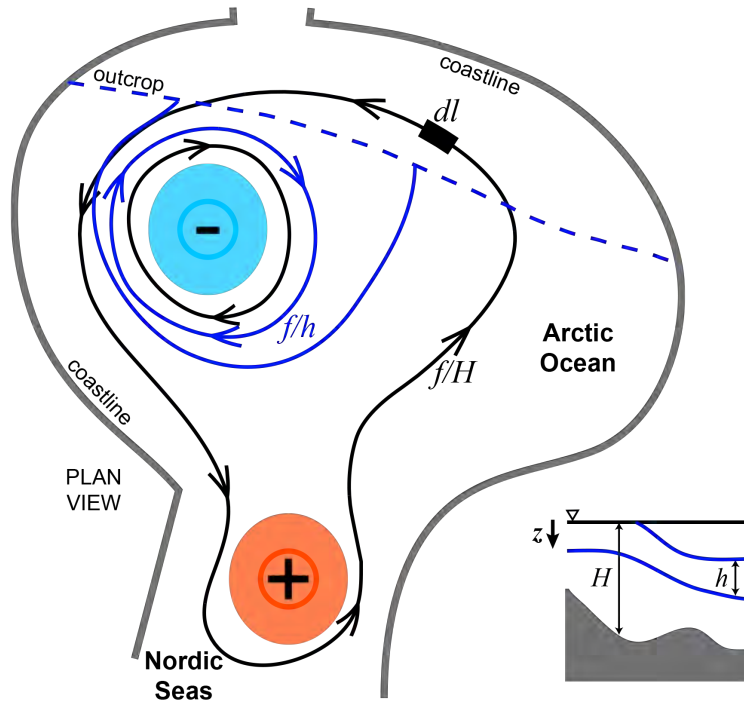


Figure 8. Plan-view schematic showing the main features of a wind-driven model of the circulation. f/H contours are shown in black with the direction of circulation along the contour governed by the sign of the wind-stress curl integrated over the area enclosed by the contour. The blue patch depicts the dominance of anticyclonic wind-stress curl in the Arctic Ocean (specifically the Beaufort Gyre region), and the red patch depicts the cyclonic wind-stress curl that dominates in the Nordic Seas. Blue contours indicate lines of constant potential vorticity for a layer bounded by two isopycnals (the section view shown in the inset shows isopycnals in blue). The blue dashed line indicates where the isopycnal bounding the top of the layer outcrops the surface, as shown in the inset schematic.

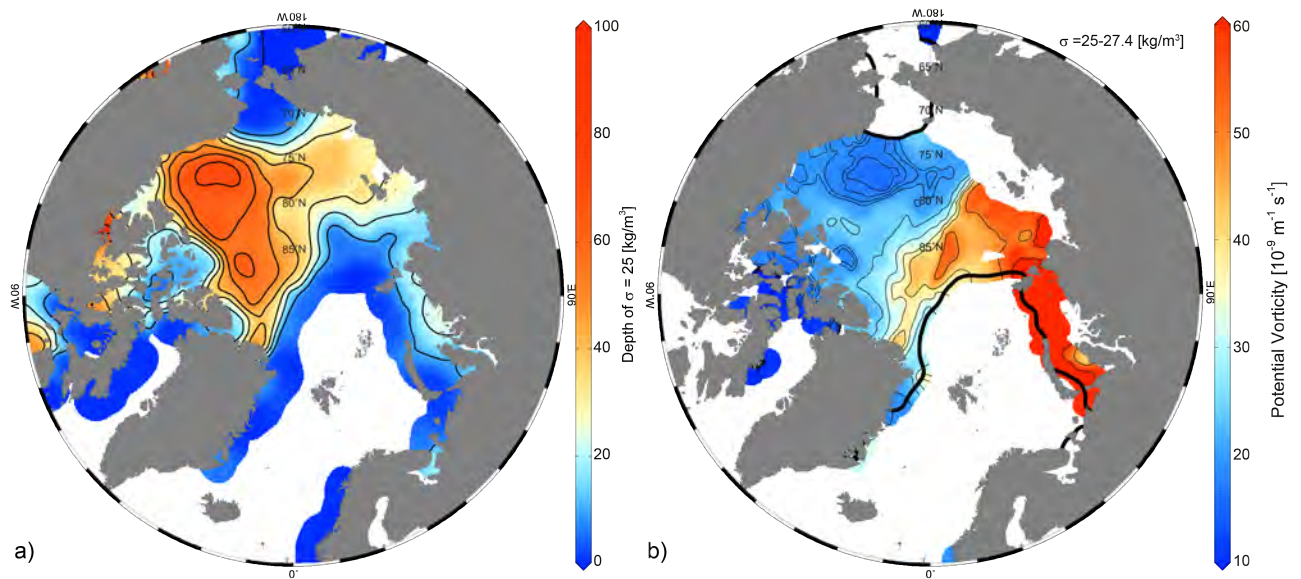


Figure 9. a) Depth of the $\sigma=25 \text{ kg m}^{-3}$ isopycnal. b) Potential vorticity ($\text{m}^{-1}\text{s}^{-1}$) of the $\sigma=25 - 27.4 \text{ kg m}^{-3}$ layer estimated by $f\delta\sigma/(h\rho_0)$, where $\delta\sigma$ is the density difference between the two density surfaces separated by a vertical distance h . The thick black contours indicate the $\sigma=25 \text{ kg m}^{-3}$ outcrop.

- 1278 Bebieva, Y., & Timmermans, M.-L. (2016). An examination of double-diffusive
 1279 processes in a mesoscale eddy in the Arctic Ocean. *Journal of Geophysical Re-*
 1280 *search: Oceans*, 121(1), 457–475.
- 1281 Bebieva, Y., & Timmermans, M.-L. (2017). The relationship between double-
 1282 diffusive intrusions and staircases in the Arctic Ocean. *Journal of Physical*
 1283 *Oceanography*, 47(4), 867–878.
- 1284 Bebieva, Y., & Timmermans, M.-L. (2019). Double-diffusive layering in the Canada
 1285 Basin: An explanation of along-layer temperature and salinity gradients. *Jour-*
 1286 *nal of Geophysical Research: Oceans*, 124(1), 723–735.
- 1287 Belkin, I. M., & Levitus, S. (1996). Temporal variability of the subarctic front near
 1288 the Charlie-Gibbs Fracture Zone. *Journal of Geophysical Research: Oceans*,
 1289 101(C12), 28317–28324.
- 1290 Belkin, I. M., Levitus, S., Antonov, J., & Malmberg, S.-A. (1998). “great salinity
 1291 anomalies” in the North Atlantic. *Progress in Oceanography*, 41(1), 1–68.
- 1292 Beszczynska-Möller, A., Fahrbach, E., Schauer, U., & Hansen, E. (2012). Variabil-
 1293 ity in Atlantic water temperature and transport at the entrance to the Arctic

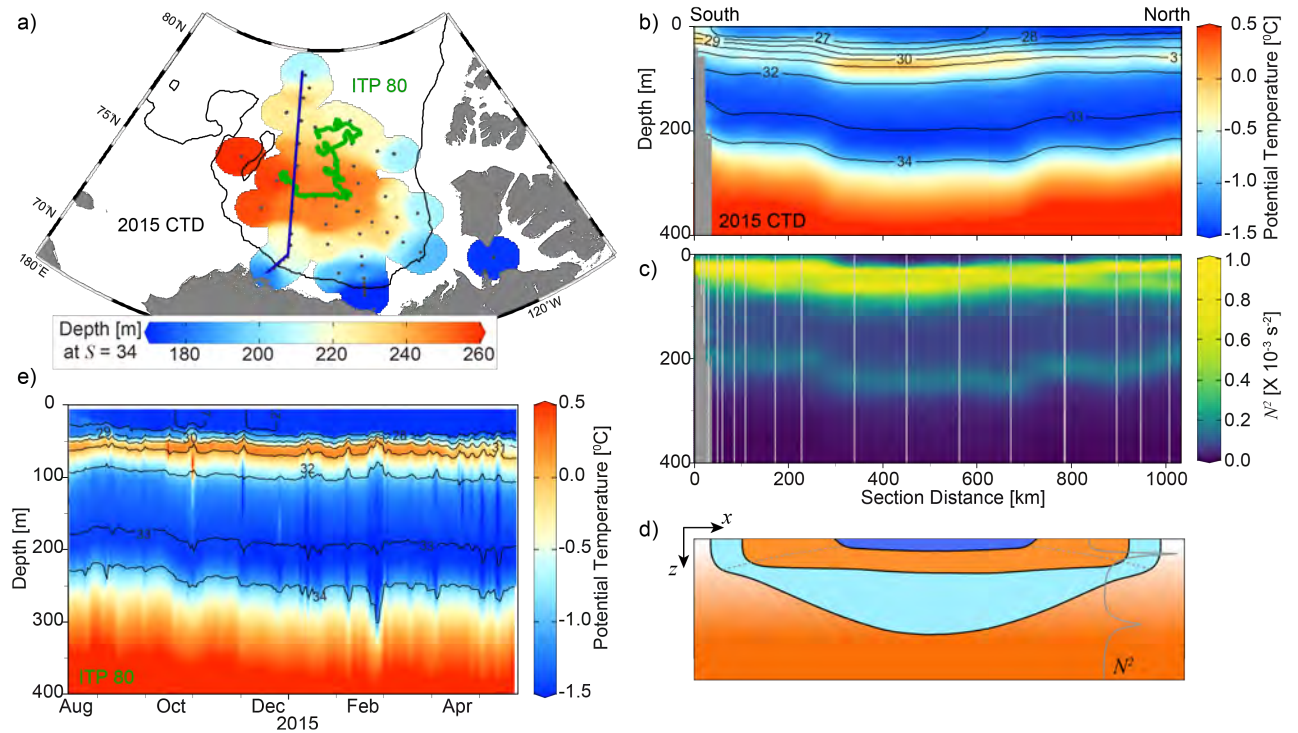


Figure 10. a) Depth of the $S=34$ isohaline from the 2015 Beaufort Gyre hydrographic expedition; CTD station locations are indicated by black dots. Sections from 2015 CTD data of b) potential temperature ($^{\circ}\text{C}$, colors) and salinity (black contours) and c) buoyancy frequency (N^2 , s^{-2}) from south (left) to north (right) along the blue line shown in panel a). d) Schematic cross section of the Beaufort Gyre where black lines represent isopycnals and colors represent temperature (blues, cold and oranges, warm); a layered configuration is shown to approximate the continuous stratification of the Beaufort Gyre, while the grey contour represents a typical stratification profile; grey dashed lines mark the base of the mixed layer. e) Depth-time section of potential temperature ($^{\circ}\text{C}$, colors) and salinity (black contours) from an Ice-Tethered Profiler (ITP) that sampled in the Canada Basin in 2014-2015 along the green drift track shown in a), where the ITP drifted from north (August 2014) to south (May 2015).

1294 Ocean, 1997–2010. *ICES Journal of Marine Science*, 69(5), 852–863.

1295 Boyd, T. J., Steele, M., Muench, R. D., & Gunn, J. T. (2002). Partial recovery of
1296 the Arctic Ocean halocline. *Geophysical Research Letters*, 29(14), 2–1.

1297 Boyer, T. P. (2018). World ocean database 2018. *NOAA Atlas NESDIS 87*.

1298 Bretherton, F. P., & Haidvogel, D. B. (1976). Two-dimensional turbulence above to-
1299 pography. *Journal of Fluid Mechanics*, 78(1), 129–154.

1300 Carmack, E., Aagaard, K., Swift, J., Perkin, R., McLaughlin, F., Macdonald, R., &
1301 Jones, E. (1998). Thermohaline transitions. *Coastal and Estuarine Studies*,
1302 179–186.

1303 Carmack, E., Polyakov, I., Padman, L., Fer, I., Hunke, E., Hutchings, J., . . . others
1304 (2015). Toward quantifying the increasing role of oceanic heat in sea ice loss
1305 in the new Arctic. *Bulletin of the American Meteorological Society*, 96(12),
1306 2079–2105.

1307 Carmack, E. C. (2000). The Arctic Ocean’s freshwater budget: Sources, storage and
1308 export. In *The freshwater budget of the Arctic Ocean* (pp. 91–126). Springer.

1309 Carmack, E. C. (2007). The alpha/beta ocean distinction: A perspective on fresh-
1310 water fluxes, convection, nutrients and productivity in high-latitude seas. *Deep*
1311 *Sea Research Part II: Topical Studies in Oceanography*, 54(23), 2578–2598.

1312 Carmack, E. C., Yamamoto-Kawai, M., Haine, T. W., Bacon, S., Bluhm, B. A.,
1313 Lique, C., . . . others (2016). Freshwater and its role in the Arctic marine
1314 System: Sources, disposition, storage, export, and physical and biogeochemical
1315 consequences in the Arctic and global oceans. *Journal of Geophysical Research:*
1316 *Biogeosciences*, 121(3), 675–717.

1317 Carpenter, J. R., & Timmermans, M.-L. (2012). Deep mesoscale eddies in the
1318 Canada Basin, Arctic Ocean. *Geophysical Research Letters*, 39(20), 1–
1319 6. Retrieved from <http://doi.wiley.com/10.1029/2012GL053025> doi:
1320 10.1029/2012GL053025

1321 Cavalieri, D. J., & Martin, S. (1994). The contribution of alaskan, Siberian, and
1322 canadian coastal polynyas to the cold halocline layer of the Arctic Ocean.
1323 *Journal of Geophysical Research: Oceans*, 99(C9), 18343–18362.

1324 Chelton, D. B., Deszoeke, R. A., Schlax, M. G., El Naggar, K., & Siwertz, N. (1998).
1325 Geographical variability of the first baroclinic Rossby radius of deformation.
1326 *Journal of Physical Oceanography*, 28(3), 433–460.

- 1327 Coachman, L., & Barnes, C. (1963). The movement of Atlantic water in the Arctic
1328 Ocean. *Arctic*, *16*(1), 8–16.
- 1329 Coachman, L. K. (1969). Physical oceanography in the Arctic Ocean: 1968. *Arctic*,
1330 *22*(3), 214–224.
- 1331 Cochran, J. R., Edwards, M. H., & Coakley, B. J. (2006). Morphology and structure
1332 of the Lomonosov Ridge, Arctic Ocean. *Geochemistry, Geophysics, Geosys-*
1333 *tems*, *7*(5).
- 1334 Collins, M., Knutti, R., Arblaster, J., Dufresne, J.-L., Fichet, T., Friedlingstein,
1335 P., . . . Wehner, M. (2013). Long-term climate change: Projections, commit-
1336 ments and irreversibility [Book Section]. In T. Stocker et al. (Eds.), *Climate*
1337 *change 2013: The physical science basis. contribution of working group i to*
1338 *the fifth assessment report of the intergovernmental panel on climate change*
1339 (p. 1029–1136). Cambridge, United Kingdom and New York, NY, USA: Cam-
1340 bridge University Press. Retrieved from www.climatechange2013.org doi:
1341 10.1017/CBO9781107415324.024
- 1342 Comiso, J. C. (2012). Large decadal decline of the Arctic multiyear ice cover. *Jour-*
1343 *nal of Climate*, *25*(4), 1176–1193.
- 1344 Danielson, S. L., Weingartner, T. J., Hedstrom, K. S., Aagaard, K., Woodgate, R.,
1345 Curchitser, E., & Stabeno, P. J. (2014). Coupled wind-forced controls of the
1346 Bering–Chukchi shelf circulation and the Bering Strait throughflow: Ekman
1347 transport, continental shelf waves, and variations of the Pacific–Arctic sea
1348 surface height gradient. *Progress in Oceanography*, *125*, 40–61.
- 1349 D’Asaro, E. A., & Morison, J. H. (1992). Internal waves and mixing in the Arc-
1350 tic Ocean. *Deep Sea Research Part A. Oceanographic Research Papers*, *39*(2),
1351 S459–S484.
- 1352 Davis, P. E. D., Lique, C., & Johnson, H. L. (2014). On the link between Arc-
1353 tic sea ice decline and the freshwater content of the Beaufort Gyre: Insights
1354 from a simple process model. *Journal of Climate*, *27*(21), 8170–8184. doi:
1355 10.1175/JCLI-D-14-00090.1
- 1356 Delworth, T. L., Zeng, F., Vecchi, G. A., Yang, X., Zhang, L., & Zhang, R. (2016).
1357 The North Atlantic Oscillation as a driver of rapid climate change in the
1358 Northern Hemisphere. *Nature Geoscience*, *9*(7), 509.
- 1359 de Steur, L., Hansen, E., Mauritzen, C., Beszczynska-Möller, A., & Fahrback, E.

- 1360 (2014). Impact of recirculation on the East Greenland Current in Fram Strait:
1361 Results from moored current meter measurements between 1997 and 2009.
1362 *Deep Sea Research Part I: Oceanographic Research Papers*, 92, 26–40.
- 1363 Dewar, W. K. (1998). Topography and barotropic transport control by bottom fric-
1364 tion. *Journal of marine research*, 56(2), 295–328.
- 1365 Dewey, S., Morison, J., Kwok, R., Dickinson, S., Morison, D., & Andersen, R. (2018,
1366 2). Arctic Ice-Ocean Coupling and Gyre Equilibration Observed With Remote
1367 Sensing. *Geophysical Research Letters*. Retrieved from [http://doi.wiley](http://doi.wiley.com/10.1002/2017GL076229)
1368 [.com/10.1002/2017GL076229](http://doi.wiley.com/10.1002/2017GL076229) doi: 10.1002/2017GL076229
- 1369 Dmitrenko, I. A., Kirillov, S. A., Forest, A., Gratton, Y., Volkov, D. L., Williams,
1370 W. J., ... Barber, D. G. (2016). Shelfbreak current over the canadian Beau-
1371 fort Sea continental slope: Wind-driven events in January 2005. *Journal of*
1372 *Geophysical Research: Oceans*, 121(4), 2447–2468.
- 1373 Dosser, H. V., & Rainville, L. (2016). Dynamics of the changing near-inertial inter-
1374 nal wave field in the Arctic Ocean. *Journal of Physical Oceanography*, 46(2),
1375 395–415.
- 1376 Dosser, H. V., Rainville, L., & Toole, J. M. (2014). Near-inertial internal wave field
1377 in the Canada Basin from ice-tethered profilers. *Journal of Physical Oceanog-*
1378 *raphy*, 44(2), 413–426.
- 1379 Dosser, H. V., & Timmermans, M.-L. (2018). Inferring circulation and lateral
1380 eddy fluxes in the Arctic Ocean’s deep Canada Basin using an inverse method.
1381 *Journal of Physical Oceanography*, 48(2), 245–260.
- 1382 Ekman, V. W., et al. (1905). On the influence of the Earth’s rotation on ocean-
1383 currents. *Almqvist & Wiksells boktryckeri, A.-B.*,
- 1384 Eldevik, T., & Nilsen, J. E. Ø. (2013). The Arctic–Atlantic thermohaline circulation.
1385 *Journal of Climate*, 26(21), 8698–8705.
- 1386 Fer, I. (2009). Weak vertical diffusion allows maintenance of cold halocline in the
1387 central Arctic. *Atmospheric and Oceanic Science Letters*, 2(3), 148–152.
- 1388 Fetterer, F., Knowles, K., Meier, W., Savoie, M., & Windnagel, A. (2017). Updated
1389 daily Sea Ice Index version 3 Boulder Colorado USA. *NSIDC: National Snow*
1390 *and Ice Data Center*. doi: 10.7265/N5K072F8
- 1391 Garcia, H., Boyer, T., Baranova, O., Locarnini, R., Mishonov, A., Grodsky, A., ...
1392 Zweng, M. (2019). World Ocean Atlas 2018: Product documentation. *Ocean*

- 1393 *Climate Laboratory NCEI, NESDIS, NOAA.*
- 1394 Garrett, C., & Horne, E. (1978). Frontal circulation due to cabbeling and double dif-
1395 fusion. *Journal of Geophysical Research: Oceans*, 83(C9), 4651–4656.
- 1396 Gent, P. R., & McWilliams, J. C. (1990). Isopycnal mixing in ocean circulation mod-
1397 els. *Journal of Physical Oceanography*, 20(1), 150–155.
- 1398 Gray, A. R., & Riser, S. C. (2014). A global analysis of Sverdrup balance using
1399 absolute geostrophic velocities from Argo. *Journal of Physical Oceanography*,
1400 44(4), 1213–1229.
- 1401 Guthrie, J. D., Fer, I., & Morison, J. (2015). Observational validation of the dif-
1402 fusive convection flux laws in the Amundsen Basin, Arctic Ocean. *Journal of*
1403 *Geophysical Research: Oceans*, 120(12), 7880–7896.
- 1404 Haine, T. W., & Martin, T. (2017). The Arctic-Subarctic sea ice system is entering a
1405 seasonal regime: Implications for future Arctic amplification. *Scientific reports*,
1406 7(1), 4618.
- 1407 Haine, T. W. N., Curry, B., Gerdes, R., Hansen, E., Karcher, M., Lee, C., . . .
1408 Woodgate, R. (2015). Arctic freshwater export: Status, mechanisms,
1409 and prospects. *Global and Planetary Change*, 125, 13–35. Retrieved
1410 from <http://dx.doi.org/10.1016/j.gloplacha.2014.11.013> doi:
1411 10.1016/j.gloplacha.2014.11.013
- 1412 Halle, C., & Pinkel, R. (2003). Internal wave variability in the Beaufort Sea during
1413 the winter of 1993/1994. *Journal of Geophysical Research: Oceans*, 108(C7).
- 1414 Hansen, B., Østerhus, S., Turrell, W. R., Jónsson, S., Valdimarsson, H., Hátún, H.,
1415 & Olsen, S. M. (2008). The inflow of Atlantic water, heat, and salt to the
1416 Nordic seas across the Greenland–Scotland ridge. In *Arctic–Subarctic ocean*
1417 *fluxes* (pp. 15–43). Springer.
- 1418 Holloway, G. (1992). Representing topographic stress for large-scale ocean models.
1419 *Journal of Physical Oceanography*, 22(9), 1033–1046.
- 1420 Holloway, G. (2004). From classical to statistical ocean dynamics. *Surveys in Geo-*
1421 *physics*, 25(3-4), 203–219.
- 1422 Holloway, G., & Proshutinsky, A. (2007). Role of tides in Arctic ocean/ice climate.
1423 *Journal of Geophysical Research: Oceans*, 112(C4).
- 1424 Holmes, R. M., McClelland, J. W., Peterson, B. J., Tank, S. E., Bulygina, E., Eglin-
1425 ton, T. I., . . . others (2012). Seasonal and annual fluxes of nutrients and

1426 organic matter from large rivers to the Arctic Ocean and surrounding seas.
1427 *Estuaries and Coasts*, 35(2), 369–382.

1428 Hughes, C. W., Meredith, M. P., & Heywood, K. J. (1999). Wind-driven trans-
1429 port fluctuations through drake passage: A southern mode. *Journal of Physical*
1430 *Oceanography*, 29(8), 1971–1992.

1431 Hunkins, K. L. (1974). Subsurface eddies in the arctic ocean. In *Deep sea research*
1432 *and oceanographic abstracts* (Vol. 21, pp. 1017–1033).

1433 Ingvaldsen, R., Loeng, H., & Asplin, L. (2002). Variability in the Atlantic inflow to
1434 the barents Sea based on a one-year time series from moored current meters.
1435 *Continental Shelf Research*, 22(3), 505–519.

1436 Isachsen, P., LaCasce, J., Mauritzen, C., & Häkkinen, S. (2003). Wind-driven
1437 variability of the large-scale recirculating flow in the Nordic Seas and Arctic
1438 Ocean. *Journal of Physical Oceanography*, 33(12), 2534–2550.

1439 Iselin, C. (1939). The influence of vertical and lateral turbulence on the character-
1440 istics of the waters at mid-depths. *Eos Trans. Am. Geophys. Union*, 20, 414–
1441 417.

1442 Ivanov, V., Alexeev, V., Koldunov, N. V., Repina, I., Sandø, A. B., Smedsrud, L. H.,
1443 & Smirnov, A. (2016). Arctic Ocean heat impact on regional ice decay: A sug-
1444 gested positive feedback. *Journal of Physical Oceanography*, 46(5), 1437–1456.

1445 Ivanov, V., Shapiro, G., Huthnance, J., Aleynik, D., & Golovin, P. (2004). Dense
1446 water cascades around the world ocean. *Progress in Oceanography*, 60, 47–98.

1447 Ivanov, V. V., & Golovin, P. N. (2007). Observations and modeling of dense water
1448 cascading from the northwestern laptev sea shelf. *Journal of Geophysical Re-*
1449 *search: Oceans*, 112(C9).

1450 Jakobsson, M., & Macnab, R. (2006). A comparison between GEBCO sheet 5.17
1451 and the International Bathymetric Chart of the Arctic Ocean (IBCAO) version
1452 1.0. *Marine Geophysical Researches*, 27(1), 35–48.

1453 Jakobsson, M., Macnab, R., Mayer, L., Anderson, R., Edwards, M., Hatzky, J., ...
1454 Johnson, P. (2008). An improved bathymetric portrayal of the Arctic Ocean:
1455 Implications for ocean modeling and geological, geophysical and oceanographic
1456 analyses. *Geophysical Research Letters*, 35(7).

1457 Jakobsson, M., Mayer, L., Coakley, B., Dowdeswell, J. A., Forbes, S., Fridman, B.,
1458 ... others (2012). The international bathymetric chart of the Arctic Ocean

- 1459 (ibcao) version 3.0. *Geophysical Research Letters*, 39(12).
- 1460 Johnson, H. L., Cornish, S. B., Kostov, Y., Beer, E., & Lique, C. (2018). Arctic
1461 Ocean freshwater content and its decadal memory of sea-level pressure. *Geo-*
1462 *physical Research Letters*, 45(10), 4991–5001.
- 1463 Kalnay, E., Kanamitsu, M., Kistler, R., Collins, W., Deaven, D., Gandin, L., . . .
1464 others (1996). The NCEP/NCAR 40-year reanalysis project. *Bulletin of the*
1465 *American meteorological Society*, 77(3), 437–472.
- 1466 Karcher, M., Kauker, F., Gerdes, R., Hunke, E., & Zhang, J. (2007). On the dy-
1467 namics of Atlantic water circulation in the Arctic Ocean. *Journal of Geophysi-*
1468 *cal Research: Oceans*, 112(C4).
- 1469 Kowalik, Z., & Proshutinsky, A. Y. (1993). Diurnal tides in the Arctic Ocean. *Jour-*
1470 *nal of Geophysical Research: Oceans*, 98(C9), 16449–16468.
- 1471 Kowalik, Z., & Proshutinsky, A. Y. (1995). Topographic enhancement of tidal mo-
1472 tion in the western Barents Sea. *Journal of Geophysical Research: Oceans*,
1473 100(C2), 2613–2637.
- 1474 Kozlov, I., Artamonova, A., Manucharyan, G., & Kubryakov, A. (2019). Eddies in
1475 the western Arctic Ocean from spaceborne SAR observations over open ocean
1476 and marginal ice zones. *Journal of Geophysical Research: Oceans*.
- 1477 Krishfield, R., Toole, J., Proshutinsky, A., & Timmermans, M.-L. (2008). Auto-
1478 mated ice-tethered profilers for seawater observations under pack ice in all
1479 seasons. *Journal of Atmospheric and Oceanic Technology*, 25(11), 2091–2105.
1480 doi: 10.1175/2008JTECHO587.1
- 1481 Krishfield, R. A., & Perovich, D. K. (2005). Spatial and temporal variability of
1482 oceanic heat flux to the Arctic ice pack. *Journal of Geophysical Research:*
1483 *Oceans*, 110(C7).
- 1484 Krishfield, R. A., Proshutinsky, A., Tateyama, K., Williams, W. J., Carmack, E. C.,
1485 McLaughlin, F. A., & Timmermans, M.-L. (2014). Deterioration of perennial
1486 sea ice in the Beaufort Gyre from 2003 to 2012 and its impact on the oceanic
1487 freshwater cycle. *Journal of Geophysical Research: Oceans*, 119(2), 1271–1305.
1488 doi: 10.1002/2013JC008999
- 1489 Kwok, R. (2009). Outflow of Arctic Ocean sea ice into the Greenland and Barents
1490 Seas: 1979–2007. *Journal of Climate*, 22(9), 2438–2457.
- 1491 Kwok, R. (2018). Arctic sea ice thickness, volume, and multiyear ice coverage: losses

- 1492 and coupled variability (1958–2018). *Environmental Research Letters*, *13*(10),
1493 105005.
- 1494 Kwok, R., Spreen, G., & Pang, S. (2013). Arctic sea ice circulation and drift speed:
1495 Decadal trends and ocean currents. *Journal of Geophysical Research: Oceans*,
1496 *118*(5), 2408–2425.
- 1497 LaCasce, J., Nøst, O., & Isachsen, P. (2008). Asymmetry of free circulations in
1498 closed ocean gyres. *Journal of physical oceanography*, *38*(2), 517–526.
- 1499 Lambert, E., Eldevik, T., & Haugan, P. M. (2016). How northern freshwater in-
1500 put can stabilise thermohaline circulation. *Tellus A: Dynamic Meteorology and*
1501 *Oceanography*, *68*(1), 31051.
- 1502 LeBlond, P. H. (1980). On the surface circulation in some channels of the Canadian
1503 Arctic archipelago. *Arctic*, 189–197.
- 1504 Ledwell, J., Montgomery, E., Polzin, K., Laurent, L. S., Schmitt, R., & Toole, J.
1505 (2000). Evidence for enhanced mixing over rough topography in the abyssal
1506 ocean. *Nature*, *403*(6766), 179.
- 1507 Lenn, Y.-D., Wiles, P., Torres-Valdes, S., Abrahamsen, E., Rippeth, T., Simpson,
1508 J., ... others (2009). Vertical mixing at intermediate depths in the Arctic
1509 boundary current. *Geophysical Research Letters*, *36*(5).
- 1510 Lincoln, B. J., Rippeth, T. P., Lenn, Y.-D., Timmermans, M. L., Williams, W. J.,
1511 & Bacon, S. (2016). Wind-driven mixing at intermediate depths in an ice-free
1512 Arctic Ocean. *Geophysical Research Letters*, *43*(18), 9749–9756.
- 1513 Lind, S., Ingvaldsen, R. B., & Furevik, T. (2018). Arctic warming hotspot in
1514 the northern Barents Sea linked to declining sea-ice import. *Nature climate*
1515 *change*, *8*(7), 634.
- 1516 Lique, C., Johnson, H. L., & Davis, P. E. D. (2015). On the Interplay between
1517 the Circulation in the Surface and the Intermediate Layers of the Arctic
1518 Ocean. *Journal of Physical Oceanography*, *45*(5), 1393–1409. Retrieved
1519 from <http://journals.ametsoc.org/doi/10.1175/JPO-D-14-0183.1> doi:
1520 10.1175/JPO-D-14-0183.1
- 1521 Luneva, M. V., Aksenov, Y., Harle, J. D., & Holt, J. T. (2015). The effects of
1522 tides on the water mass mixing and sea ice in the Arctic Ocean. *Journal of*
1523 *Geophysical Research: Oceans*, *120*(10), 6669–6699.
- 1524 Luyten, J., Pedlosky, J., & Stommel, H. (1983). The ventilated thermocline. *J.*

- 1525 *Phys. Oceanogr.*, *13*, 292–309.
- 1526 Manley, T. O., & Hunkins, K. (1985). Mesoscale Eddies of the Arctic Ocean. *Jour-*
1527 *nal of Geophysical Research C Oceans*, *90*(C3), 19. Retrieved from [http://](http://onlinelibrary.wiley.com/doi/10.1029/JC090iC03p04911/abstract)
1528 onlinelibrary.wiley.com/doi/10.1029/JC090iC03p04911/abstract doi:
1529 10.1029/JC090iC03p04911
- 1530 Manucharyan, G., & Isachsen, P. (2019). Critical role of continental slopes in halo-
1531 cline and eddy dynamics of the ekman-driven Beaufort Gyre. *Journal of Geo-*
1532 *physical Research: Oceans*, *124*(4), 2679–2696.
- 1533 Manucharyan, G. E., Spall, M. A., & Thompson, A. F. (2016). A Theory of the
1534 Wind-Driven Beaufort Gyre Variability. *Journal of Physical Oceanogra-*
1535 *phy*(2013), 3263–3278. doi: 10.1175/JPO-D-16-0091.1
- 1536 Manucharyan, G. E., Thompson, A. F., & Spall, M. A. (2017). Eddy Memory
1537 Mode of Multidecadal Variability in Residual-Mean Ocean Circulations with
1538 Application to the Beaufort Gyre. *Journal of Physical Oceanography*, *47*(4),
1539 855–866. Retrieved from [http://journals.ametsoc.org/doi/10.1175/](http://journals.ametsoc.org/doi/10.1175/JPO-D-16-0194.1)
1540 [JPO-D-16-0194.1](http://journals.ametsoc.org/doi/10.1175/JPO-D-16-0194.1) doi: 10.1175/JPO-D-16-0194.1
- 1541 Marshall, J., Jamous, D., & Nilsson, J. (2001). Entry, flux, and exit of potential vorticity in ocean circulation. *Journal of physical oceanography*, *31*(3), 777–789.
- 1542 Marshall, J., & Radko, T. (2003). Residual-mean solutions for the Antarctic Circumpolar Current and its associated overturning circulation. *Journal of Physical Oceanography*, *33*(11), 2341–2354.
- 1543 Marshall, J., Scott, J., & Proshutinsky, A. (2017). “climate response functions” for
1544 the Arctic Ocean: a proposed coordinated modelling experiment. *Geoscientific*
1545 *Model Development*, *10*(7).
- 1546 Marshall, J., & Speer, K. (2012). Closure of the meridional overturning circulation
1547 through Southern Ocean upwelling. *Nature Geoscience*, *5*(3), 171.
- 1548 Marshall, J., Schlosser, P., Newton, R., Smethie Jr, W., Bayer, R., Rhein, M., &
1549 Jones, E. P. (2010). The velocity and mixing time scale of the Arctic Ocean
1550 Boundary Current estimated with transient tracers. *Journal of Geophysical*
1551 *Research: Oceans*, *115*(C8).
- 1552 Mauritzen, C. (1996). Production of dense overflow waters feeding the North At-
1553 lantic across the Greenland-Scotland ridge. part 2: An inverse model. *Deep Sea*
1554 *Research Part I: Oceanographic Research Papers*, *43*(6), 807–835.
- 1555
1556
1557

- 1558 Maykut, G., & McPhee, M. G. (1995). Solar heating of the Arctic mixed layer. *Journal of Geophysical Research: Oceans*, *100*(C12), 24691–24703.
- 1559
- 1560 Maykut, G. A., & Untersteiner, N. (1971). Some results from a time-dependent
1561 thermodynamic model of sea ice. *Journal of Geophysical Research*, *76*(6),
1562 1550–1575.
- 1563 McClelland, J. W., Holmes, R., Dunton, K., & Macdonald, R. (2012). The Arctic
1564 Ocean estuary. *Estuaries and Coasts*, *35*(2), 353–368.
- 1565 McLaughlin, F., Carmack, E., Macdonald, R., & Bishop, J. (1996). Physical and
1566 geochemical properties across the Atlantic/Pacific water mass front in the
1567 southern Canadian Basin. *Journal of Geophysical Research: Oceans*, *101*(C1),
1568 1183–1197.
- 1569 McLaughlin, F., Carmack, E., Macdonald, R., Melling, H., Swift, J., Wheeler, P., ...
1570 Sherr, E. (2004). The joint roles of Pacific and Atlantic-origin waters in the
1571 Canada Basin, 1997–1998. *Deep Sea Research Part I: Oceanographic Research*
1572 *Papers*, *51*(1), 107–128.
- 1573 McLaughlin, F. A., Carmack, E. C., Williams, W. J., Zimmermann, S., Shimada,
1574 K., & Itoh, M. (2009). Joint effects of boundary currents and thermohaline
1575 intrusions on the warming of Atlantic water in the Canada Basin, 1993–2007.
1576 *Journal of Geophysical Research: Oceans*, *114*(C1).
- 1577 McPhee, M. G. (2013). Intensification of geostrophic currents in the Canada Basin,
1578 Arctic Ocean. *Journal of Climate*, *26*(10), 3130–3138. doi: 10.1175/JCLI-D-12
1579 -00289.1
- 1580 Meneghello, G., Doddridge, E., Marshall, J., Scott, J., & Campin, J.-M. (2020).
1581 Exploring the role of the “ice–ocean governor” and mesoscale eddies in the
1582 equilibration of the Beaufort Gyre: Lessons from observations. *Journal of*
1583 *Physical Oceanography*, *50*(1), 269–277.
- 1584 Meneghello, G., Marshall, J., Campin, J.-M., Doddridge, E., & Timmermans, M.-L.
1585 (2018). The ice-ocean governor: Ice-ocean stress feedback limits Beaufort Gyre
1586 spin-up. *Geophysical Research Letters*, *45*(20), 11–293.
- 1587 Meneghello, G., Marshall, J., Cole, S. T., & Timmermans, M.-L. (2017, 11).
1588 Observational inferences of lateral eddy diffusivity in the halocline of the
1589 Beaufort Gyre. *Geophysical Research Letters*, *44*. Retrieved from [http://](http://doi.wiley.com/10.1002/2017GL075126)
1590 doi.wiley.com/10.1002/2017GL075126 doi: 10.1002/2017GL075126

- 1591 Meneghello, G., Marshall, J., Timmermans, M.-L., & Scott, J. (2018). Observations
1592 of seasonal upwelling and downwelling in the Beaufort Sea mediated by sea ice.
1593 *J. Phys. Oceanogr.*, *in press*. doi: 10.1175/JPO-D-17-0188.1
- 1594 Mensa, J., Timmermans, M.-L., Kozlov, I., Williams, W., & Özgökmen, T. (2018).
1595 Surface drifter observations from the Arctic Ocean’s Beaufort Sea: Evidence
1596 for submesoscale dynamics. *Journal of Geophysical Research: Oceans*, *123*(4),
1597 2635–2645.
- 1598 Moore, G., Schweiger, A., Zhang, J., & Steele, M. (2018). Collapse of the 2017 win-
1599 ter Beaufort High: A response to thinning sea ice? *Geophysical Research Let-
1600 ters*, *45*(6), 2860–2869.
- 1601 Morison, J., Kwok, R., Peralta-Ferriz, C., Alkire, M., Rigor, I., Andersen, R., &
1602 Steele, M. (2012). Changing Arctic Ocean freshwater pathways. *Nature*,
1603 *481*(7379), 66.
- 1604 Morison, J., Long, C., & Levine, M. (1985). The dissipation of internal wave energy
1605 under Arctic ice. *J. Geophys. Res.*, *90*, 11–959.
- 1606 Morison, J., Steele, M., & Andersen, R. (1998). Hydrography of the upper Arc-
1607 tic Ocean measured from the nuclear submarine USS pargo. *Deep Sea Research
1608 Part I: Oceanographic Research Papers*, *45*(1), 15–38.
- 1609 Morison, J., Steele, M., Kikuchi, T., Falkner, K., & Smethie, W. (2006). Relaxation
1610 of central Arctic Ocean hydrography to pre-1990s climatology. *Geophysical Re-
1611 search Letters*, *33*(17).
- 1612 Moros, M., Jansen, E., Oppo, D. W., Giraudeau, J., & Kuijpers, A. (2012). Recon-
1613 struction of the late-holocene changes in the sub-Arctic front position at the
1614 Reykjanes Ridge, North Atlantic. *The Holocene*, *22*(8), 877–886.
- 1615 Muilwijk, M., Ilicak, M., Cornish, S. B., Danilov, S., Gelderloos, R., Gerdes, R., ...
1616 others (2019). Arctic Ocean response to greenland sea wind anomalies in a
1617 suite of model simulations. *Journal of Geophysical Research: Oceans*.
- 1618 Muilwijk, M., Smedsrud, L. H., Ilicak, M., & Drange, H. (2018). Atlantic water heat
1619 transport variability in the 20th century Arctic Ocean from a global ocean
1620 model and observations. *Journal of Geophysical Research: Oceans*, *123*(11),
1621 8159–8179.
- 1622 Münchow, A., Melling, H., & Falkner, K. K. (2006). An observational estimate of
1623 volume and freshwater flux leaving the Arctic Ocean through Nares Strait.

- 1624 *Journal of Physical Oceanography*, 36(11), 2025–2041.
- 1625 Munk, W. H. (1950). On the wind-driven ocean circulation. *Journal of meteorology*,
1626 7(2), 80–93.
- 1627 Nansen, F. (1897). Some results of the Norwegian Arctic expedition, 1893–96. *Scot-*
1628 *tish Geographical Magazine*, 13(5), 225–246.
- 1629 Nansen, F. (1902). The oceanography of the North Polar Basin. the Norwegian
1630 North Polar Expedition 1893-1896. *Scient. Results*, 3(9).
- 1631 Nazarenko, L., Holloway, G., & Tausnev, N. (1998). Dynamics of transport of
1632 “Atlantic signature” in the Arctic Ocean. *Journal of Geophysical Research:*
1633 *Oceans*, 103(C13), 31003–31015.
- 1634 Nikolopoulos, A., Pickart, R. S., Fratantoni, P. S., Shimada, K., Torres, D. J., &
1635 Jones, E. P. (2009). The western Arctic boundary current at 152 w: Struc-
1636 ture, variability, and transport. *Deep Sea Research Part II: Topical Studies in*
1637 *Oceanography*, 56(17), 1164–1181.
- 1638 Nøst, O. A., & Isachsen, P. E. (2003). The large-scale time-mean ocean circula-
1639 tion in the Nordic Seas and Arctic Ocean estimated from simplified dynamics.
1640 *Journal of Marine Research*, 61(2), 175–210.
- 1641 Nurser, A. J. G., & Bacon, S. (2014). The Rossby radius in the Arctic Ocean. *Ocean*
1642 *Science*, 10(6), 967–975. doi: 10.5194/os-10-967-2014
- 1643 Oldenburg, D., Armour, K. C., Thompson, L., & Bitz, C. M. (2018). Distinct mech-
1644 anisms of ocean heat transport into the Arctic under internal variability and
1645 climate change. *Geophysical Research Letters*, 45(15), 7692–7700.
- 1646 Onarheim, I. H., Eldevik, T., Smedsrud, L. H., & Stroeve, J. C. (2018). Seasonal
1647 and regional manifestation of Arctic sea ice loss. *Journal of Climate*, 31(12),
1648 4917–4932.
- 1649 Orvik, K. A., & Niiler, P. (2002). Major pathways of atlantic water in the northern
1650 North Atlantic and Nordic Seas toward Arctic. *Geophysical Research Letters*,
1651 29(19), 2–1.
- 1652 Östlund, H. G., Possnert, G., & Swift, J. H. (1987). Ventilation rate of the deep
1653 arctic ocean from carbon 14 data. *Journal of Geophysical Research: Oceans*,
1654 92(C4), 3769–3777.
- 1655 Overland, J., Hanna, E., Hanssen-Bauer, I., Kim, S.-J., Walsh, J., Wang, M., &
1656 Bhatt, U. (2019). [the Arctic] surface air temperature [in “State of the

- 1657 Climate in 2018”]. *Bull. Amer. Meteor. Soc.*, 100(9), S142–S144. doi:
1658 10.1175/2019BAMSStateoftheClimate.1
- 1659 Padman, L. (1995). Small-scale physical processes in the Arctic Ocean. *COASTAL*
1660 *AND ESTUARINE STUDIES*, 97–97.
- 1661 Padman, L., & Dillon, T. M. (1987). Vertical heat fluxes through the Beaufort Sea
1662 thermohaline staircase. *Journal of Geophysical Research: Oceans*, 92(C10),
1663 10799–10806.
- 1664 Padman, L., & Dillon, T. M. (1989). Thermal microstructure and internal waves
1665 in the Canada Basin diffusive staircase. *Deep Sea Research Part A. Oceanographic Research Papers*, 36(4), 531–542.
- 1667 Padman, L., Plueddemann, A. J., Muench, R. D., & Pinkel, R. (1992). Diurnal tides
1668 near the Yermak Plateau. *Journal of Geophysical Research: Oceans*, 97(C8),
1669 12639–12652.
- 1670 Peralta-Ferriz, C., & Woodgate, R. A. (2015). Seasonal and interannual variability
1671 of pan-arctic surface mixed layer properties from 1979 to 2012 from hydro-
1672 graphic data, and the dominance of stratification for multiyear mixed layer
1673 depth shoaling. *Progress in Oceanography*, 134, 19–53.
- 1674 Peralta-Ferriz, C., & Woodgate, R. A. (2017). The dominant role of the east
1675 Siberian Sea in driving the oceanic flow through the bering Strait—conclusions
1676 from GRACE ocean mass satellite data and in situ mooring observations be-
1677 tween 2002 and 2016. *Geophysical Research Letters*, 44(22).
- 1678 Perner, K., Moros, M., Jansen, E., Kuijpers, A., Troelstra, S. R., & Prins, M. A.
1679 (2018). Subarctic front migration at the Reykjanes Ridge during the mid-to
1680 late holocene: evidence from planktic foraminifera. *Boreas*, 47(1), 175–188.
- 1681 Perovich, D., Meier, W., Tschudi, M., Farrell, S., Hendricks, S., Gerland, S.,
1682 ... Webster, M. (2019). [the Arctic] sea ice cover [in “State of the Cli-
1683 mate in 2018”]. *Bull. Amer. Meteor. Soc.*, 100(9), S146–S150. doi:
1684 10.1175/2019BAMSStateoftheClimate.1
- 1685 Perovich, D. K., & Richter-Menge, J. A. (2009). Loss of sea ice in the Arctic. *An-
1686 nual review of marine science*, 1, 417–441.
- 1687 Perovich, D. K., Richter-Menge, J. A., Jones, K. F., & Light, B. (2008). Sunlight,
1688 water, and ice: Extreme Arctic sea ice melt during the summer of 2007. *Geo-
1689 physical Research Letters*, 35(11).

1690 Perovich, D. K., Richter-Menge, J. A., Jones, K. F., Light, B., Elder, B. C., Po-
1691 lashenski, C., . . . Lindsay, R. (2011). Arctic sea-ice melt in 2008 and the role
1692 of solar heating. *Annals of Glaciology*, *52*(57), 355–359.

1693 Peterson, A. K., Fer, I., McPhee, M. G., & Randelhoff, A. (2017). Turbulent heat
1694 and momentum fluxes in the upper ocean under Arctic sea ice. *Journal of Geo-*
1695 *physical Research: Oceans*, *122*(2), 1439–1456.

1696 Pickart, R. S. (2004). Shelfbreak circulation in the Alaskan Beaufort Sea: Mean
1697 structure and variability. *Journal of Geophysical Research: Oceans*, *109*(C4).

1698 Pickart, R. S., Nobre, C., Lin, P., Arrigo, K. R., Ashjian, C. J., Berchok, C., . . . oth-
1699 ers (2019). Seasonal to mesoscale variability of water masses and atmospheric
1700 conditions in barrow canyon, chukchi sea. *Deep Sea Research Part II: Topical*
1701 *Studies in Oceanography*.

1702 Pickart, R. S., Weingartner, T. J., Pratt, L. J., Zimmermann, S., & Torres, D. J.
1703 (2005). Flow of winter-transformed Pacific water into the Western Arctic.
1704 *Deep Sea Research Part II: Topical Studies in Oceanography*, *52*(24-26), 3175–
1705 3198.

1706 Pinkel, R. (2005). Near-inertial wave propagation in the western Arctic. *Journal of*
1707 *physical oceanography*, *35*(5), 645–665.

1708 Pistone, K., Eisenman, I., & Ramanathan, V. (2014). Observational determination
1709 of albedo decrease caused by vanishing Arctic sea ice. *Proceedings of the Na-*
1710 *tional Academy of Sciences*, *111*(9), 3322–3326.

1711 Plueddemann, A., Krishfield, R., Takizawa, T., Hatakeyama, K., & Honjo, S. (1998).
1712 Upper ocean velocities in the Beaufort Gyre. *Geophysical research letters*,
1713 *25*(2), 183–186.

1714 Pnyushkov, A., Polyakov, I. V., Padman, L., & Nguyen, A. T. (2018). Structure
1715 and dynamics of mesoscale eddies over the Laptev Sea continental slope in the
1716 Arctic Ocean. *Ocean Science*, *14*(5), 1329–1347.

1717 Polyakov, I. (2001). An eddy parameterization based on maximum entropy produc-
1718 tion with application to modeling of the Arctic Ocean circulation. *Journal of*
1719 *physical oceanography*, *31*(8), 2255–2270.

1720 Polyakov, I. V., Pnyushkov, A. V., Alkire, M. B., Ashik, I. M., Baumann, T. M.,
1721 Carmack, E. C., . . . others (2017). Greater role for atlantic inflows on sea-ice
1722 loss in the Eurasian Basin of the Arctic Ocean. *Science*, *356*(6335), 285–291.

- 1723 Polyakov, I. V., Pnyushkov, A. V., Rember, R., Ivanov, V. V., Lenn, Y.-D., Padman,
1724 L., & Carmack, E. C. (2012). Mooring-based observations of double-diffusive
1725 staircases over the Laptev Sea slope. *Journal of Physical Oceanography*, *42*(1),
1726 95–109.
- 1727 Polyakov, I. V., Timokhov, L. A., Alexeev, V. A., Bacon, S., Dmitrenko, I. A.,
1728 Fortier, L., ... others (2010). Arctic Ocean warming contributes to reduced
1729 polar ice cap. *Journal of Physical Oceanography*, *40*(12), 2743–2756.
- 1730 Proshutinsky, A., Bourke, R., & McLaughlin, F. (2002). The role of the Beaufort
1731 Gyre in Arctic climate variability: Seasonal to decadal climate scales. *Geophys-*
1732 *ical Research Letters*, *29*(23), 15–1.
- 1733 Proshutinsky, A., Dukhovskoy, D., Timmermans, M.-l., Krishfield, R., & Bamber,
1734 J. L. (2015). Arctic circulation regimes. *Philosophical transactions. Series*
1735 *A, Mathematical, physical, and engineering sciences*, *373*(2052), 20140160.
1736 Retrieved from [http://rsta.royalsocietypublishing.org/content/373/](http://rsta.royalsocietypublishing.org/content/373/2052/20140160)
1737 [2052/20140160](http://rsta.royalsocietypublishing.org/content/373/2052/20140160) doi: 10.1098/rsta.2014.0160
- 1738 Proshutinsky, A., Krishfield, R., & Timmermans, M.-L. (2019). Preface to special
1739 issue forum for Arctic Ocean Modeling and Observational Synthesis (FAMOS)
1740 2: Beaufort Gyre phenomenon. *Journal of Geophysical Research: Oceans*.
- 1741 Proshutinsky, A., Krishfield, R., Timmermans, M.-l., Toole, J., Carmack, E.,
1742 McLaughlin, F., ... Shimada, K. (2009). Beaufort Gyre freshwater reservoir :
1743 State and variability from observations. *Journal of Geophysical Research*, *114*,
1744 1–25. doi: 10.1029/2008JC005104
- 1745 Proshutinsky, A. e. a. (2019). Analysis of the Beaufort Gyre freshwater content in
1746 2003-2018. *Journal of Geophysical Research*, *xxx*(xxx), xxx. doi: 1xxx
- 1747 Proshutinsky, A. Y., & Johnson, M. A. (1997). Two circulation regimes of the
1748 wind-driven Arctic Ocean. *Journal of Geophysical Research: Oceans*, *102*(C6),
1749 12493–12514. doi: 10.1029/97JC00738
- 1750 Rabe, B., Karcher, M., Kauker, F., Schauer, U., Toole, J. M., Krishfield, R. A., ...
1751 Su, J. (2014). Arctic Ocean basin liquid freshwater storage trend 1992–2012.
1752 *Geophysical Research Letters*, *41*(3), 961–968.
- 1753 Rainville, L., Lee, C. M., & Woodgate, R. A. (2011). Impact of wind-driven mixing
1754 in the Arctic Ocean. *Oceanography*, *24*(3), 136–145.
- 1755 Rainville, L., & Winsor, P. (2008). Mixing across the Arctic Ocean: Microstructure

1756 observations during the Beringia 2005 expedition. *Geophysical Research Let-*
1757 *ters*, 35(8).

1758 Rainville, L., & Woodgate, R. A. (2009). Observations of internal wave generation in
1759 the seasonally ice-free Arctic. *Geophysical Research Letters*, 36(23).

1760 Reynolds, R. W., Smith, T. M., Liu, C., Chelton, D. B., Casey, K. S., & Schlax,
1761 M. G. (2007). Daily high-resolution-blended analyses for sea surface tempera-
1762 ture. *Journal of Climate*, 20(22), 5473–5496.

1763 Rhines, P. B. (1975). Waves and turbulence on a beta-plane. *Journal of Fluid Me-*
1764 *chanics*, 69(3), 417–443.

1765 Richter-Menge, J., Jeffries, M., & Osborne, E. (2018). The Arctic [in “State of the
1766 Climate in 2017”]. *Bull. Amer. Meteor. Soc.*, 99(8), S143–S173. doi: 10.1175/
1767 2018BAMSSStateoftheClimate.1

1768 Rigor, I. G., Wallace, J. M., & Colony, R. L. (2002). Response of sea ice to the Arc-
1769 tic Oscillation. *Journal of Climate*, 15(18), 2648–2663.

1770 Rippeth, T. P., Lincoln, B. J., Lenn, Y.-D., Green, J. M., Sundfjord, A., & Bacon, S.
1771 (2015). Tide-mediated warming of Arctic halocline by Atlantic heat fluxes over
1772 rough topography. *Nature Geoscience*, 8(3), 191.

1773 Rippeth, T. P., Vlasenko, V., Stashchuk, N., Scannell, B. D., Green, J. M., Lincoln,
1774 B. J., & Bacon, S. (2017). Tidal conversion and mixing poleward of the critical
1775 latitude (an Arctic case study). *Geophysical Research Letters*, 44(24), 12–349.

1776 Roden, G. I. (1970). Aspects of the mid-Pacific transition zone. *Journal of Geophys-*
1777 *ical Research*, 75(6), 1097–1109.

1778 Roden, G. I. (1991). Subarctic-subtropical transition zone of the North Pacific:
1779 large-scale aspects and mesoscale structure. *NOAA Technical Report NMFS*,
1780 105, 1–38.

1781 Rudels, B. (1989). The formation of polar surface water, the ice export and the ex-
1782 changes through the Fram Strait. *Progress in Oceanography*, 22(3), 205–248.

1783 Rudels, B. (2015). Arctic Ocean circulation, processes and water masses: A descrip-
1784 tion of observations and ideas with focus on the period prior to the Interna-
1785 tional Polar Year 2007–2009. *Progress in Oceanography*, 132, 22–67.

1786 Rudels, B., Anderson, L., & Jones, E. (1996). Formation and evolution of the sur-
1787 face mixed layer and halocline of the Arctic Ocean. *Journal of Geophysical Re-*
1788 *search: Oceans*, 101(C4), 8807–8821.

- 1789 Rudels, B., Jones, E., Anderson, L., & Kattner, G. (1994). On the intermediate
1790 depth waters of the Arctic Ocean. *The polar oceans and their role in shaping*
1791 *the global environment*, 85, 33–46.
- 1792 Rudels, B., Kuzmina, N., Schauer, U., Stipa, T., & Zhurbas, V. (2009). Double-
1793 diffusive convection and interleaving in the Arctic Ocean—distribution and
1794 importance. *Geophysica*, 45(1-2), 199–213.
- 1795 Rudels, B., et al. (2012). Arctic Ocean circulation and variability—advection and ex-
1796 ternal forcing encounter constraints and local processes. *Ocean Science*.
- 1797 Schanze, J. J., & Schmitt, R. W. (2013). Estimates of cabbeling in the global ocean.
1798 *Journal of physical oceanography*, 43(4), 698–705.
- 1799 Schauer, U., & Beszczynska-Möller, A. (2009). Problems with estimating oceanic
1800 heat transport—conceptual remarks for the case of Fram Strait in the Arctic
1801 Ocean. *Ocean Science Discussions*, 6, 1007–1029.
- 1802 Schauer, U., Fahrback, E., Osterhus, S., & Rohardt, G. (2004). Arctic warming
1803 through the Fram Strait: Oceanic heat transport from 3 years of measure-
1804 ments. *Journal of Geophysical Research: Oceans*, 109(C6).
- 1805 Schauer, U., Loeng, H., Rudels, B., Ozhigin, V. K., & Dieck, W. (2002). Atlantic
1806 water flow through the Barents and Kara Seas. *Deep Sea Research Part I:*
1807 *Oceanographic Research Papers*, 49(12), 2281–2298.
- 1808 Serreze, M., Barrett, A., Stroeve, J., Kindig, D., & Holland, M. (2009). The emer-
1809 gence of surface-based Arctic amplification. *The Cryosphere*, 3(1), 11.
- 1810 Serreze, M. C., Barrett, A. P., Slater, A. G., Steele, M., Zhang, J., & Trenberth,
1811 K. E. (2007). The large-scale energy budget of the Arctic. *Journal of Geophys-*
1812 *ical Research: Atmospheres*, 112(D11).
- 1813 Serreze, M. C., Barrett, A. P., Slater, A. G., Woodgate, R. A., Aagaard, K., Lam-
1814 mers, R. B., . . . Lee, C. M. (2006). The large-scale freshwater cycle of the
1815 Arctic. *Journal of Geophysical Research: Oceans*, 111(C11).
- 1816 Serreze, M. C., Crawford, A. D., Stroeve, J. C., Barrett, A. P., & Woodgate, R. A.
1817 (2016). Variability, trends, and predictability of seasonal sea ice retreat
1818 and advance in the Chukchi Sea. *Journal of Geophysical Research: Oceans*,
1819 121(10), 7308–7325.
- 1820 Serreze, M. C., McLaren, A. S., & Barry, R. G. (1989). Seasonal variations of sea ice
1821 motion in the Transpolar Drift Stream. *Geophysical Research Letters*, 16(8),

1822 811–814.

1823 Shibley, N. C., Timmermans, M.-L., Carpenter, J. R., & Toole, J. M. (2017). Spatial
1824 variability of the Arctic Ocean’s double-diffusive staircase. *Journal of Geophys-*
1825 *ical Research: Oceans*, *122*(2), 980–994.

1826 Sirevaag, A., & Fer, I. (2012). Vertical heat transfer in the Arctic Ocean: The role of
1827 double-diffusive mixing. *Journal of Geophysical Research: Oceans*, *117*(C7).

1828 Smedsrud, L. H., Esau, I., Ingvaldsen, R. B., Eldevik, T., Haugan, P. M., Li, C.,
1829 ... others (2013). The role of the barents sea in the Arctic climate system.
1830 *Reviews of Geophysics*, *51*(3), 415–449.

1831 Smith, K. S. (2007). The geography of linear baroclinic instability in Earth’s oceans.
1832 *Journal of Marine Research*, *65*(5), 655–683.

1833 Spall, M. A. (2013). On the circulation of Atlantic water in the Arctic Ocean. *Jour-*
1834 *nal of Physical Oceanography*, *43*(11), 2352–2371.

1835 Spall, M. A., Pickart, R. S., Fratantoni, P. S., & Plueddemann, A. J. (2008). West-
1836 ern Arctic shelfbreak eddies: Formation and transport. *Journal of Physical*
1837 *Oceanography*, *38*(8), 1644–1668.

1838 Spall, M. A., Pickart, R. S., Li, M., Itoh, M., Lin, P., Kikuchi, T., & Qi, Y. (2018).
1839 Transport of Pacific water into the Canada Basin and the formation of the
1840 Chukchi slope current. *Journal of Geophysical Research: Oceans*, *123*(10),
1841 7453–7471.

1842 Steele, M., & Boyd, T. (1998). Retreat of the cold halocline layer in the Arctic
1843 Ocean. *Journal of Geophysical Research: Oceans*, *103*(C5), 10419–10435.

1844 Steele, M., Ermold, W., & Zhang, J. (2008). Arctic Ocean surface warming trends
1845 over the past 100 years. *Geophysical Research Letters*, *35*(2).

1846 Steele, M., Morison, J., Ermold, W., Rigor, I., Ortmeyer, M., & Shimada, K. (2004).
1847 Circulation of summer Pacific halocline water in the Arctic Ocean. *Journal of*
1848 *Geophysical Research: Oceans*, *109*(C2).

1849 Stein, R., Fahl, K., Gierz, P., Niessen, F., & Lohmann, G. (2017). Arctic Ocean sea
1850 ice cover during the penultimate glacial and the last interglacial. *Nature com-*
1851 *munications*, *8*(1), 373.

1852 Stigebrandt, A. (1981). A model for the thickness and salinity of the upper layer
1853 in the Arctic Ocean and the relationship between the ice thickness and some
1854 external parameters. *Journal of Physical Oceanography*, *11*(10), 1407–1422.

- 1855 Stommel, H. (1948). The westward intensification of wind-driven ocean currents.
1856 *Eos, Transactions American Geophysical Union*, 29(2), 202–206.
- 1857 Stommel, H. M. (1979). Determination of water mass properties of water pumped
1858 down from the Ekman layer to the geostrophic flow below. *Proc. Nat. Acad.*
1859 *Sci.*, 76, 3051–3055.
- 1860 Sverdrup, H. U., Johnson, M. W., Fleming, R. H., et al. (1942). *The oceans: Their*
1861 *physics, chemistry, and general biology* (Vol. 7). Prentice-Hall New York.
- 1862 Timmermans, M.-L. (2015). The impact of stored solar heat on Arctic sea ice
1863 growth. *Geophysical Research Letters*(May). doi: 10.1002/2015GL064541.1.
- 1864 Timmermans, M.-L., & Jayne, S. R. (2016). The Arctic Ocean spices up. *Journal of*
1865 *Physical Oceanography*, 46(4), 1277–1284.
- 1866 Timmermans, M.-L., Krishfield, R., Lee, C., & Toole, J. (2018). ALPS in the Arctic
1867 Ocean. In D. Rudnick, D. Costa, K. Johnson, C. Lee, & M.-L. Timmermans
1868 (Eds.), *ALPS ii – autonomous lagrangian platforms and sensors. a report of*
1869 *the ALPS ii workshop* (p. 37-39). La Jolla CA: 66 pp.
- 1870 Timmermans, M.-L., & Ladd, C. (2019). [the Arctic] sea surface temperature [in
1871 “State of the Climate in 2018”]. *Bull. Amer. Meteor. Soc.*, 100(9), S144-S146.
1872 doi: 10.1175/2019BAMSStateoftheClimate.1
- 1873 Timmermans, M.-L., Marshall, J., Proshutinsky, A., & Scott, J. (2017). Seasonally
1874 derived components of the Canada Basin halocline. *Geophysical Research Let-*
1875 *ters*, 44(10), 5008–5015. doi: 10.1002/2017GL073042
- 1876 Timmermans, M.-L., Proshutinsky, A., Golubeva, E., Jackson, J. M., Krishfield, R.,
1877 McCall, M., . . . others (2014). Mechanisms of Pacific summer water variabil-
1878 ity in the Arctic’s central Canada Basin. *Journal of Geophysical Research:*
1879 *Oceans*, 119(11), 7523–7548.
- 1880 Timmermans, M.-L., Proshutinsky, A., Krishfield, R. A., Perovich, D. K., Richter-
1881 Menge, J. A., Stanton, T. P., & Toole, J. M. (2011). Surface freshening in the
1882 Arctic Ocean’s Eurasian Basin: An apparent consequence of recent change in
1883 the wind-driven circulation. *Journal of Geophysical Research: Oceans*, 116(7).
1884 doi: 10.1029/2011JC006975
- 1885 Timmermans, M.-L., Rainville, L., Thomas, L., & Proshutinsky, A. (2010). Moored
1886 observations of bottom-intensified motions in the deep Canada Basin, Arctic
1887 Ocean. *Journal of Marine Research*, 68(3-4), 625–641.

- 1888 Timmermans, M.-L., Toole, J., & Krishfield, R. (2018). Warming of the interior Arc-
1889 tic Ocean linked to sea ice losses at the basin margins. *Science advances*, *4*(8),
1890 eaat6773.
- 1891 Timmermans, M.-L., Toole, J., Krishfield, R., & Winsor, P. (2008). Ice-tethered
1892 profiler observations of the double-diffusive staircase in the Canada Basin
1893 thermocline. *Journal of Geophysical Research: Oceans*, *113*(C1).
- 1894 Timmermans, M.-L., Toole, J., Proshutinsky, A., Krishfield, R., & Plueddemann, A.
1895 (2008). Eddies in the Canada Basin, Arctic Ocean, Observed from Ice-Tethered
1896 Profilers. *Journal of Physical Oceanography*, *38*(1), 133–145. Retrieved from
1897 <http://journals.ametsoc.org/doi/abs/10.1175/2007JP03782.1> doi:
1898 10.1175/2007JPO3782.1
- 1899 Toole, J., Krishfield, R., Timmermans, M.-L., & Proshutinsky, A. (2011). The
1900 Ice-Tethered Profiler: Argo of the Arctic. *Oceanography*, *24*(3), 126–135. Re-
1901 trieved from <https://tos.org/oceanography/article/the-ice-tethered>
1902 [-profiler-argo-of-the-arctic](https://tos.org/oceanography/article/the-ice-tethered) doi: 10.5670/oceanog.2011.64
- 1903 Toole, J. M., Schmitt, R. W., & Polzin, K. L. (1994). Estimates of diapycnal mixing
1904 in the abyssal ocean. *Science*, *264*(5162), 1120–1123.
- 1905 Toole, J. M., Timmermans, M.-L., Perovich, D. K., Krishfield, R. A., Proshutinsky,
1906 A., & Richter-Menge, J. A. (2010). Influences of the ocean surface mixed layer
1907 and thermohaline stratification on Arctic sea ice in the central Canada Basin.
1908 *Journal of Geophysical Research: Oceans*, *115*(C10).
- 1909 Tschudi, M., Fowler, C., Maslanik, J., Stewart, J., & Meier, W. (2016). Polar
1910 Pathfinder daily 25 km ease-grid sea ice motion vectors, version 3. *National*
1911 *Snow and Ice Data Center Distributed Active Archive Center, accessed Febru-*
1912 *ary*.
- 1913 Tulloch, R., Marshall, J., Hill, C., & Smith, K. S. (2011). Scales, growth rates,
1914 and spectral fluxes of baroclinic instability in the ocean. *Journal of Physical*
1915 *Oceanography*, *41*(6), 1057–1076.
- 1916 Untersteiner, N. (1988). On the ice and heat balance in Fram Strait. *Journal of*
1917 *Geophysical Research: Oceans*, *93*(C1), 527–531.
- 1918 Vihma, T., Screen, J., Tjernström, M., Newton, B., Zhang, X., Popova, V., . . .
1919 Prowse, T. (2016). The atmospheric role in the Arctic water cycle: A review
1920 on processes, past and future changes, and their impacts. *Journal of Geophysi-*

1921 *cal Research: Biogeosciences*, 121(3), 586–620.

1922 Walsh, D., & Carmack, E. (2003). The nested structure of Arctic thermohaline in-
1923 trusions. *Ocean Modelling*, 5(3), 267–289.

1924 Weingartner, T., Aagaard, K., Woodgate, R., Danielson, S., Sasaki, Y., & Cavalieri,
1925 D. (2005). Circulation on the north central Chukchi Sea shelf. *Deep Sea*
1926 *Research Part II: Topical Studies in Oceanography*, 52(24-26), 3150–3174.

1927 Wettlaufer, J. (1991). Heat flux at the ice-ocean interface. *Journal of Geophysical*
1928 *Research: Oceans*, 96(C4), 7215–7236.

1929 Whitehead, J. (1998). Topographic control of oceanic flows in deep passages and
1930 straits. *Reviews of Geophysics*, 36(3), 423–440.

1931 Woodgate, R. A. (2018). Increases in the Pacific inflow to the Arctic from 1990
1932 to 2015, and insights into seasonal trends and driving mechanisms from year-
1933 round bering Strait mooring data. *Progress in Oceanography*, 160, 124–154.

1934 Woodgate, R. A., & Aagaard, K. (2005). Revising the Bering Strait freshwater flux
1935 into the Arctic Ocean. *Geophysical Research Letters*, 32(2).

1936 Woodgate, R. A., Aagaard, K., Muench, R. D., Gunn, J., Björk, G., Rudels, B., ...
1937 Schauer, U. (2001). The Arctic Ocean boundary current along the Eurasian
1938 slope and the adjacent Lomonosov Ridge: Water mass properties, transports
1939 and transformations from moored instruments. *Deep Sea Research Part I:*
1940 *Oceanographic Research Papers*, 48(8), 1757–1792.

1941 Woodgate, R. A., Aagaard, K., Swift, J. H., Smethie Jr, W. M., & Falkner, K. K.
1942 (2007). Atlantic water circulation over the Mendeleev Ridge and Chukchi bor-
1943 derland from thermohaline intrusions and water mass properties. *Journal of*
1944 *Geophysical Research: Oceans*, 112(C2).

1945 Woodgate, R. A., Fahrbach, E., & Rohardt, G. (1999). Structure and transports
1946 of the East Greenland Current at 75 n from moored current meters. *Journal of*
1947 *Geophysical Research: Oceans*, 104(C8), 18059–18072.

1948 Woodgate, R. A., Stafford, K. M., & Prahl, F. G. (2015). A synthesis of year-round
1949 interdisciplinary mooring measurements in the bering strait (1990–2014) and
1950 the rusalka years (2004–2011). *Oceanography*, 28(3), 46–67.

1951 Woodgate, R. A., Weingartner, T., & Lindsay, R. (2010). The 2007 Bering Strait
1952 oceanic heat flux and anomalous Arctic sea-ice retreat. *Geophysical Research*
1953 *Letters*, 37(1).

- 1954 Woodgate, R. A., Weingartner, T. J., & Lindsay, R. (2012). Observed increases in
1955 Bering Strait oceanic fluxes from the Pacific to the Arctic from 2001 to 2011
1956 and their impacts on the Arctic Ocean water column. *Geophysical Research
1957 Letters*, *39*(24).
- 1958 Worthington, L. (1953). Oceanographic results of project skijump i and skijump ii
1959 in the polar Sea, 1951–1952. *Eos, Transactions American Geophysical Union*,
1960 *34*(4), 543–551.
- 1961 Wunsch, C. (2011). The decadal mean ocean circulation and Sverdrup balance.
1962 *Journal of Marine Research*, *69*(2-3), 417–434.
- 1963 Yang, J. (2005). The Arctic and subarctic ocean flux of potential vorticity and
1964 the Arctic Ocean circulation. *Journal of Physical Oceanography*, *35*(12), 2387–
1965 2407.
- 1966 Yang, J., Proshutinsky, A., & Lin, X. (2016). Dynamics of an idealized
1967 Beaufort Gyre: 1. the effect of a small beta and lack of western bound-
1968 aries. *Journal of Geophysical Research: Oceans*, *121*(2), 1249–1261. doi:
1969 10.1002/2015JC011296
- 1970 Zhang, J., Rothrock, D. A., & Steele, M. (1998). Warming of the Arctic Ocean by
1971 a strengthened Atlantic inflow: Model results. *Geophysical Research Letters*,
1972 *25*(10), 1745–1748.
- 1973 Zhang, J., & Steele, M. (2007). Effect of vertical mixing on the Atlantic water layer
1974 circulation in the Arctic Ocean. *Journal of Geophysical Research: Oceans*,
1975 *112*(C4).
- 1976 Zhao, B., & Timmermans, M.-L. (2018). Topographic Rossby waves in the Arc-
1977 tic Ocean’s Beaufort Gyre. *Journal of Geophysical Research: Oceans*, *123*(9),
1978 6521–6530.
- 1979 Zhao, M., & Timmermans, M.-L. (2015). Vertical scales and dynamics of eddies
1980 in the arctic ocean’s Canada basin. *Journal of Geophysical Research: Oceans*,
1981 *120*(12), 8195–8209.
- 1982 Zhao, M., Timmermans, M.-L., Cole, S., Krishfield, R., Proshutinsky, A., & Toole,
1983 J. (2014). Characterizing the eddy field in the Arctic Ocean halocline.
1984 *Journal of Geophysical Research C: Oceans*, *119*(12), 8800–8817. doi:
1985 10.1002/2014JC010488
- 1986 Zhao, M., Timmermans, M.-L., Cole, S., Krishfield, R., & Toole, J. (2016). Evolu-

1987 tion of the eddy field in the Arctic Ocean's Canada Basin, 2005-2015. *Geophys-*
1988 *ical Research Letters*, 43(15), 8106–8114. doi: 10.1002/2016GL069671
1989 Zhao, M., Timmermans, M.-L., Krishfield, R., & Manucharyan, G. (2018). Partition-
1990 ing of kinetic energy in the arctic ocean's beaufort gyre. *Journal of Geophys-*
1991 *ical Research: Oceans*, 123(7), 4806–4819.